MINERALOGICAL AND GEOCHEMICAL CHARACTERISATION OF CORES FROM AN IN SITU RECOVERY URANIUM MINE

A Thesis Submitted to the College of
Graduate and Postdoctoral Studies
In Partial Fulfillment of the Requirements
For the Degree of Masters of Science
In the Department of Geological Sciences
University of Saskatchewan
Saskatoon

By

SAMIRA SUMAILA

PERMISSION TO USE

In presenting this thesis in partial fulfillment of the requirements for a Postgraduate degree from the University of Saskatchewan, I agree that the Libraries of this University may make it freely available for inspection. I further agree that permission for copying of this thesis/dissertation in any manner, in whole or in part, for scholarly purposes may be granted by the professor or professors who supervised my thesis/dissertation work or, in their absence, by the Head of the Department or the Dean of the College in which my thesis work was done. It is understood that any copying or publication or use of this thesis/dissertation or parts thereof for financial gain shall not be allowed without my written permission. It is also understood that due recognition shall be given to me and to the University of Saskatchewan in any scholarly use which may be made of any material in my thesis.

Requests for permission to copy or to make other uses of materials in this thesis in whole or part should be addressed to:

Head of the Department of Geological Sciences
University of Saskatchewan
114 Science Place
Saskatoon, Saskatchewan
S7N 5E2, Canada

OR

Dean of the College of Graduate Studies and Research
University of Saskatchewan
107 Administration Place
Saskatoon, Saskatchewan
S7N 5A2, Canada

ABSTRACT

This study investigates the mineralogy and geochemistry of natural aquifer materials associated with a uranium (U) ore deposit at the Smith Ranch-Highlands Mine, Wyoming, USA. The ore occurs in a roll front deposit and is mined via in situ recovery (ISR). This method of mining is used to recover U from low-grade deposits while producing no tailings or waste rock. This method of mining can, however, contaminate adjacent aquifers with residual U and other elements. The objective of this project is to characterize core taken down-gradient of a mined unit to provide information on the capacity of down-gradient aquifer solids to attenuate U. Core samples were obtained from hydraulically down-gradient of the mine unit B at two locations. Powder X-ray diffraction analyses showed the presence of quartz, clays, feldspar, goethite and pyrite. Electron microprobe analysis, scanning electron microscopy and physical examination confirmed that the core is a heterogeneous mixture of grain sizes with different shapes and composed of clays, sandy materials and coal lenses. Synchrotron X-ray fluorescence mapping revealed the close association of U with Fe, V, Ca and coal lenses in the sediments. Uranium X-ray absorption spectroscopy (XANES) showed the presence of both U(IV) and U(VI) in samples containing coal lenses. Carbon (C) XANES indicated the presence of several C functional groups representative of organic C; however, inorganic C was not identified in the C-K-edge XANES analysis. Iron and S XANES also confirmed the presence of reduced and oxidised Fe and S species. Clays, coal lenses, Fe-oxides and pyrite observed in the core samples may control U concentrations and mobility in groundwater. Geochemical modelling using PHREEQC software showed that primary and secondary U minerals may not control U mobility in these materials but the presence of carbonate, Fe oxides and clays may control U concentrations and mobility through sorption, reduction and precipitation processes. Information from this work can contribute to the quantification and estimation of the risk of downstream/down-gradient human exposure in fate-and-transport models.

ACKNOWLEDGEMENTS

I would like to acknowledge that the Smith-Ranch Highlands Mine is located in Wyoming, the homeland of the Sioux and Cheyenne people. The University of Saskatchewan's main campus is located on Treaty 6 Territory and is also the homeland of the Métis people.

The completion of this thesis would not have been possible without the care and support of many people and institutions. I am very grateful to my supervisors Dr. Joyce McBeth and Dr. Jim Hendry for their mentorship, time, patience and guidance throughout my MSc programme. I would also like to thank my committee member Dr. Mat Lindsey for his guidance and insightful comments.

A big thank you to Cameco Resources for providing samples for this work. I would also like to thank Jim Clay and Jeff Warner for their guidance, technical advice and support for this project. A special thank you to Dr. Janet Schramke for providing access to the PHREEQC database needed for this work.

My sincere thanks to Dr. Joseph Essilfie-Dughan for his mentorship and help in my XANES and modelling analysis. A special thanks to Tom Bonli for my PXRD and EMPA data collection, Dr. Joel Reid for teaching me PXRD data analysis, Ibi Bondici for listening, sharing and helping me with some data analysis and members of the McBeth group for all their supports and advice.

Funding for this project was provided through direct and in-kind support from Cameco Corporation, a MITACs Accelerate grant (ITO4936), Natural Sciences and Engineering Research Council of Canada (NSERC) Discovery Grant to Joyce McBeth (RGPIN-2014-03719). We acknowledge stipend support provided by the University of Saskatchewan, Department of Geological Sciences devolved scholarships, the Canadian Light Source (CLS), and the NSERC TERRE-CREATE training program (449124-2014). Synchrotron research described in this thesis was performed at the CLS, which is supported by the Canada Foundation for Innovation, the NSERC, the University of Saskatchewan, the Government of Saskatchewan, Western Economic Diversification Canada, the National Research Council Canada, and the Canadian Institutes of Health Research. I am also appreciative of the beamline support provided by Aimee Maclennan (CLS SXRMB), Ning Chen (CLS HXMA), Peter Blanchard (CLS VESPERS) and all members of the CLS CMCF beamline.

DEDICATION

I dedicate this dissertation to my kids (Hafeez and Shukura), my mum, Ababa, my siblings and my dear husband who has been my support, my friend and my inspiration.

TABLE CONTENTS

LIST OF TABLES

LIST OF FIGURES

LIST OF ABBREVIATIONS

ALS	Advance Light Source
BPT	Best practicable technology
BSE	Backscattered electron image
CFR	Code of federal regulations
CLS	Canadian Light Source
CMCF-BM	Canadian Macromolecular Crystallography Facility
DOE	U.S. Department of Energy
EDS	Energy dispersive spectra
EMPA	Electron microprobe
EPA	Environmental Protection Agency
ESRF	European Synchrotron Facility
HXMA	Canadian Light Source Hard X-ray Micro-Analysis beamline
ICP-MS	Inductively coupled plasma-mass spectrometry
ICP-OES	Inductively coupled plasma-optical emission spectrometry
ISR	In situ recovery mining
LCF	Linear combination fitting
LQD	Land Quality Division
MUB	Mine Unit B
NRC	United States Nuclear Regulatory Commission
PCA	Principal Component Analysis
PXRD	Powder X-ray diffraction
SEM	Scanning electron microscopy
SGM	Canadian Light Source Spherical Grating Monochromator beamline
SM	Standard Methods
SXRMB	Canadian Light Source Soft X-ray Microcharacterization Beamline
WDEQ	Wyoming Department of Environmental Quality
XANES	X-ray absorption near edge spectroscopy
XAS	X-ray absorption spectroscopy
µXRF	Micro X-ray fluorescence
w/w	Weight per weigh

1. INTRODUCTION AND LITERATURE REVIEW

Uranium (U) is a fissile element and used in nuclear power plants to produce low-carbon energy. In 2011, about 12% of global electricity was generated by fission reactions using U in power plants (Canadian Nuclear Association, 2015). Currently there are 434 operable reactors in the world generating approximately 372 gigawatts of electricity (Canadian Nuclear Association, 2015). The United States is home to 99 nuclear power generating stations that provided 19.5% of the country's electricity in 2014 (World Nuclear Association, Last updated; June, 2016). Other countries also generate an appreciable percentage of their electricity from nuclear energy. For example, in 2015, France generated 76.3% of its electricity from nuclear energy, Canada (16.6%), China (3%) and United Kingdom (18.9 %) (World Nuclear Association, Last updated; September, 2016). Uranium is also used in medical isotope production and in propulsion of naval submarines.

In 2013, 47% of the U produced worldwide was generated from in situ recovery mining (ISR) (World Nuclear Association, updated May 2017). In situ Recovery is one of the most economical methods used for U mining (IAEA, 2016). The use of ISR in U production has grown from 13% in 1995 to 46% in 2011 due to its competitive production cost and lesser impact on the surface environment (IAEA, 2016). A major concern associated with ISR mining is the possibility of groundwater contamination with U and other dissolved metals which may be consumed by humans and livestock (Borch et al., 2012).

In situ recovery mining, also known as in situ leach (ISL) or solution mining is used to mine U in permeable deposits, such as the roll front U deposits present at the Smith Ranch-Highlands Mine in the Wyoming Basin, USA. The roll front U ore deposits at this mine occur in a loosely consolidated, permeable sandstone host formation located below the groundwater table and is vertically confined above and below by low permeability layers such as shale and mudstones (Dahlkamp, 2010). In situ Recovery involves circulating native groundwater fortified with dissolved oxygen (oxidant), sodium carbonate, and/or carbon dioxide through the ore body to create a solution containing U (lixiviate). The lixiviate is extracted through a series of wells and the U is recovered using an ion exchange process. The addition of an oxidant causes the oxidation of U(IV) (highly insoluble) to U(VI) (soluble). The U(VI) then forms soluble complexes with carbonate ions which are brought to the surface. The redox state of U is crucial in determining the

mobility of U in aquifers. U(VI) is the most stable oxidation state of U in oxidizing environment and its mobility is primarily controlled by sorption to mineral surfaces (clays, iron minerals) and redox processes. Predicting U mobility in groundwater requires understanding several factors (pH, Eh, availability or absence of complexing ligands such as sulfate, phosphate, and carbonates) that affect sorption and redox processes (Bachmaf et al., 2008; Du et al., 2011). After ISR mining is complete, groundwater restoration is done to remove remaining dissolved U from the mined zone. Groundwater restoration is normally achieved using 'groundwater sweep' or groundwater flush (i.e. flushing the ore formation with aquifer water obtained from outside the mine zone), reverse osmosis, bioremediation, natural attenuation and the application of a chemical reducing agent (Mays, 1994; Hall, 2009; Hu et al., 2011).

In recent years, several studies have been conducted to look at groundwater restoration in aquifers contaminated by U and other radioisotopes (Borch et al., 2012). The mobility of U in shallow groundwater (Stewart et al., 2010; Dong et al., 2012) and groundwater bioremediation studies in areas contaminated with acidic plating waste containing high levels of U have been studied (Wei-min et al., 2006; Wu et al., 2006; Wu et al., 2007; Kelly et al., 2008). None of these studies addressed groundwater restoration under conditions typical of ISR mining. The ISR mining zone is usually located one hundred meters or more beneath the ground surface. For example, the Crow Butte ISR mine extract U from sandstone aquifers at a depth that varies between 121 – 244 m below the ground surface. Moreover, aquifers at ISR sites tend to be less severely contaminated than those at sites associated with weapons production. For example, the groundwater beneath the S-3 ponds (where liquid wastes from U processing were dumped) of the U.S. Department of Energy (DOE) Field Research Center at Oak Ridge, TN contains up to 210 µM of U along with high concentrations of nitrate, mercury, and transuranic elements (Brooks, 2001). A United States Geological Survey study on restoration outcomes at ISR facilities in Texas concluded that pre-mining baseline values for U, Se, As, Pb, Ra and Cd were high, and after mining and restoration the values were below baseline except for U and Se (Hall, 2009), thus returning U to baseline condition after mining and restoration remains a challenge to the mining companies.

Before commencing ISR mining in the USA, companies are required to get licenses from the United States Nuclear Regulatory Commission (NRC). These companies are also required by the NRC to return the mine site to pre-mining or baseline condition after mining. As such, companies

maintain a surety bond (financial commitment) for the purposes of decommissioning their facilities. When pre-mining conditions are not attained during restoration of groundwater and if it can be demonstrated that the extent of restoration is sufficient to protect down-gradient water (i.e. outside the aquifer exemption boundary), the surety bond for the mine unit can be released by regulators (United States Nuclear Regulatory Commission, Last updated August 22, 2013). A key question underpinning restoration goals is whether the residual contamination (particularly U and other radio-isotopes as well as heavy metals) left after restoration is immobilized by down-gradient solids present immediately outside the mined aquifer zone. In this work, I used core samples collected from two boreholes located at Mine Unit B (MUB), a mined and restored zone at the Smith Ranch-Highland U mine and data from within the mined area of the site to develop conceptual models to help guide restoration strategies. The goal of this study is to characterise core taken down-gradient of the mining zone to provide information on the capacity of down-gradient aquifer solids to attenuate U. Geochemical modelling using groundwater data from the site can help confirm experimental data and explain U chemistry. This is important for quantifying and estimating the risk of downstream/down-gradient human exposure in fate-and-transport models.

1.1 Hypothesis

In this work, we hypothesised that solids located downstream of the Smith Ranch-Highland Mine Unit B mine may control U mobility in groundwater. To test this hypothesis, I have the following set of objectives:

- Characterize the bulk mineralogy of the core samples from MUB
- Characterize C, Fe, S and U phases present in the core samples
- Map mineralogy and elemental distributions in the core samples
- Develop a geochemical model for U chemistry at MUB
- Develop a conceptual model for the interactions of U with minerals within the ore and in the groundwater.

1.2 Literature review

1.2.1 Uranium

Uranium is a naturally-occurring fissile element that occurs throughout the earth's crust, normally in the form of U(VI) and U(IV)-containing minerals in phosphate rock deposits and in minerals such as uraninite in U-rich ore. Uranium was first discovered in a mineral called pitchblende by a German chemist called Martin Klaproth in 1789. Uranium ore deposits are distributed globally with the highest ore grade found in the Athabasca Basin located in Northern Saskatchewan, Canada (Jamieson & Frost, 1997).

Uranium is one of the heaviest naturally-occurring element with no stable isotopes. The three naturally-occurring U isotopes are U-238 (99.275%), U-235 (0.72%) and U-234 (0.005%). These U isotopes can undergo radioactive decay releasing alpha particles, beta particles, and gamma rays that may pose ill-effects to living cells. U-238, the most common U isotope, decays until a stable non-radiative decay product is formed. The decay process results in the formation of radionuclides including radium-226 and radon-222 that are very harmful when ingested. U-238 has a half-life of about 4.47 billion years which is almost the same as the age of the earth, while U-235 and U-234 have half-lives of 704 million and 245,000 years respectively (Monreal & Diaconescu, 2010). Uranium mining is part of the nuclear fuel cycle which is a series of industrial processes used in the generation of electricity from U. Uranium (U-235) undergoes a fission reaction when it is bombarded with neutrons, thereby releasing energy for production of electricity. One U-235 atom produces about 50 million times more energy than a single carbon atom, therefore three tiny pellets of U (about 0.24 ounce each) can produce as much energy as 7000 pounds of coal or 12 barrels of oil (Kaufman & Franz, 2000; Alan & George, 2007).

1.2.2 Uranium speciation in natural waters

Uranium is a lithophilic metal and exists in several oxidation states (+2, +3, +4, +5, and +6). In natural waters U exists as ions containing U(IV), U(V), and U(VI) (Vivo et al., 1984). The hexavalent U(VI), which is water soluble, and the much less soluble tetravalent U(IV) are of practical importance in geochemical studies (Vivo et al., 1984). In groundwater systems, U may exist as complexed, sorbed or precipitated uranyl carbonates, uraninite or hydroxide minerals (Hua et al., 2006). According to Langmuir (1978) , in groundwater systems, dissolved U concentrations

are controlled by several factors that include (a) the pH and the redox condition of the water, (b) the proximity of the groundwater to the U source, (c) the content and leachability of U in the aquifer sediments, (d) evapotranspiration processes (climatic effects and their seasonal variabilities), (e) the presence and concentrations of species that can form complexes with U or precipitate insoluble U minerals, and (f) the availability of sorptive materials (e.g. organic matter, Fe oxyhydroxides). The interactions between these factors may eventually lead to U precipitation, adsorption and redox transformation all of which are essential in understanding U chemistry (Langmuir, 1978; Hua et al., 2006). A recent study has confirmed biotic reduction as an important mechanism in the formation of U roll front deposit (Bhattacharyya et al., 2017). Uranium in natural waters forms aqueous complexes with carbonates, hydroxyls, phosphates, fluorides and sulfates. The formation of these complexes increases the solubility and mobility of U (Langmuir, 1978; Bostick et al., 2002). The activities of these complexing species are a function of pH and temperature. Among the most important of these complexing species is carbonate that is usually obtained from atmospheric carbon dioxide and carbonate minerals (Giblin et al., 1981). Casas et al. (1998) demonstrated that U complexation in natural groundwater is highly pH dependent and U mineral solubility and precipitation are also dependent on Eh and pH. Figure 1-1 shows a Pourbaix diagram for U in natural water containing carbonate, at a temperature of 13˚C and 1 atm pressure. The figure shows uranyl dicarbonate and tricarbonate complexes as the main forms of dissolved U with their fields widening with increasing pH. Carbonate ions control the circulation of U in the high pH region, thus water containing high concentrations of carbonate species will increase the formation of complexes that in turn will increase the solubility and mobility of U in these waters (Langmuir, 1978; Vivo et al., 1984).

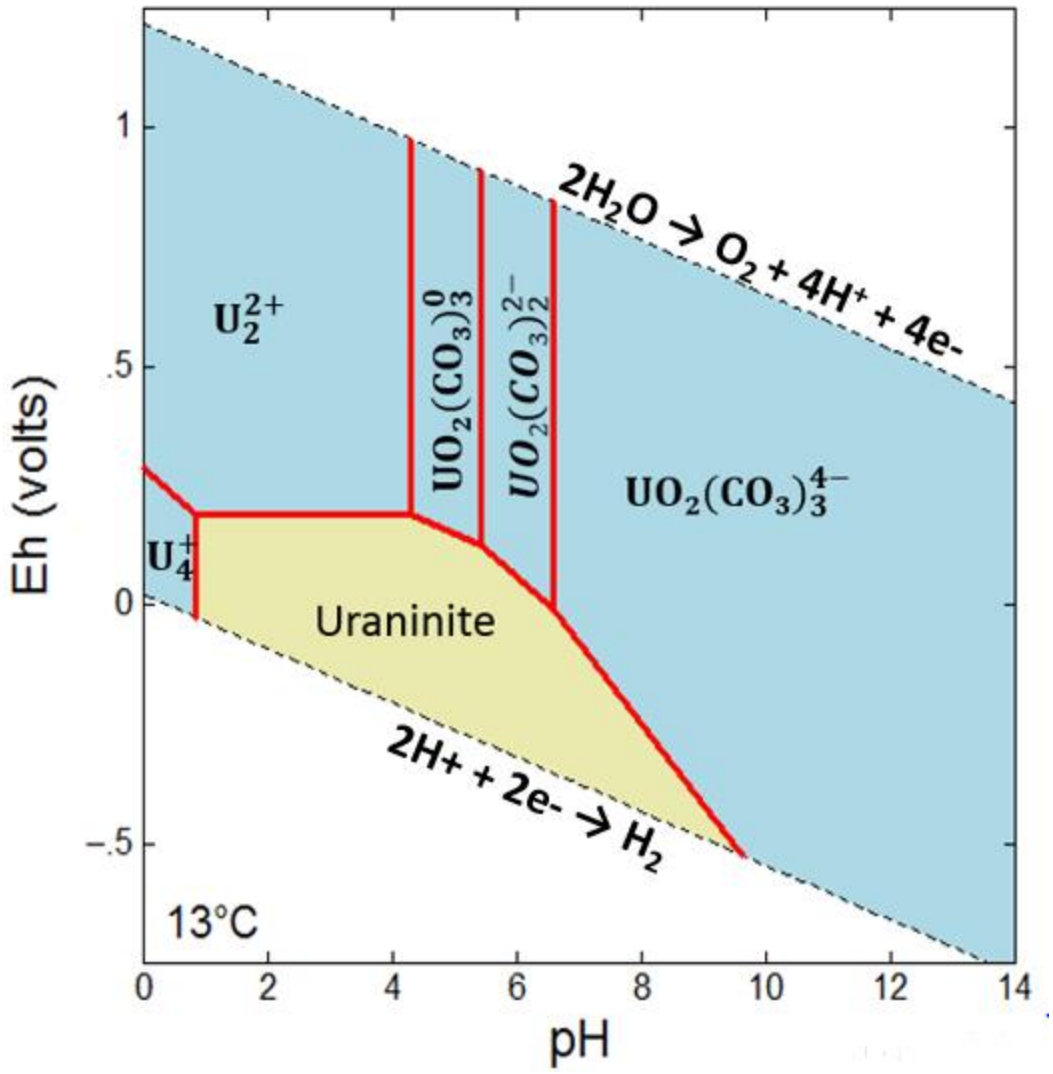

Figure 1-1: Eh-pH diagram for UO_2-H_2O-CO_2 system at 13˚C (a typical groundwater temperature) and 1 atm for U=3.8 x10^{-8}M and PCO_2 =10^{-2} atm. The dashed lines show the thermodynamically stable area of water.

In U-bearing groundwater containing high concentration of carbonate mineral, stable carbonate uranyl complex are reported to dominate the total dissolved U species (Gorby & Lovley, 1992). Thermodynamic modelling using MINTEQA2 database for 30 mM of carbonate at neutral pH shows that U speciation under these conditions is dominated by $UO_2(CO_3)_2^{2-}$ and $UO_2(CO_3)_3^{4-}$ (Sani et al., 2002). These carbonate complexes can readily be reduced by dissimilatory metal-reducing bacteria (Lovley et al., 1991; Phillips et al., 1995; Stewart et al.,

2011). In the presence of Ca, Ca-UO_3-CO_3 complex becomes the dominant dissolved U species and these complex have been reported to have the ability to limit biotic reduction of U (Brooks et al., 2003; Neiss et al., 2007).

1.2.3 Redox processes

Redox processes play key roles in the formation and dissolution of minerals by oxidation and reduction processes. They control the mobility, bioavailability and chemical speciation of many important trace element including U (Borch et al., 2010). Under oxic condition U exists generally as uranyl [U(VI)] which is soluble. The solubility of uranyl is enhanced by forming complexes with carbonates; the most common ligand found in most groundwaters. U(IV) is sparingly soluble even in the presence of carbonate and thus tends to be immobile (Guillaumont et al., 2003). Reduction plays an important role in precipitating insoluble U minerals (e.g. uraninite). This is achieved by using reducing agents such as organic matter, Fe (II) minerals and sulfides. Reduction can be biotic (enzymatic) or abiotic (chemical). Vivo et al. (1984) proposed the following redox reactions for the reduction of U(VI) to U(IV):

$$4UO_2^{2+} + HS^- + 4H_2O \rightarrow 4UO_2 + SO_4^{2-} + 9H^+ \quad (1)$$

Or $$4UO_2(CO_3)_3^{4-} + HS^- + 15H^+ \rightarrow 4UO_2 + SO_4^{2-} + 12CO_2 + 8H_2O \quad (2)$$

Or $$4UO_2^{2+} + CH_4 + 2H_2O \rightarrow 4UO_2 + CO_2 + 8H^+ \quad (3)$$

The presence of anaerobic bacteria in such a reducing environment are known to play a crucial role in the formation of non-crystalline U(IV) minerals (Bhattacharyya et al., 2017). Uranium reduction using bacteria have been extensively studied (Lovley et al., 1991; Mays, 1994; Ganesh et al., 1997; Wan et al., 2005) and viewed as an important mechanism for sequestering environmental U and accumulation of economical important U deposit in some parts of the United States (e.g. U ore deposits in Colorado and Wyoming) (Wall & Krumholz, 2006). The feasibility of microbial reduction by bacteria in groundwater and sediments have been demonstrated by several laboratory-based experiments (Uhrie et al., 1996; Abdelouas et al., 1998a; Elias et al., 2003; Ortiz-Bernad et al., 2004; Gu et al., 2005). These studies concluded that naturally-occurring bacteria present in groundwater and aquifer sediments are capable of reducing U, but the groundwater and the aquifer sediments are mostly limited by readily-available electron donors.

Thus, addition of electron donors (e.g. ethanol, molasses, tryptone, acetate) to the groundwater will increase the growth of bacteria and that will enhance bioreduction.

Recent studies have provided further evidence of UO_2 (uraninite) formation as a result of reduction of U(VI) by sulfide (Barnes & Cochran, 1993; Beyenal et al., 2004; Hua et al., 2006). Beyenal et al. (2004) demonstrated that in the absence of bicarbonate in a continuous flow system both enzymatic and chemical reduction of U can be achieved using sulfide. Hua et al. (2006) also demonstrated U reduction using hydrogen sulfide to produce uraninite. Hua et al. (2006) again noted that the kinetics of U reduction is highly controlled by pH and carbonate concentration. Uranium reduction with sulfide minerals has also been reported to yield U_3O_8 (pitchblende) (Wersin et al., 1994; Moyes et al., 2000; Livens et al., 2004; Hua et al., 2006). Hua et al. (2006) proposed the following equation for the reduction of U(VI) to pitchblende:

$$12UO_2(CO_3)_3^{4-} + HS^- + 47H^+ \rightarrow 4U_3O_8 + SO_4^{2-} + 36CO_2 + 24H_2O \quad (4)$$

Reduction processes have also proven effective in precipitating reduced U minerals from oxidised solutions. Uranium reduction using hydrogen sulfide and organic matter have been observed and compared to U adsorption on organic matter and minerals surfaces (Nash et al., 1981). Swanson (1956) proposed that both adsorption and reduction by organic matter are responsible for U deposit in black shales (e.g. New Albany shales of USA) as higher U content correlate with higher organic matter and the presence of pyrite (form from reduction of sulfate by organic matter) in close associated with U confirms reduction processes.

Equilibrium speciation models mostly predict uranyl-carbonate complexes as the dominant U(VI) aqueous species in U-bearing groundwater containing carbonates minerals (Clark et al., 1995; Abdelouas et al., 1998b). In the presence of Ca, ternary Ca-uranyl-carbonates complexes are reported to dominate over other carbonate complexes (Abdelouas et al., 1998b; Neiss et al., 2007). An example is shown in a groundwater study from Tuba City, AZ, U Mill Tailing Remedial Action (UMTRA) site. The study results reveal that in groundwater that did not contain Ca, the U(VI) species distribution was 56% $UO_2(CO_3)_2^{2-}$ and 38% $UO_2(CO_3)_3^{4-}$. Recalculating the species distribution with the addition of Ca and the same water composition resulted in the formation of both $Ca_2UO_2(CO_3)_3$ and $CaUO_2(CO_3)_3^{2-}$ accounting for 99.3% and 0.3% respectively of the total dissolved species while $UO_2(CO_3)_2^{2-}$ and $UO_2(CO_3)_3^{4-}$ both accounted for less than 0.4% of the

dissolved U species (Abdelouas et al., 1998b). The formation of ternary Ca-uranyl-carbonates complexes has been reported to decrease the rate of biotic reduction of U(VI) (Brooks et al., 2003; Neiss et al., 2007). Brooks et al. (2003) demonstrated that in the presence of Ca in mM concentrations (0.45-5 mM) the rate and extent of biotic U reduction by both facultative (*Shewanella putrefaciens*) and obligate (*Desulfovibrio desulfuricans*, *Geobacter sulfurreducens*) anaerobic bacteria decreases. A reduction study by Neiss et al. (2007) using *Shewanella putrefaciens* within a packed mineral column containing U, Ca, and ferrihydrite-coated quartz sand concluded that in the absence of Ca, uranyl-carbonate complexes dominate and U reduction occurs but when Ca was added to the system, U reduction is inhibited due the formation of Ca-uranyl-carbonates complexes (Neiss et al., 2007). Thus the presence of Ca in groundwater can have a profound effect on U reduction. Thermodynamic calculation and experimental results have demonstrated U(VI) reduction by soluble Fe (II) as a function of pH (Du et al., 2011). Du et al. (2011) reported that in a system containing soluble Fe (II) and U, reduction of U(VI) occurs only at pH greater than 5.4.

1.2.4 Adsorption processes

Sorption processes have also been reported to offer important controls on the concentrations of many radionuclide including U (Moyes et al., 2000; Waite et al., 2000; Giammar & Hering, 2001) The presence of clay and hydrous metal oxide in groundwater provide surfaces for sorption of metals and other contaminants (Han et al., 2007). Sorption is pH dependant thus Vivo et al. (1984) proposed that U sorption should follow reduction of U(VI) to U(IV). If reduction does not occur, there may be remobilization following changes in the groundwater pH and Eh.

The adsorption of U(VI) on different iron oxides has been extensively documented (Murphy et al., 1999; Giammar & Hering, 2001; Wazne et al., 2003). Fe minerals have highly reactive surfaces that can greatly influence U adsorption. Uranium adsorption on iron oxyhydroxides is highly pH dependent and also depend on carbonate concentrations in waters containing carbonates minerals (Wazne et al., 2003). Moyes et al. (2000) reported that U uptake by iron oxyhydroxides (goethite, lepidocrocite) is by surface complexation and stops when their surfaces get saturated. Uranium uptake by ferrihydrite is reported to increase with increasing concentrations of ferrihydrite but the uptake decreases in the presence of carbonate due the increased pH and the formation of uranyl-

carbonate complexes (Um et al., 2008). Uranyl-carbonate complexes form negatively-($UO_2(CO_3)_2^{2-}$ and neutrally (UO_2CO_3) charged ions thus making it difficult for the complexes to adhere to the surfaces of negatively-charged iron oxyhydroxides (Ho & Miller, 1986; Geipel et al., 1998). Modelling experiments using goethite [α-FeO(OH)] and kaolinite [$Al_2Si_2O_5(OH)_4$] show kaolinite dominating U adsorption at pH<4 and goethite at pH > 6 (Dong et al., 2011). The adsorption of U onto goethite was reported to be strongly dependant on pH. Below pH 4 and at total iron concentration of 3.15×10^{-4} almost all the U(VI) was found to remain in solution but the adsorption increased sharply between pH 4-6 with more than 99% of U(VI) adsorption above pH 6 (Cheng et al., 2004).

Phosphates are important minerals that can play a role in sequestering metals and radionuclides (Wright et al., 2011). In a system containing U and iron oxides, phosphate may compete with U(VI) for surface site of iron oxide or may form complexes with U(VI) thereby decreasing U(VI) adsorption (Bachmaf et al., 2008). The formation of uranyl-phosphate complexes in oxidizing surfaces and groundwater containing phosphate are expected to occurs at pH 4 -7 and $PCO_2 = 10^{-2}$, such complexes enhance U transport (Langmuir, 1978). Cheng et al. (2004) studied the effect of phosphate on U(VI) adsorption to goethite-coated sand and reported an increase in U(VI) adsorption using the following parameters: pH 4–6, total iron concentration 3.15×10^{-4} M, and phosphate 5×10^{-5} M. The increase was due to the formation of ternary surface complex ($FePO_4UO_2$); the likely dominant surface species at these pHs. They added that at high pH (> 8.5) the formation of soluble U phosphate complex at the same concentrations of phosphate and iron will decrease the adsorption of U(VI) onto goethite.

Clay minerals possess several features (e.g. high surface area and layered structure) that are useful for adsorbing environmental contaminants. Uranium (VI) adsorption on bentonite and montmorillonite has been reported to be high at a low total U(VI) concentration. The adsorption was attributed to the fact that at low U concentration, sorption occurs at the most energetically favorably sites but at high U concentration the favourable sites are fully occupied, hence sorption is weaker (Pabalan et al., 1996; Hyun et al., 2001; Bachmaf et al., 2008). Bachmaf et al. (2008) reported that U(VI) sorption on bentonite depends on pH, U(VI) concentration, presence of carbonate, phosphate and sulfate concentrations. At pH less than 6, and in the presence of 0.005 M of sulfate, U(VI) sorption on bentonite is limited due to competition between sulfate and uranyl

ion for surface site of bentonite or due to the formation of uranyl-sulfate complexes. This has also been observed using montmorillonite (Pabalan et al., 1996). The sorption of U(VI) on montmorillonite have been reported to be controlled by ion exchange process and surface complexation all of which are dependent on pH and ionic strength.

1.2.5 Biogeochemistry of uranium deposits

A type of U deposit that has provided strong evidence about the importance of reduction in U solubility is observed in roll front deposit (Figure 1-2). Roll front deposits (typically found in arkosic sandstone) are believed to form from meteoric water (approximate equilibrium with atmosphere) in reduced zones with low Eh following oxygen consumption by iron sulfide minerals and generation of kinetically active sulfur minerals that are capable of reducing U (Granger & Warren, 1979). Roll fronts are typically found at a location of an abrupt change in redox condition (Harshman & Adams, 1981). On the up-gradient side of the aquifer, the host sandstone is greenish-yellow to orange in color with low organic matter, low pyrite and more ferric than ferrous iron minerals. The colour may be due to oxidation of pyrite to other forms of iron oxides (e.g. hematite). On the down-gradient side, the host sandstone is light to gray in color and contain pyrite, organic matter and more ferrous than ferric iron minerals. The ore region normally lies at the boundary between the altered and unaltered zone of the sandstone (Harshman & Adams, 1981; Spirakis, 1996).

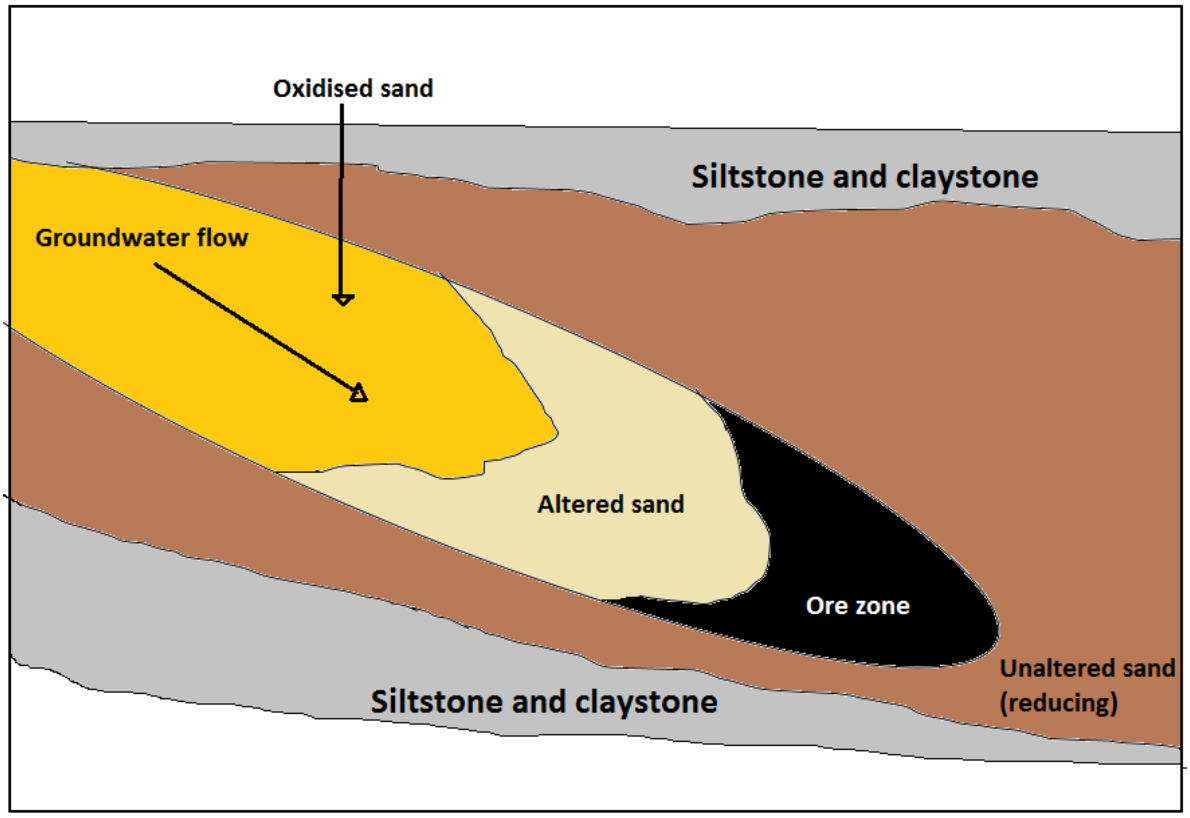

Figure 1-2: Model of a roll front U deposit after Harshman and Adams (1981).

There is a general agreement on the concept of migration of a redox front leading to the deposition of U but there still remain some disagreement on the redox processes involved (Dahlkamp, 2010). Granger and Warren (1969) reported that inorganic chemical reactions without bacterial influence are the main processes influencing the migration and deposition of U and other minerals along the roll front. They postulated that the oxidation of pyrite at the roll front is influenced by the presence of mineralised solution (oxygenated water) which in the case of insufficient oxygen results in the partial oxidation of the sulfide minerals. These partially-oxidised minerals produce soluble, metastable sulfur species (e.g. sulfite and thiosulfate) that are carried down gradient by the mineralised solution into reducing zones where they eventually undergo disproportionation; a reaction that disintegrates the sulfur species into equivalent amount of reduced species (e.g. H_2S) and oxidised species (e.g. SO_4^{2-}). The reduced S species can bind to Fe(II) minerals forming Fe(II) sulfide minerals that are capable of reducing and precipitating U minerals.

Other studies have also highlighted the importance of biological processes that are involved in U deposition (Rackley, 1972; Harshman & Adams, 1981; Shchetochkin & Kislyakov, 1993). Rackley (1972) hypothesised that biogenic processes associated with U mineral deposition are influenced by two distinct groups of bacteria that function in different pH and Eh environment and are separated from one another by a redox boundary. On the oxidized part of the roll front, aerobic bacterial such as *Thiobacillus ferrooxidans* and related bacterial are believed to be active. They can survive a pH as low as zero; their optimum pH is 2 - 4. They derive energy from sulfur, iron, nitrogen compounds and hydrogen, and produce high Eh conditions (up to +760 mV). The catalytic activity of this bacteria greatly increases the rate of oxidation of pyrite; here the oxidation is 200x faster than with atmospheric oxygen. Three main reactions are believed to occur in this zone (Figure 1-3). First is a reaction of pyrite, ferric sulfate and water to produce ferrous sulfate and sulfuric acid, followed by a biochemical oxidation (by *Thiobacillus*) of the ferrous sulfate and sulfuric acid to produce more ferric sulfate which can be further used to oxidised other pyrite. The final step involves hydrolysis of the ferric sulfate to produce ferric hydroxide and sulfuric acid. Excess sulfate from the system is carried to the reduced side of the roll front deposit.

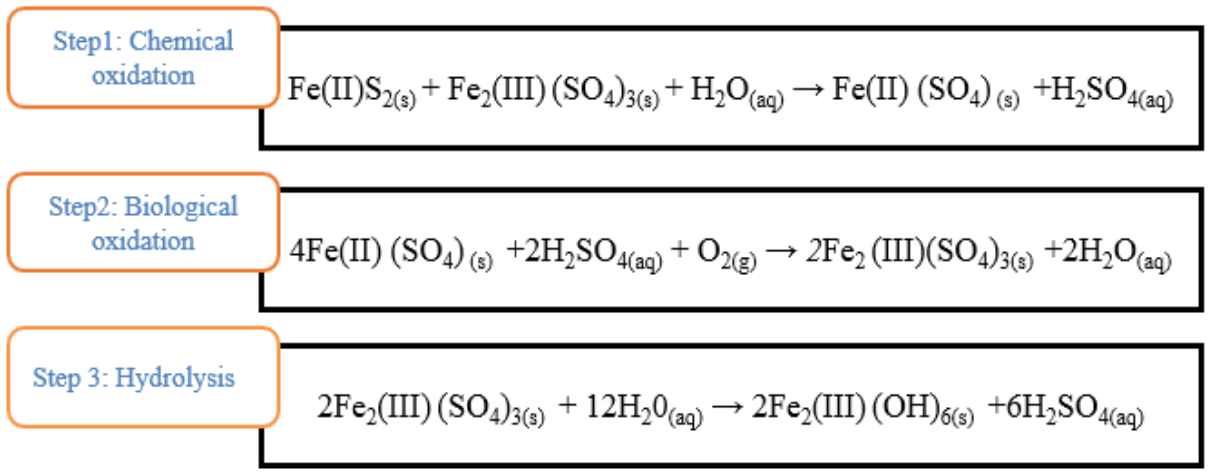

Figure 1-3: Probable reactions occurring in the oxidizing zone during U deposition.

On the reduced side, it has been hypothesized that sulfate-reducing bacteria such as *Desulfovibrio* govern the biogeochemistry. They are strict anaerobes and rely on organic matter for energy. Their optimal pH conditions for growth are from 7.8 - 8.4, and they require Eh conditions on the order of -200 mV. They produce hydrogen sulfide in the reduced zone through anaerobic respiration. The generation of hydrogen sulfide favor the formation of pyrite in the reduced zone thereby

facilitating the precipitation of insoluble U(IV) minerals and other elements associated with U deposits (Rackley, 1972; Harshman & Adams, 1981; Wall & Krumholz, 2006).

1.2.6 The Wyoming Basins

The Wyoming Basins host a roll-type (roll front) U mineral deposit; a distinctive type of U deposit found in sandstones (roll front deposits only form in permeable strata between confining layers such as shales). These sandstones are mostly fine to coarse-grained, friable and contain carbonaceous matter, pyrite, and iron stained mudstones (Dahlkamp, 2010). The U deposits found in the Wyoming Basin occur in rocks of Paleocene and Eocene age (Harshman & Adams, 1981) Sources of the U in these deposits are the granite rocks of the Sweetwater arch (Rackley, 1972) and the intraformational tuffaceous sediments of the White River Formation; this was determined by examining the geochemistry and the hydrochemistry of the groundwater flowing through the deposits (Dahlkamp, 2010). Other sources may include volcanic ashes, where the U is mobilized by oxygenated rainwater dissolving the U and carrying it down into sandstone outcrops; this rainwater containing the dissolved U will continue deep in the sandstone deposit until it reaches reducing conditions where the U will be precipitated (Freeman & Stover, 1999). Weathering and erosion of the granite in the early Eocene time may have cause the release of U into the vadose zone and subsequently transported by groundwater and deposited in a favourable host sediment (Dahlkamp, 2010).

The main U-bearing minerals found in Wyoming roll-front deposits include uraninite, and coffinite. Other secondary minerals present include autunite, carnotite, tyuyamunite, metaautunite, schroeckingerite, and uranophane (Page et al., 1956; Stewart et al., 2000; Dahlkamp, 2010) (Table 1-1).

Table 1-1: Uranium-bearing minerals, their chemical formulae and their oxidation state in the Wyoming Basin.

Minerals	**Chemical formulae**	**Oxidation state**
Uraninite	UO_2	+4
Coffinite	$USiO_4$	+4
Autunite	$Ca(UO_2)_2(PO_4)_2 \cdot 10\text{-}12H_2O$	+6
Carnotite	$K_2(UO_2)_2(VO_4)_2 \cdot 3H_2O$	+6
Tyuyamunite	$Ca(UO_2)_2(VO_4)_2 \cdot 5\text{-}8H_2O$	+6
Uranophane	$Ca(UO_2)_2(SiO_3OH)_2 \cdot 5H_2O$	+6
Schroeckingerite	$NaCa_3(UO_2)(CO_3)_3(SO_4)F \cdot 10H_2O$	+6

Uraninite and coffinite are reported to be the principal U minerals that are found in the Wyoming roll front deposit. They replace organic matter in sandstone by filling voids and sometimes are found to coat grains of sandstones (Dahlkamp, 2010). Uranium minerals in the Wyoming Basin are accompanied by several other elements (e.g. selenium, molybdenum, vanadium, carbon, sulfur, calcium, arsenic, phosphorus, and copper) that have biogeochemical importance. Some of these elements are of concern toxicologically because of their known effect on human health. The deposits are composed of mainly U-V minerals, U-silicates, U-phosphates, and carbonates. This composition varies depending on the location of the ore deposit; the Powder River Basin (located at the southern end of the Highland mine) contains deposits of U-V minerals on its oxidised front and mainly pitchblende and coffinite at its reduced front (Langen & Kidwell, 1974; Dahlkamp, 2010). Exposed roll front deposits at the Wyoming Basins reported by Stewart (2002) are characterised by two distinct regions separated by a well-defined mineralised redox boundary; oxidised /altered side and reduced /unaltered side On the oxidised side, groundwater carries mobile U(VI) until it encounters the reduced side where precipitation of insoluble U(IV) occurs. This explains the presence of calcite, pyrite and high U concentrations in the reduced side as compared to the oxidised side where there are iron oxides (including goethite and haematite), low calcite and low U concentrations (Langen & Kidwell, 1974; Stewart, 2002).

In the southern Powder River Basin (Figure 1-4), the principal host rocks for U mineralization are the Wasatch Formation and the arenites of the Upper Fort Union Formation (Page et al., 1956; Dahlkamp, 2010). The Wasatch Formation is of Eocene age and has varied thicknesses of 300 -

500 m from north to south. It consists of silicates beds, siltstones, coaly shale, lignite and claystone inter-bedded with irregular-spaced coarse- to fine-grained sandstone lenses. Uranium deposits are observed at the centre part of the Wasatch outcrop where the lenses of the sandstone are red. The sandstones are friable and brittle, with horizons separated by claystones and siltstones. On the other hand, the Upper Fort Union arenites have a thickness of about 900 m are composed of mainly fluvial and poorly sorted coarse-grained sandstone that are in a form of a wedge (Stout & Stover, 1997).

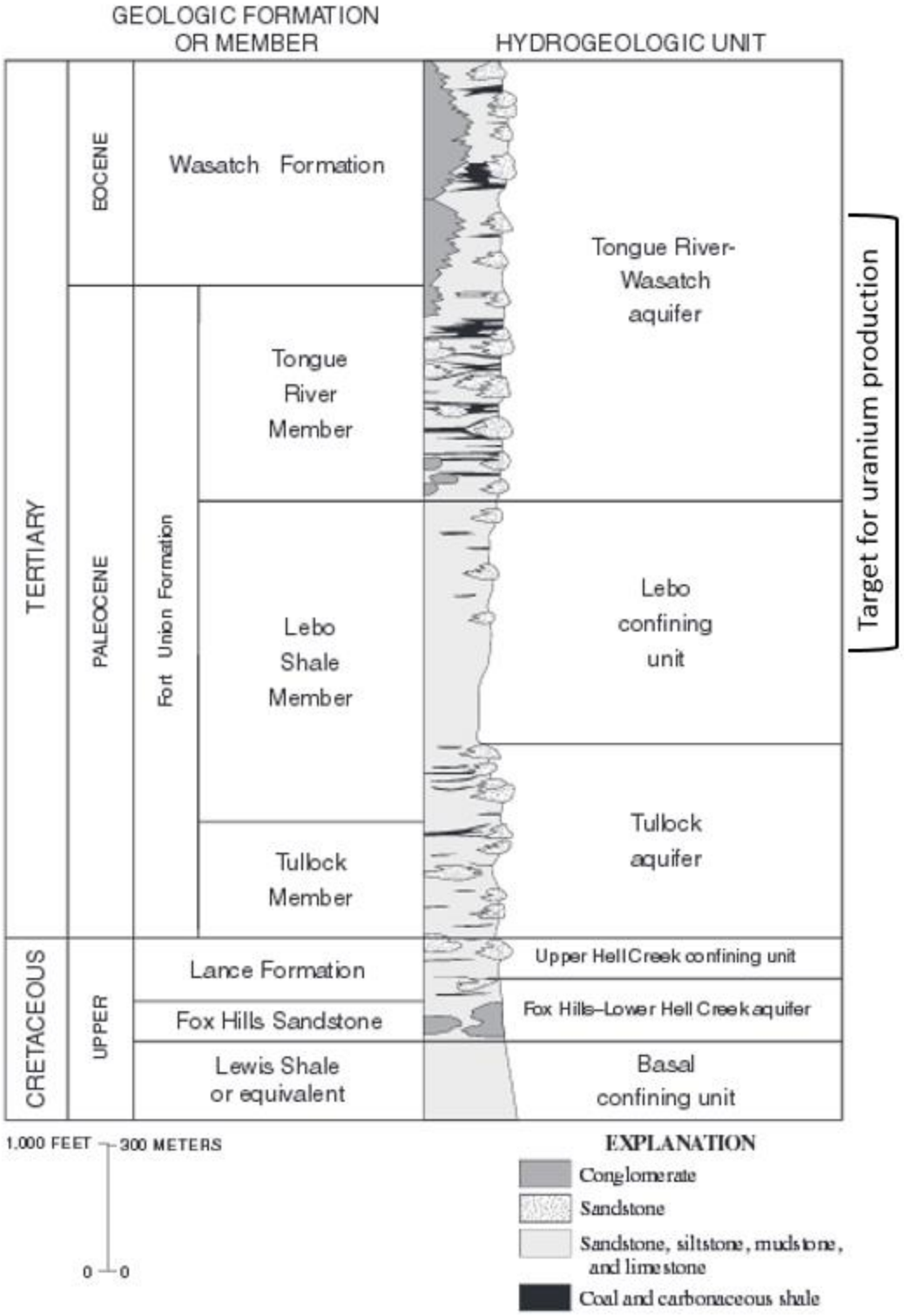

Figure 1-4: Stratigraphic column of Tertiary and Upper Cretaceous Formations in the Southern Powder River, Wyoming. Adapted from Hinaman (2005).

1.2.7 In situ recovery mining

In situ recovery mining is one of the mining processes used to recover U. It is used in some parts of the world including Kazakhstan, Uzbekistan, Australia, and the United States to recover low grade (about 0.1% of U by weight) U deposit in sandstones (Fox, 2014). It currently contributes 48% of the world's U production (IAEA, 2001). It has an advantage over other processes (open pit and underground mining) as it does not require removal of overburden rocks (Figure 1-5A and 1-5B). It causes minimum distortion of the hydrogeological system around the ore deposit and poses considerably less radiation hazard. It is a low cost recovery process and has environmental advantages especially at sites where alkaline leaching is used. In situ recovery mining produces no tailings, and no waste rock. This mining technique depends on the porosity and the permeability of the ore body to the solution used for the dissolution (Stewart, 2002).

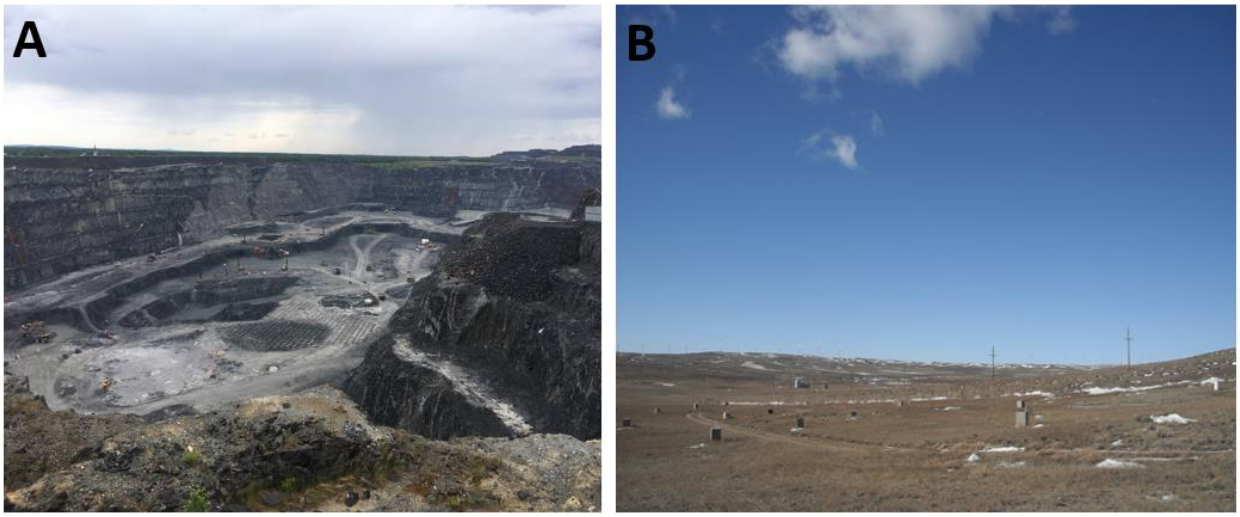

Figure 1-5: Images showing the visual difference between (A) open pit mine gold mine (B) ISR U mine (Smith Ranch-Highland Mine). Photos by J. McBeth.

An ISR mining mine unit contains wellfields (a pattern of injection and production well, Figure 1-6) over a uranium orebody. A wellfield consists of injection wells that are used to inject barren solution (solution containing oxidant and complexing agent) into the ore body, and a production well to pump U-rich solution to the surface where the U will be recovered by an ion exchange process (Frank, 1954; Stewart, 2002). Wellfield patterns are site specific and also depend on factors such as permeability and thickness of the host sand, type of deposit and the geometry of the deposit (Pelizza & Bartels, 2016). In places like Kazakhstan where sheet-like U deposit exist, the distance between an injection well and a production well is typically 50 to 60 m, thus the time

taken to recover U is longer compared to wellfields pattern that has a 20 to 30 m distance between a production and an injection well (World Nuclear Association, Last updated; September, 2016). An important factor governing the distance between wells is the time it takes for the oxidant to react with the uranium in the groundwater. In Kazakhstan, the oxidant is often naturally-occurring ferric iron sometimes supplemented with hydrogen peroxide. In North America, the oxidant is usually dissolved oxygen, which has a much shorter half-life and thus requires more closely-spaced wells (J. Clay, personal communication). A five spot wellfield (Figure 1-6) at the Smith Ranch-Highlands Mine has a distance of 20 - 30 m between the production and the injection wells and a typical flow rate of 126 -189 L/s (Freeman & Stover, 1999). To prevent the rich solution containing U and other dissolve metals from escaping the mine zone into adjacent aquifers, a higher extraction rate and a lower injection rate is maintained; resulting in excess water called 'bleed'. This process creates a cone of depression that ensures that the U-rich solution remains within the wellfield (Gallegos et al., 2015a).

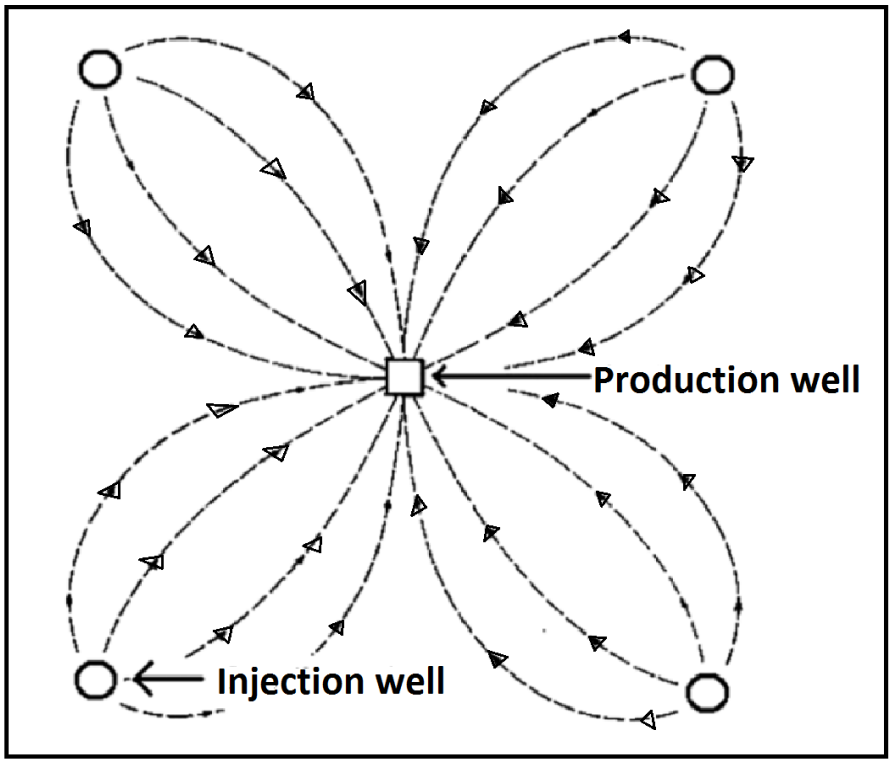

Figure 1-6: Typical wellfield pattern used in ISR mining. Prepared after Power Resources Inc. (2000).

The ISR process starts with native groundwater mixed with oxidant (e.g. oxygen gas, hydrogen peroxide) and carbonates (CO_2 or $NaHCO_3$) to form a solution called a lixiviant. The lixiviant is then pumped into the U ore bearing sandstone through a series of injection wells which then travels through the ore body. As the lixiviant moves through the ore body, the oxidant reacts to oxidise the U(IV) to U(VI), which then forms a soluble complex (uranyl dicarbonate) with the carbonate and water. The U rich solution (pregnant solution) is recovered using the production well and then passed through an ion exchanger where the U is extracted from the pregnant solution and the remaining groundwater from the ion exchanger is re-fortified with oxidants and carbonates and reinjected in to the ground. The flow path is essentially a closed loop save for a slight "bleed" (typically about 1% or less of the total flow) skimmed off and disposed of to ensure that fortified mining water (lixiviate) does not move horizontally out of the mining zone (Mays, 1992; Edwards & Oliver, 2000; Borch et al., 2012; WoldeGabriel et al., 2014). Figure 1-7 shows an overview of the ISR mining process. The ion exchange method uses a resin bed; when the resin bed is fully saturated with U it is flushed with strong acid or chloride solution to release U into solution. The U is then precipitated by the addition of ammonia, hydrogen peroxide, or caustic soda, and dried to make a variety of different U oxides (e.g U_3O_8, UO_3) depending on the temperature of the oven (Merritt, 1971). The process of injection, pumping and recovery will continue for several months and even years until the U concentration gets to a level where recovery is no longer economically feasible.

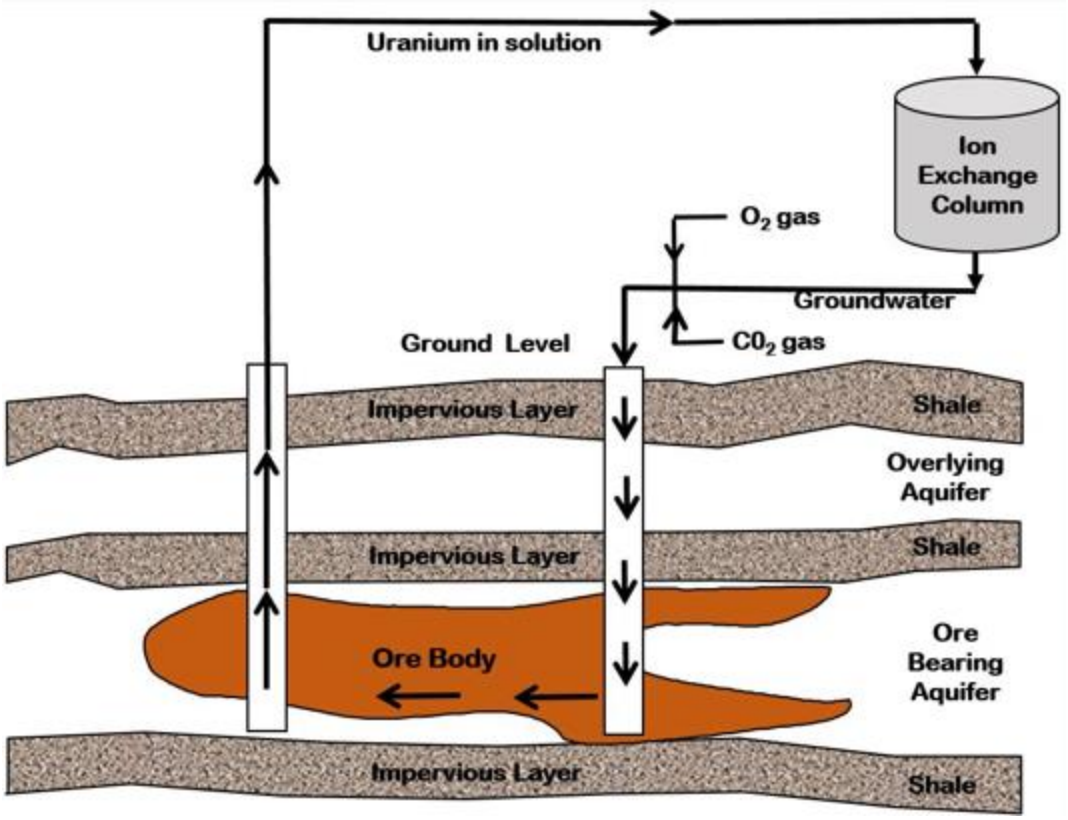

Figure 1-7: Schematic of ISR mining process. Modified from Stewart (2002).

1.2.8 Reclamation methods

After U mining, a major challenge for the mining companies is to return the mine site to pre-existing conditions or to a composition that is reasonably close to the pre-mining condition. Reclamation entails ensuring groundwater contaminants are close to the concentrations that were present before mining. Current reclamation practices at the Smith Ranch Highlands Mine include the use of groundwater flush, reverse osmosis, and the application of a chemical reducing agent. Natural attenuation and bioremediation (using naturally-occurring bacteria) methods for restoring ISR mine sites are also becoming more popular and well accepted (Hall, 2009; Borch et al., 2012). The choice of treatment options depends on factors present at the site of interest, for example, the level of restoration required by regulators, aridity of the site (i.e. water availability), and cost of chemicals.

Groundwater flush involves pumping contaminated groundwater and disposing of it or treating it as waste. This contaminated water is then replaced by groundwater from surrounding aquifers that flows through the pore spaces. Groundwater flushing alone may be insufficient and expensive as

it requires removal of large volumes of pore water from the ore formation. Furthermore, groundwater flushing may introduce oxic condition from up-gradient groundwater that enters the ore zone, making it difficult to establish reducing conditions that may be useful in immobilizing U (Gallegos et al., 2015a).

During ISR mining, the groundwater acquires ions from the rich lixiviant containing U and these ions may bind to soil surfaces present in the aquifer. During restoration, clean surrounding groundwater introduces lower concentrations of ions causing exchange of ions off the soil surfaces into the water. This increases the concentration of ions of the water as it moves towards the pumping well; thus assisting with the restoration of the aquifers (Mays, 1994; Hall, 2009).

During reclamation, companies will sometimes follow groundwater flush with reverse osmosis. Here, the contaminated groundwater is filtered, and its pH lowered to prevent precipitation of carbonates which can plug the filtration membrane (ion filter). The pressure of the contaminated groundwater is then raised and forced through the membrane leaving behind a brine solution. This brine solution is disposed of and the treated water reinjected into the wellfields. A database obtained from ISR mining in Texas which uses groundwater flush and reverse osmosis techniques for treating mined aquifers have shown better results when the two techniques are coupled together (Hall, 2009). Using groundwater flush alone, U concentration from an ISR in Texas were reported to be 2109 % of the baseline. With the combination of groundwater flush and reverse osmosis, the value was reduced to 48 % of the baseline. Other elements of interest present in the groundwater include selenium, cadmium, arsenic, lead and molybdenum. These elements showed similar trend as the U, thus emphasising the importance of coupling the two techniques (Hall, 2009).

Reverse osmosis may be accompanied by addition of chemical reductants which are mostly sulfur-based compounds (e.g. sodium sulfide, sodium thiosulfate). These chemical reductants are added to the treated water from the reverse osmosis unit before reinjecting. The chemical reductants act to prevent further oxidation and encourage precipitation of contaminants (Borch et al., 2012). Bioremediation processes involve stimulating naturally occurring bacterial and other microbes to reduce mobile U(VI) to an immobile U(IV) and to precipitate other contaminants. This process involves the use of electron donors such as lactate, ethanol methanol, molasses, peptone, hydrogen, and/or acetate. The ideal of using bioremediation in environments containing U was first proposed by Lovley et al. (1991) when they showed that reduced immobile U, a form of uraninite can be

produced through the use of microorganisms. Bioremediation has also been recorded to be the most cost effective technique compared to other available techniques including recirculation of groundwater (Quinton et al., 1997). The bioremediation process requires many naturally-occurring microorganisms to mediate the transformation of U(VI) to U(IV) under anaerobic condition. These microorganisms include iron (III)-reducing bacteria (e.g. *Shewanella*, *Geobacter* sp.) and sulfate-reducing bacteria (e.g. *Desulfovibrio* sp.). Moreover, maintenance of such reducing microbial communities have been reported to be a complex phenomenon as other processes like subsurface heterogeneity (which affects electron donor delivery) and geochemical processes (affecting U(VI) partitioning) influence the microbes. Ecological interactions among microbial populations (e.g. competition among microbes that reduce U(VI) and those that do not, e.g. methanogens and iron-reducing bacteria) is another reason accounting for the complexity in maintaining microbial populations.(Lovley et al., 1991; Ganesh et al., 1997; Wei-min et al., 2006). In addition, oxidation of bioreduced U(IV) to U(VI) have also been reported to occur in the presence of calcium, bicarbonate and some *Geobacter* species (Wan et al., 2005).

1.2.9 Solid phase analysis of uranium ore

Uranium-bearing ores have been studied using a variety of analytical and spectroscopy techniques including the use high energy synchrotron techniques (Brandes et al., 2008; Larson, 2008; Susini, 2008; Stewart et al., 2010; Borch et al., 2012). The following are techniques employed in the present work. Powder X-Ray Diffraction is a powerful tool used to characterise the crystal structures of materials. Each mineral possesses a characteristic X-ray diffraction pattern than can be matched against a database of recorded phases. Powder X-Ray Diffraction data is produced when a beam is projected onto a sample at an angle. This produces peaks in the diffraction pattern which can be used as a "fingerprint" to identify the mineral phases present. Powder X-Ray Diffraction is only helpful in characterising crystalline mineral, thus minerals with disordered structures are difficult to characterise with this method. Potential sources of beam (X-rays) include filament X-ray tubes or a synchrotron. Powder X-Ray Diffraction has been applied extensively in studying mineral phases in U bearing ores and tailing (Reynolds et al., 2010; Gomez et al., 2013). The detection limit for U minerals using PXRD is typically 2-3 % w/w but it can be as low as 0.5% w/w (Gallegos et al., 2015b). WoldeGabriel et al. (2014) used PXRD to study post-ISR sample from the Smith Ranch-Highlands Mine Unit 4 and reported the presence of quartz, K-feldspar,

albite and some secondary minerals including pyrite, kaolinite and calcite. Reynolds et al. (2010) compared synchrotron PXRD to standard Cu source PXRD and found an improvement in the spatial resolution and intensity of the synchrotron data as compared to standard Cu source data.

Synchrotron X-Ray Absorption spectroscopy (XAS) is another technique that can be used to determine the local and electronic structures of elements. It is also useful in identifying chemical forms of elements; which is key in determining elements' toxicity and stability. X-Ray absorption spectroscopy is sensitive to the oxidation state of elements especially in the pre-edge region (Schnohr & Ridgway, 2015). This technique have been used widely in studying several elements that are relevant to U mine reclamation e.g. C, Fe, S, U, and P (Haberstroh et al., 2006; Brandes et al., 2008; Essilfie-Dughan et al., 2012). Neiss et al. (2007) employed U L_3-edge XANES to study the effect of Ca in U speciation and mobility. Beyenal et al. (2004) confirmed chemical and enzymatic reduction of U(VI) to U(IV) mineral uraninite using U L_3-edge XANES. Sulfur speciation using XANES in a naturally S-enriched lake sediment have been reported to have absorption peak near the 2470-2473 eV region, which represent reduced S species (e.g. pyrite, thiol) and another absorption peak near 2480-2487 eV region representing oxidised S species example of which include sulfonate and or sulfate (Zeng et al., 2013).

Micro-X-ray fluorescence (μXRF) mapping is another powerful technique used to probe the spatial distribution of elements (major and trace) in heterogeneous sample such as ores and mine tailings. Micron-scale heterogeneities in elemental speciation have been studied for some geological materials including U using μXRF maps (Womble et al., 2013). The technique is based on the use of X-rays to excite electrons in elements and induce emission of characteristic fluorescence X-rays from the sample for elemental analysis. Micro-X-ray fluorescence mapping provides 2D quantitative maps for elemental concentrations with minimal sample preparation. This technique is important in understanding the distribution of U and other elements e.g. Fe, V, Ca on a microscale level and the extent to which U distribution correlates with the distribution of other elements (Womble et al., 2013) .

To study micro-scale morphology and chemical composition of small crystalline minerals Scanning Electron Microscope (SEM) and Electron Microprobe Analysis (EMPA) can be used. The SEM is an instrument used to image samples at the micro to nanometer scale. It produces images by rastering a focused beam of electrons over a sample to produce signals which are

registered on a detector. The secondary electron mode of the SEM provide a close look at the morphology and the texture of the surface coatings of the ore (Tsui, 1984). Electron Microprobe Analysis on the other hand is a useful technique used to map elemental distribution over selected areas of solid samples. The EMPA technique uses a focused beam of electron to cause X-ray emission from samples. Electron Microprobe Analysis is fundamentally the same as SEM but it has an added advantage of producing precise quantitative elemental analysis at a very small spot size thanks to its energy-dispersive spectroscopy capabilities. Backscatter electron mode is available for both SEM and EMPA and provides Backscattered Electron Images (BEI). The brightness of features in these images are associated with the average atomic number of the elements in the sample. Regions of images containing elements with heavier atomic number (e.g. U) appear brighter than regions of images with only elements having lighter atomic numbers, this helps in rapid identification of disseminated mineral particles. Energy dispersive spectrometer (EDS) makes it possible for qualitative determination of elemental distribution over a sample. EMPA also have options for X-ray maps which give the location of specific elements within an area of interest. Electron Microprobe Analysis and SEM have been used in several works to study U ore samples from different locations (Stewart, 2002; Stefaniak et al., 2009; Maehata et al., 2011).

1.2.10 Modelling

Restoration of a groundwater aquifer after mining is accomplished using groundwater flush, reverse osmosis and in some cases a chemical reductant may be added to the mined-out wellfields to reduce the oxidizing conditions created in the ore zone during the mining process. Developing models to explain how the various reclamation methods may affect U availability and mobility in groundwater are important in planning restoration strategies. Modelling is a valuable tool that can be used in predicting long-term behaviour of contaminants in groundwater (Merkel, 2008). It can also help explain geochemical processes occurring in laboratory experiments and field data. Modelling offers a cheap, and non-intrusive approach for obtaining insight into the sensitivities of the different approaches used in mine site reclamation.

Geochemical modelling is a predictive tool that can be used to optimise remediation efforts. It is based on the principles of mass conservation (mass can neither be created nor destroyed but can be converted from one form to another). It is useful in interpreting and predicting long-term behaviour of geochemical systems which is often impossible to do in laboratory-based experiments

owning to the issues of complexity and time scale (Crawford, 1999). Geochemical modelling has been used in many works to study the adsorption of U on iron minerals (Hsi & Langmuir, 1985; Waite et al., 1994) and to predict fate of U and other contaminants in mine tailing (Morrison et al., 2002; Gómez et al., 2006; Essilfie-Dughan et al., 2013). In this work, a geochemical model will be performed using PHREEQC software using groundwater data from the field site and a modified database based on WATEQ4F embedded in the software.

2 METHODOLOGY

2.1 Project site (Smith Ranch-Highland Mine)

The Smith Ranch-Highland Mine is one of the largest U mining facilities in the United States and it produces U using the ISR mining method. It is situated in the south Powder River Basin, approximately 23 miles northwest of the City of Douglas in Converse County, Wyoming, USA (Figure 2-1). The mine is operated under the United State Nuclear Regulatory Commission license SUA-1548 (Golder Associates, 2010). The site is operated and owned by Cameco Resources Inc. The operations were formerly run separately; the Highland operations started commercial scale production in July 1987 and the Smith Ranch started in June 1997 (Golder Associates, 2010). By August 2003, the Highland and the Smith Ranch mines were operating together even though each of the sites has its own processing facility. The Smith Ranch central processing plant is now used for all U processing at the mine. The Smith Ranch-Highland Mine has an estimated proven and probable reserve of about 5.2 million pounds of U_3O_8 with an average grade of 0.09% (Cameco, 2013). The total U production was 17.6 million pounds between 2002 and 2013 with annual production capacity of 1.7 million pounds for the year 2013 (Cameco, 2013). The Smith Ranch-Highland Mine is divided into several mine units (Figure 2-2) among which is MUB, where this study was conducted.

Mine Unit B was the second mine unit developed and mined at the Smith Ranch-Highland Mine. It was formerly run by Power Resources Inc. on behalf of Cameco Resources. It is located at 43˚079" N, 105˚512" W close to the east boundary of the mine (Figure 2-2). Production at the MUB started in early 1988 after a baseline study in August 1987 using ISR mining (United States Nuclear Regulatory Commission, Last updated August 22, 2013). The mine units consist of a set of injection and production wells, which are surrounded by perimeter rings of monitoring wells to monitor U and other elements of concern. The monitoring wells are strategically placed in overlying aquifer, underlying aquifers and in the mineralised zones. The monitoring wells range from 106 - 180 m in depth. The production, injection, and the monitoring wells are completed in the Highland Sand Group, which consist of layers of sandstones separated by several meters (about 3 - 7 m) of shales and siltstones (Cameco, 2013; Cameco Resources Inc., 2013; United States Nuclear Regulatory Commission, Last updated August 22, 2013).

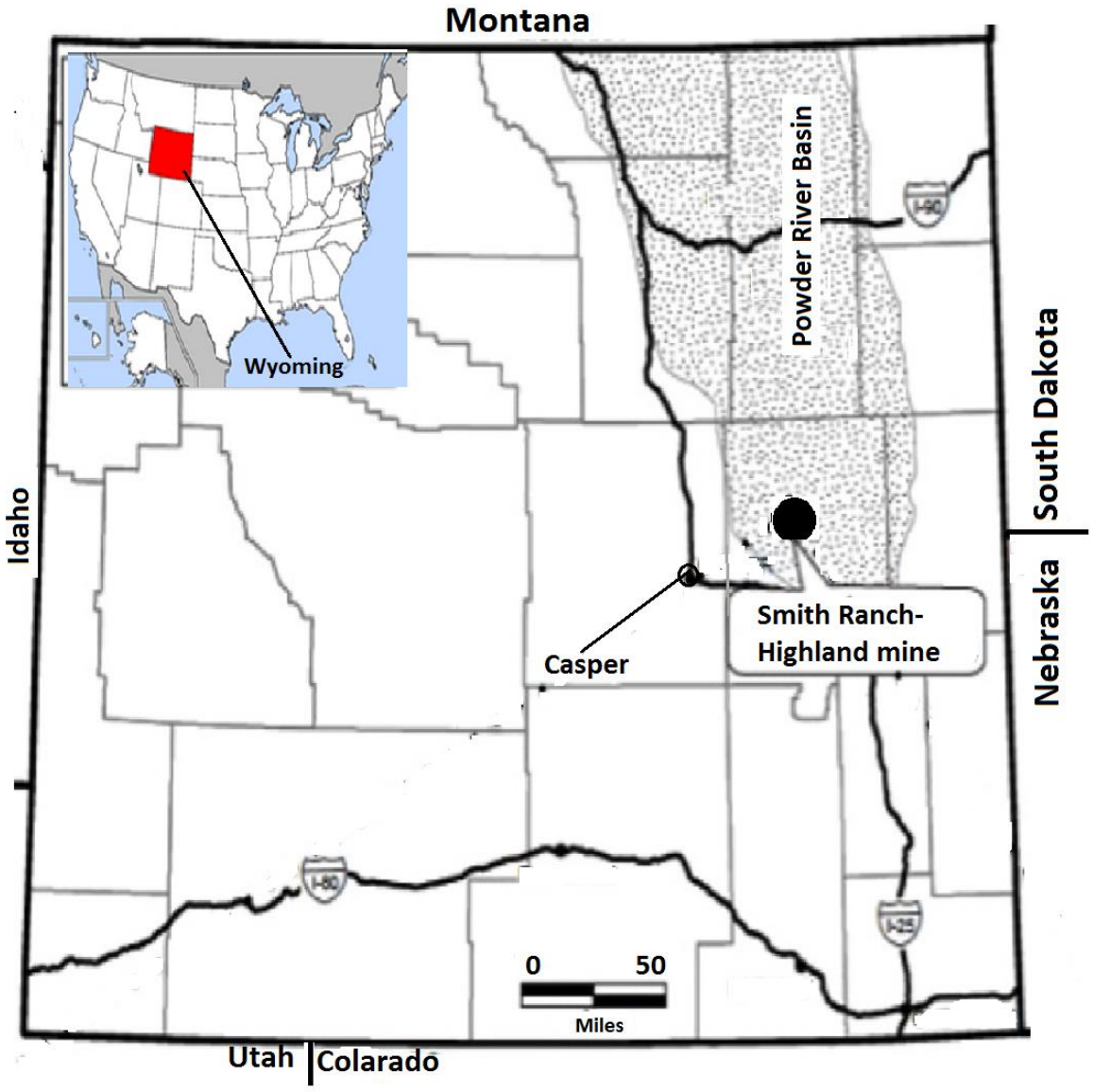

Figure 2-1: Map of Wyoming showing the Smith-Ranch Highland U operations and Powder River Basin modified from WoldeGabriel et al. (2014).

Production at the MUB continued until July 1999 when it ended and groundwater restoration started. Groundwater restoration at the site continued for about 13 years (July 1991 - June 2004), followed by a stability period of 6 months (June - December 2004) during which continuous monitoring was done to demonstrate that aquifer conditions establish at the end of restoration were stable with time. Completion of groundwater restoration was in accordance with the ISR regulations in Land Quality Division (LQD) Chapter 11, the Wyoming Department of Environmental Quality (WDEQ) LQD permit No. 603, and the WDEQ Chapter 8 Rules and

Regulations (United States Nuclear Regulatory Commission, Last updated August 22, 2013). The groundwater restoration was based on "Best Practicable Technology (BPT)", which is defined by EPA as an average of the best existing performance by well- operated plants within an industry category (EPA, Last updated December, 2016). The WDEQ analysed selected wells and approved MUB as restored in March 2008 when they confirmed that the post ISR groundwater met the criteria for "Class of Use" (i.e. Class IV (A); industrial use) after demonstrating application of BPT (Cameco Resources Inc., 2013). Even though the concentrations of some elements did not return to baseline concentrations, the demonstration of BPT includes the requirement that the restored aquifer will not degrade downstream groundwater. The NRC rejected the restoration outcome and stated that the 'class of use' standard is no longer applicable as a restoration standard for groundwater, and thus 10 CFR Part 40, Appendix A, Criteria 5C will be used. The 10 CFR Part 40, Appendix A, Criteria 5C is the code of federal regulations for domestic licensing of source materials related to operating U mills and waste disposal (United States Nuclear Regulatory Commission, Last updated January 3, 2017).

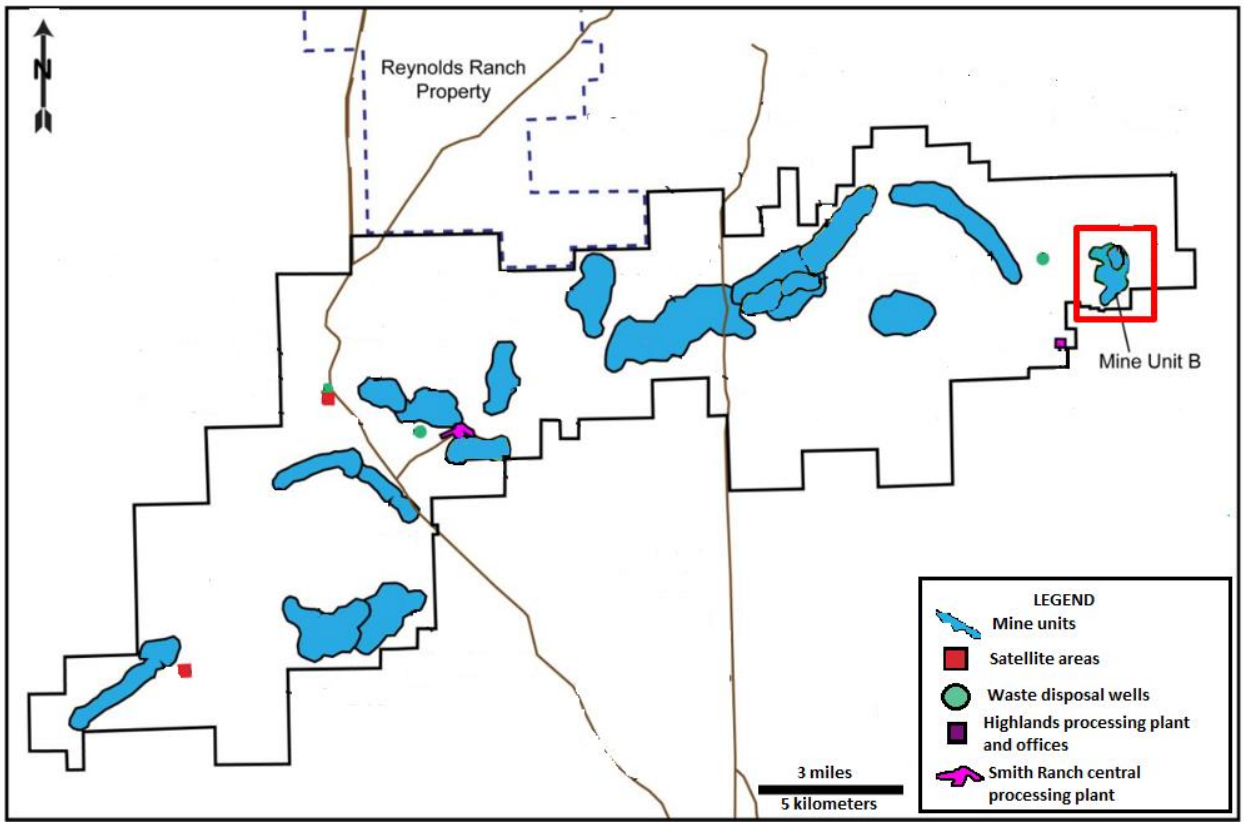

Figure 2-2: Smith Ranch–Highland U Mine Units. Modified from U.S. NRC, www.nrc.gov/info-finder/materials/uranium/licensed-facilities/is-smith-ranch.pdf

2.1.1 Geology and mineralization of the Smith Ranch-Highland Mine

The Smith Ranch and Highland Mine are situated on a roll-front U deposit and are managed as a single operation even though they have separate permits. The Highland U mine is located near the town of Glenrock, which is about 80 km north-northeast of Casper near the south end of the Powder River Basin. The U deposits are hosted in arkosic sandstones that are immature, poorly sorted and friable (Dahlkamp, 2010). The ore body is situated in 3 different sandstones (upper sand, middle sand, and lower sand) that are adjacent to each other. Each of the sandstone have a thickness of 5 - 10 m and they are separated by beds of mudstone, lignite and siltstone of about 3 - 7 m thickness (The ore body has a width of 20 - 200 m within each of the sandstones (Dahlkamp, 2010). The host sandstone (coarse grained, fluvial and poorly sorted) has good permeability and contains coaly materials. The concave side (oxidised) of the sandstone are red in color due to the presence of haematite and yellowish-brown in the ore zone due to the presence of limonite and on the front of the convex side it is grey due to the presence of pyrite-bearing minerals, organic matter, and U minerals. The predominant U-bearing minerals identified in these ores in previous studies are coffinite and lesser amounts of pitchblende. Positive mineral identification was obtained using powder X-ray diffraction (Langen & Kidwell, 1974). The U minerals are in the form of sooty layers of irregular masses (less than 10 microns thick) and they were deposited on sandstones and clays as grain coatings (Langen & Kidwell, 1974).

The Smith-Ranch portion of the mine is located 15 km west of the Highland side of the property (Figure 2-1). The area is characterised as semi-arid with rolling grassland (Freeman & Stover, 1999). Uranium deposits were exploited in the late 1970s using underground mining and open pit mining; in 1981 the mining technique was changed to ISR. The topography of the area is characterised by a rolling upland area, rounded ridge crest and broad stream valleys (Freeman & Stover, 1999). The U deposits at the Smith-Ranch mine are in tertiary strata, that is the Eocene Wasatch Formation and the Paleocene Fort Union Formation. The uppermost area of the mine (closest to the surface) consists of the Eocene Wasatch Formation; which is the youngest bedrock unit within the permit area. It is about 60 - 90 m thick in the northern and southern portions and 150 m in the central portion (Freeman & Stover, 1999; Dahlkamp, 2010). It hosts U minerals in

sandstones and has a School Coal (lignite lenses) seam at its base that forms a contact between the Wasatch and the Fort Union Formation (under layer). The Fort Union Formation has a thickness of over 300 m and hosts U mineralization of interest in arkosic sandstone within its upper 215 m. The ore body occurs as a typical oxidation-reduction roll fronts and are shaped like a crescent. The ore is believed to originate from sources that include granites from the southern part of the Powder River Basin and from volcanic ashes that were mobilised by rainwater, dissolving U as it moves down into permeable sandstone and dipping north until it reaches a reducing environment where the U was precipitated (Freeman & Stover, 1999; Norris & Drummond, 2000). The Fort Union Formation is characterised by seven sandstone horizons that alternate with shale beds and mudstones. Each of the horizon is about 3 - 60 m thick with the lower horizons containing most of the U resources (Freeman & Stover, 1999; Dahlkamp, 2010; Cameco Resources Inc., 2013).

2.2 Sample collection

Two boreholes were drilled at the Smith Ranch Highlands Site, MUB in January 2014. Eleven core samples were taken down gradient from the two bore holes (Figures 2-3 and 2-4). The drilling was performed with a diamond-tipped core barrel (0.1 m diameter). The first borehole (core 1 (MUB-N1)) was drilled between January 20th and January 21st and it extended to a depth of 165 m below ground surface. The second borehole (core 2 (MUB-S1)) was drilled between January 21st and January 22nd to a depth of 120 m below ground surface. Core samples were cut into 0.15 m sections from the two boreholes. Sections were taken throughout each borehole at 0.76 m intervals for shipment to the McBeth group at the University of Saskatchewan. Core was also sent to the Paul Reimus group (Los Alamos National Laboratory) and the Borch group (Colorado State University). Eleven 0.15 m sections of core were obtained for this project by the McBeth group. The eleven samples were chosen at regular intervals throughout the core to provide a representative sampling of the aquifer over the regions corresponding to the mined zone. The samples were vacuum-packed and shipped by Cameco in steel drums to the University of Saskatchewan via Blind River, Ontario. They arrived on April 15, 2014. Note that due to logistical challenges it was not possible to ship the samples in a refrigerated vehicle; however, the weather over the period ranged between -2.5ºC - 0ºC and prior to shipping the samples were frozen.

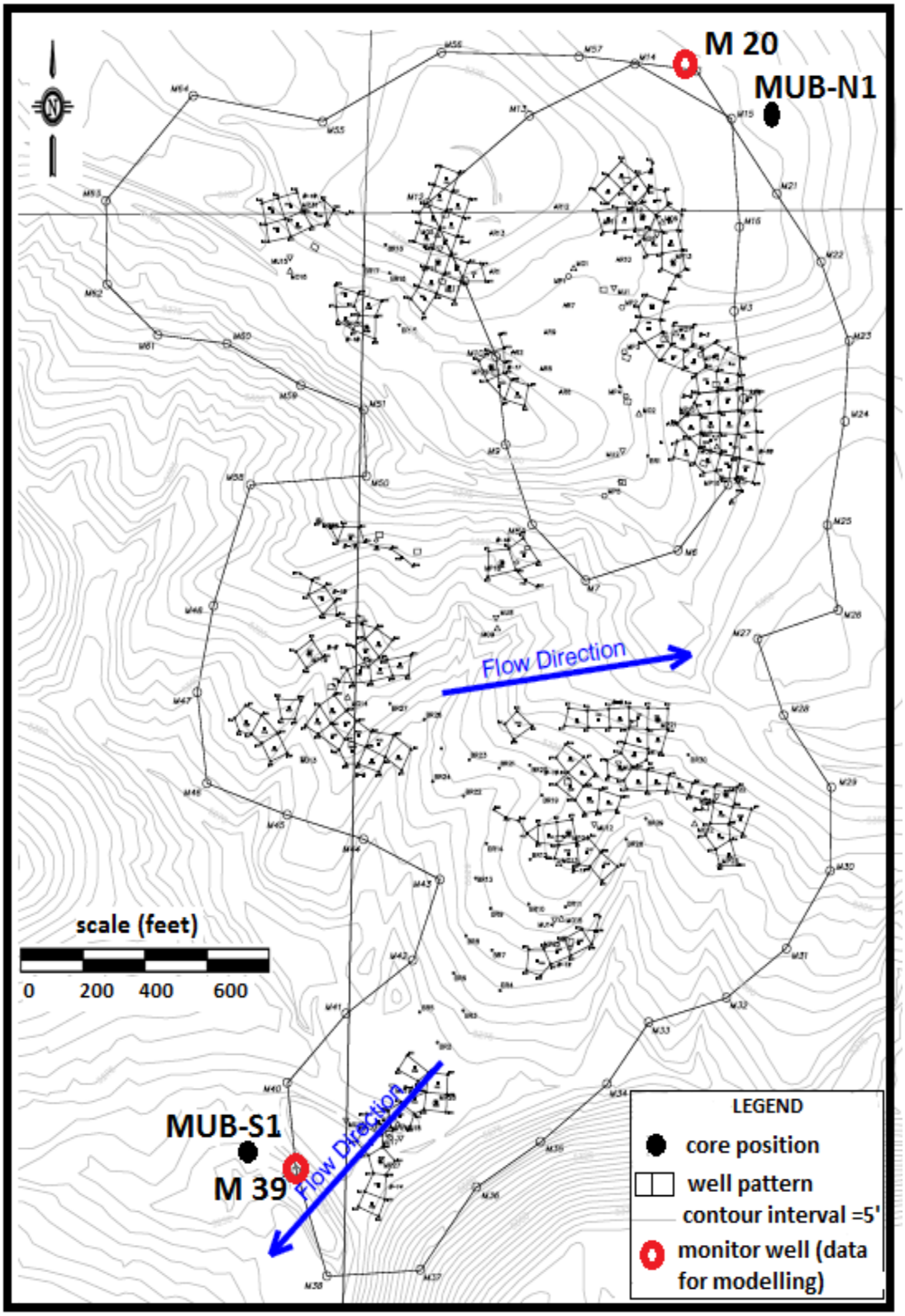

Figure 2-3: Map showing the position of the two boreholes drilled in January 2014 (Core 1 is MUB-N1 and core 2 is MUB-S1). Topographic map provided by Cameco Resources.

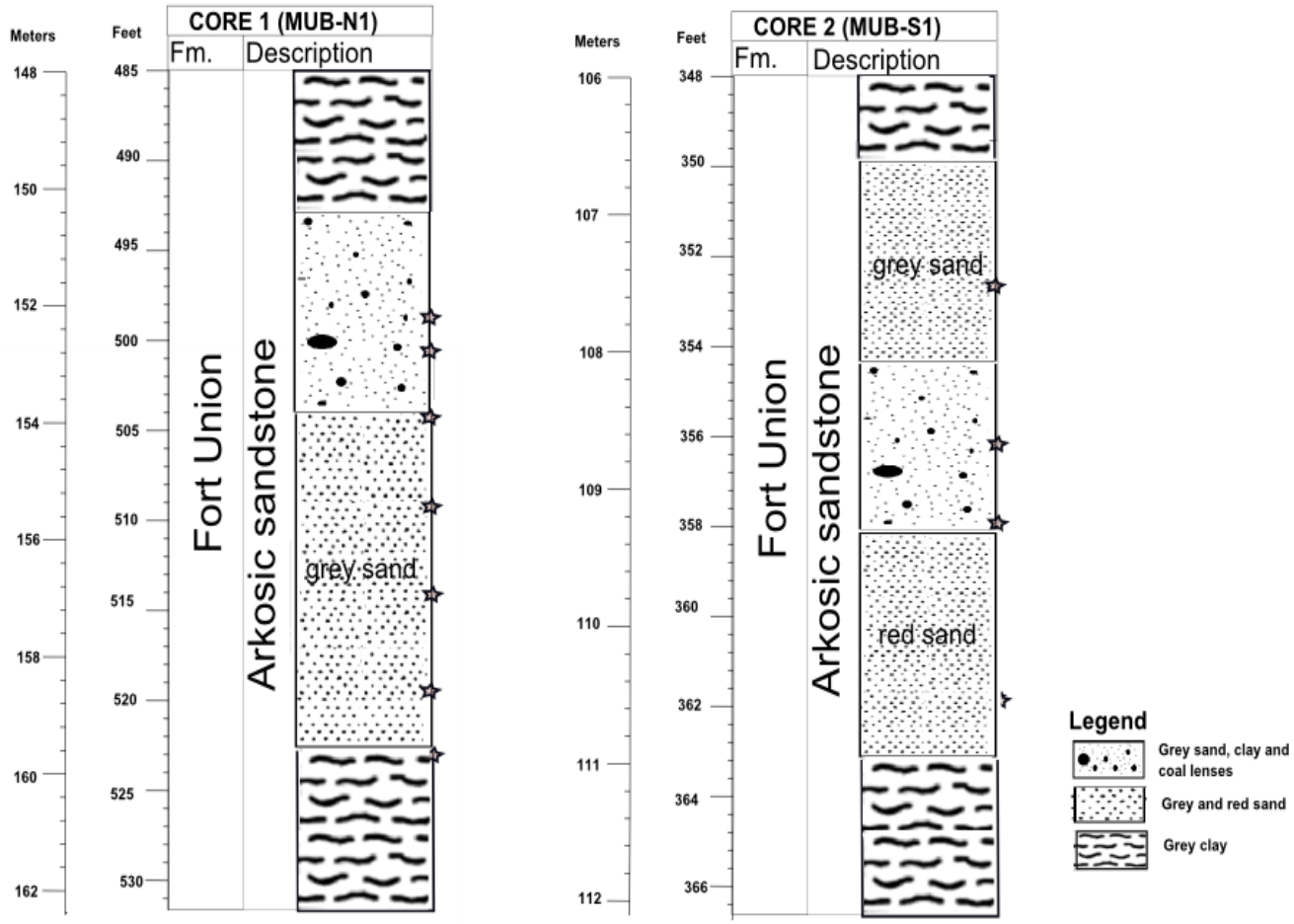

Figure 2-4: Stratigraphic section for core 1 (MUB-N1) and core 2 (MUB-S1). The stars show the positions where the core samples were taken for analyses.

2.3 Sample processing

Core samples were stored and processed for further analyses at the Department of Geological Sciences, University of Saskatchewan. Members of the McBeth lab are trained in radiation safety and Dr. McBeth possess a valid nuclear substance permit from the University of Saskatchewan for handling radioactive materials (permit GEO-08-P). Core samples were stored in a dedicated locked freezer. Samples were transferred to a fume hood in the Hendry Lab to allow venting of radon gas before sub-sampling. Sub-sampling was done under argon in a fume hood. Sub-samples (approximately 50 cm^3) were taken from each core for PXRD, XAS, XRF and inductively-coupled plasma mass spectrometry (ICP-MS) analyses, and the sub-samples were stored in the freezer until further preparation and analyses. Care was taken to separate the coal lenses (L) from the sandy

material (R) in those samples where coal lenses (small pockets of coal within the core) were present; thus, sample names with L at the end indicate that the core contains coal lenses while core with sample names that end with R indicate no coal lenses were present. Samples with coal lenses were believed to contain high U and carbon content. The remaining materials were vacuum sealed in plastic bags and stored in the freezer until disposal. Radiation monitoring was performed before and after the sub-sampling and results were recorded.

2.3.1 Radioactive material handling procedure

The McBeth group has a set of University of Saskatchewan Radiation Safety Approval Committee approved procedures for handling radioactive materials (McBeth, 2015). Radiation samples were stored in a dedicated locked freezer/fridge in Room S411, Spinks Building (Matthew Lindsay's lab) at the University of Saskatchewan. The samples were labelled and an inventory of the samples was prepared. All sample preparations were performed in Geological Sciences room 317, University of Saskatchewan. Samples were first placed in a fume hood to allow venting of radon gas. Samples that must be handled under anaerobic conditions were placed in a disposable glove bag and placed inside the fume hood. Sub-sampling was done in the fume hood or in an argon box after venting. After sampling, all the samples were transferred into an air-tight plastic bags and vacuum sealed, then returned to Room S411, Spinks Building for storage. Radiation monitoring was done before and after sample handling and counts (cpm) were measured and recorded using a handheld monitor. Waste generated from this activity was collected in sealed storage bags and arrangements were made with safety resources for disposal

2.4 Analytical Methods

2.4.1 Elemental analysis

For the solids from core 1 and core 2, bulk quantitative analysis of major and minor elements were determined at the Saskatchewan Research Council (SRC), Saskatoon. The total percentage of organic and inorganic carbon were determine using a LECO CS230 analyser with a detection limit of 0.01 % (LECO Corporation, 2008); for organic carbon, an aliquot of sample was combusted in a LECO induction furnace with an oxygen supply while for the inorganic carbon, the combustion is with argon supply and the percentage of either the organic or inorganic carbon determined from

instrument calibration. Elemental concentration for Al, As, Ba, Fe, Cu, Pb, V, Ti, Zn, Sr, Se, M, Ag, B, Ni, Cr, Ca, Mg, K, Na and Mn were determined using ICP-MS (EPA METHOD 3052). A portion (0.5 g) of the sample was digested in 9 mL of nitric acid and 3 mL of hydrofluoric acid using microwave heating at 180˚C for 15 minutes, the reaction was allowed to cooled, filtered and analysed using ICP-MS. Concentration of Cl was determined by leaching approximately 30 g of dry soil sample in 90 mL of deionised water for about 11 hours. The solution was filtered using a high retentive filter and the filtrate analysed using ion chromatography (Carter, 1993). The detection limit for this analysis was 0.05 mg/g.

For the groundwater, bulk quantitative analysis of all elements was determined at Inter-Mountains labs, Sheridan, Wyoming in September 2015. Total dissolved concentrations of Al, Be, B, Cr, Fe, Mn, Ni, Zn, Na, K, Mg and Ca were determined by ICP-optical emission spectroscopy (ICP-OES; EPA Method 200.7), whereas total dissolved concentrations of As, Ba, Cd, Cu, Se, U, and V were determined by ICP-MS (EPA Method 200.8). Samples for both ICP-OES and ICP-MS analysis were filtered using 0.45µm filter and acidified to pH below 2 using HNO_3. Carbonate, bicarbonates and total alkalinity were measured using titration methods (Standard Methods for the Examination of Water and Wastewater (SM 2320B). Chloride and sulfate concentrations were measured by ion chromatography (IC; EPA Method 300.1) and that of ammonia was measured using colorimetry (EPA Method 350.1). Nitrate and Nitrite were also determined using colorimetry (EPA Method 353.2). The reporting limit of the elemental concentrations ranges from 0.0003 mg/L to 5 mg/L.

2.4.2 Powder X-Ray Diffraction

Powder X-Ray Diffraction was performed using a conventional copper X-rays source and synchrotron X-rays source. Results from these two techniques were used to identify bulk mineral phases that are present in the ore. For the conventional PXRD analysis, samples were dried in an oven at 40°C for 10 hours. The samples were then ground with mortar and pestle and mounted on a rotating disk holder for bulk X-ray diffractogram measurement (Department of Geology, University of Saskatchewan). The measurements were done with Empryream Pro PANanalytical diffractometer equipped with a copper target and a scintillation detector. The diffractometer was set to a current of 40 mA and a voltage of 45 kV. The scans were measured from 3^o to 80^o 2θ with

a step size of 0.01°. Phase identification was performed with HighScore Plus software from PAN analytical.

High energy synchrotron PXRD measurements were performed using the Macromolecular Crystallography beamline (CMCF-BM) at the CLS. The CMCF-BM beamline is a bending magnet beamline with a Si (111) double crystal monochromator. Powdered samples were loaded into 0.032 inch kapton (polyimide) capillaries and sealed at both ends with Loctite 454 gel epoxy. The samples and a sample of lanthanum hexaboride (LaB_6; used as calibrant) were analysed to obtain 2D X-ray diffraction patterns using an incident energy of 18 KeV (wavelength: 0.68878Å) and a Rayonix MX300HE detector with an active area of 300 mm x 300 mm. The 2D X-ray diffraction patterns were calibrated and integrated using GSASII software (Toby & Von Dreele, 2013). The LaB_6 was used to calibrate the sample-detector distance, detector centering, and detector tilt. The calibration parameters obtained were applied to the entire pattern before integration. Phase identification semi-quantitative analysis were done on the integrated pattern using Powder Diffraction File (PDF-4) software (Powder Diffraction File, 2012).

To study the differences between the two PXRD techniques used in this study, a comparison of the PXRD patterns from the synchrotron and the Cu source was performed. To allow for a direct comparison, a wavelength of 0.154 A˚ was used for the Cu source and 0.688A˚ for the synchrotron source in the Braggs equation ($n\lambda = 2d \sin\Theta$). The data obtained using the different wavelength were plotted as shown in Figure 2-5. The Cu source PXRD patterns were noisier and had higher background compared to the synchrotron source data. The synchrotron PXRD data provided a higher level of resolution thus making it easier to resolve minor peaks of the crystalline phases present in the ore. The synchrotron PXRD facilitates the detection of peaks not visible using the conventional Cu source due to better signal to noise ratio. An example is a peak for kaolinite at 18.33˚ 2Θ visible in the synchrotron PXRD pattern (Figure 2-5 inset). This superior resolution of synchrotron data makes it better for peak indexing, thus better for phase identification. The remainder of the data presented in this thesis was obtained using the synchrotron PXRD analyses.

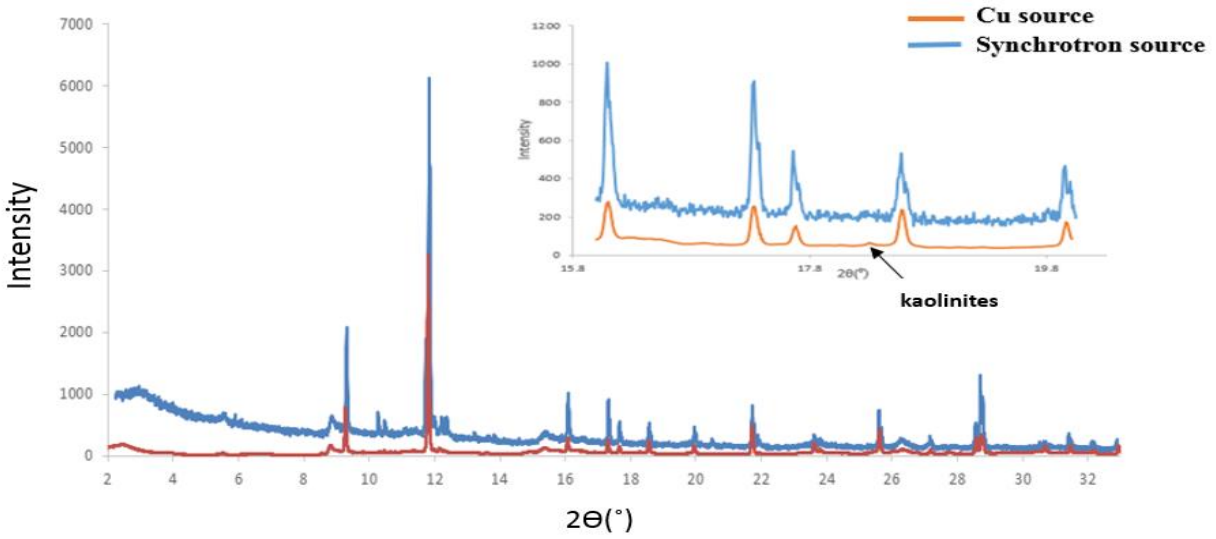

Figure 2-5: Comparing X-ray diffraction patterns from Cu source (blue) and synchrotron source (red) from core 1 (MUB-N1), sample 498R. The inserted figure shows a peak for kaolinite which was not visible in Cu-source PXRD pattern.

2.4.3 Electron Microprobe Analysis and Scanning Electron Microscopy

Samples were placed on a plate holder and gold-coated using a JOEL JEE Vacuum Evaporator to prevent the surface from charging and promote the emission of secondary electrons. Scanning Electron Microscopy images were obtained using a JEOL JSM-840A Scanning Electron Microscope at 12 mA and 15 kV. For the EMPA, BEI were collected to locate the higher atomic number elements using JOEL JXA-8600 Super probe Micro-analyzer at 12 mA and 15 kV. Both experiments were performed at the Department of Geological Sciences, University of Saskatchewan. This is then followed by elemental mapping of single grain within the higher atomic number region. Energy dispersive spectra were also collected at selected spots for elemental analysis.

2.4.4 X-Ray Absorption Spectroscopy

Synchrotron-based XAS was performed for C, Fe, S, and U at the CLS, Saskatoon. The CLS is a third- generation synchrotron facility operating at an electron energy of 2.9 GeV. Carbon XANES spectra were collected using the Spherical Grating Monochromator beamline (SGM). The beamline uses a 45 mm planer undulator over the energy range 250 and 2000 eV. The spot size on

the beamline was 1000 µm × 100 µm. Samples were ground and mixed with methanol and loaded onto a gold-plated silicon wafer on a copper sample holder. Samples were dried in a vacuum desiccator before analysis. Citric acid was used to calibrate the energy scale, assuming a value of 288.6 eV (Gillespie et al., 2015). Normal scans were collected using a silicon drift detector over the energy range 280 eV to 320 eV at 1 s dwell time and 0.1 step size. The entrance and exit slit gaps were set to 249.9 µm and 25 µm respectively. The carbon K-edge is at 284.2 eV. A titanium filter was used to reject higher order harmonics. Normalization of the data involved collecting an I_0 by measuring the scatter of the incident beam from a freshly Au-coated Si wafer using a silicon drift detector. The scatter in the sample data was removed by adjusting the pre-edge baseline to near zero before normalizing with the I_0. Acquaman software was used for data collection and the data was analysed using Axis2000 (Hitchcock, 2011) and OriginPro (OriginLab, Northampton, MA).

Uranium L_3-edge and Fe K-edge XANES were performed using the CLS Hard X-ray Micro-Analysis beamline (HXMA, 06ID-1). The beamline uses a super conducting wiggler to produce high flux and brilliance at an energy level of 5 - 40 keV, it is thus suitable for conducting XAS analyses of most transition elements. Freeze dried powdered sample (approximately 0.1 g) was placed in a Teflon sample holder and covered on both sides using an X-ray transparent kapton tape. A focused beam of 0.1 x 0.1mm for U and 1mm x 3 mm for Fe (JJ slit apertures) was chosen with the sample oriented at 45º to the incident beam. The U spectra were collected at the L_3 edge (17166 eV) over 5 energy regions: -200 eV to -160 eV, 10 eV steps; -160 eV to -100 eV, 0.5 eV steps (covering the yttrium foil calibration standard); -100 eV to -30 eV, 10 eV steps; -30 eV to +40 eV, 0.5 eV steps (uranium L_3 edge); and +40 eV to 14.2 KeV, 0.05K steps. The dwell time for each step was 1 s and the data was collected in fluorescence mode with a 32 element solid-state germanium detector. Carnotite (U(VI)), uranyl nitrate (U(VI)) and uraninite (U(IV)) standards were also collected in transmission mode; standard samples were oriented 90º to the incident beam. The beamline was calibrated to a yttrium foil at the first inflection point of the yttrium K-edge (17038 eV) Yttrium foil calibration spectra were collected simultaneously along with each U spectrum.

The Fe standards (goethite, ferrihydrite, hematite, pyrite and lepidocrocite) were obtained from Joseph Essilfie-Dughan (Essilfie-Dughan et al., 2013), siderite and magnetite from Derek Peak,

and spectra for illite, chlorite, ilmenite and vivianite were obtained from the Advance Light Source (ALS), Lawrence Berkeley National Lab. Collection of Fe K-edge data has been described by Essilfie-Dughan et al. (2013). The Fe K-edge spectra were collected over three energy regions:- 200 eV to -30 eV, 10 eV; -30 to +40 eV, 0.25 eV steps; +40 to 9 K eV, 0.1 KeV steps. The dwell time for each step was 1 s and a manganese filter was used to reject unwanted harmonics. Absorption spectra for an in-line Fe foil was collected simultaneously during sample spectra acquisition (CLS) at the Fe K-edge to use for energy calibration of sample spectra. Data reduction including energy calibration, averaging of multiple scans, background subtraction, and normalization were performed using ATHENA software (Ravel & Newville, 2005).

Sulfur XANES spectra were also collected at the CLS 06-B1-1 soft X-ray micro-characterization beamline (SXRMB). The beamline uses a bending magnet and toroidal mirror to produce a focused beam in the energy range of 1.7-10 keV. Freeze-dried samples were ground using mortar and pestle in a glove box and mounted on carbon tape on a copper sample holder. Sulfur K-edge spectra were collected under high vacuum (~5×10^{-8} Torr) using both fluorescence and total electron yield mode. The scans were obtain over three energy regions: -50 to -6 eV, 2 eV steps, 1 s dwell time, -6 to +15 eV, 0.15 eV steps, 4 s dwell time, +15 to +50 eV, 0.75 eV steps, and 1 s dwell time. Two scans were obtained for each sample and averaged to increase the signal to noise ratio. Sulfur standard K-edge XANES spectra were obtained from the European Synchrotron Facility (ESRF) XANES database for organic and inorganic sulfur compounds. Data analysis and processing including energy calibration, background subtraction, pre-edge and post edge subtraction were performed using Athena software (version 0.9.25)(Ravel & Newville, 2005).

The normalised spectra for both Fe and S were analysed to identify and quantify molecular species of Fe and S that are present in the ore. Principal component analysis (PCA) was first employed to determine the number of principal components present in the samples using SixPACK (Webb, 2005). The PCA can provide the value of the minimum number of components needed to fit data. Target transform is performed after the PCA to check the likelihood that each of the spectra of the selected reference standards is a main component of the XANES spectra from the two cores. SixPACK reports a spoil value (a measure of increasing in fit error when replacing a component with a target spectra). The spoil value gives a statistical basis of accepting the most appropriate reference spectra to be used for spectral fitting, thus reference compounds with smaller spoil

values are best used for least square linear combination fitting (LCF) (Malinowski, 1978). Spoil values are considered excellent for fitting if they are less than 1.5, good between 1.5 to 3, fair between 3 to 4.5, poor between 4.5 to 6 and unacceptable for any value greater than 6 (Malinowski, 1978). Based on the outcome of PCA and target transform, LCF was then performed. Quantitative information about the different S and Fe species present in the ore sample were obtained from the linear combination of the XANES spectra to a set of reference spectra with ATHENA (Ravel & Newville, 2005). The LCF reconstruct a simple spectrum using a combination of selected reference spectra and reports goodness of fit parameters (R-factor and Chi square values) and the percentages of each reference contribution to the fit.

2.4.5 Synchrotron Micro-X-Ray Fluorescence Mapping (μXRF mapping)

Micro-XRF maps were collected on the VESPERS beamline (07B2-1). VESPERS is a bending magnet beamline with an energy range of 6 - 30 keV, ideal for mapping transition elements. Samples for micro XRF analyses were freeze-dried and ground with a mortar and pestle under argon gas. The ground samples were then loaded onto kapton tape and sealed. A second layer of kapton tape was applied to prevent leakage and provide secondary containment. The sample was made very flat and air spaces were avoided to prevent pinhole effects. Data was collected with a pink beam (i.e. photon from a bending magnet with a wide energy range) of spot size 3.5 μm. Regions of interest (ROIs) were set for As K_{α}, As K_{β}, Pb L_{α}, Pb L_{β}, Ca K_{α}, Ca K_{β}, Ge K_{α}, Ge K_{β}, Ni K_{α}, Ni K_{β}, Fe K_{α}, Fe K_{β}, Mo K_{α}, Mo K_{β}, Rb K_{α}, Rb K_{β}, Ti K_{α}, Ti K_{β}, V K_{α}, V K_{β}, U L_{α}, U L_{β}, Zn K_{α} and Zn K_{β}. It is important to note that the emission peaks for some elements overlap; examples include the emission peaks for: U L_{α} and Rb K_{α}; Ti K_{β} and V K_{α}; and As K_{α} and Pb L_{α},. The ROIs selected were based on reported elements from ICP-MS and the operating limit of the beamline. Elements with emission spectra below the Ar K-edge (2950.7 eV) (e.g. P, Si, S and Al) can not be detected due to the operating energy and setup of this beamline. The intensity of the scattering X-rays were monitored using a 4 element vortex detector at a distance of 125 mm. The maps were obtained using 5 μm x 5 μm step sizes and a dwell time of 1s per pixel. The maps were generally 300 μm by 300 μm in size. The detector dead time was set such that the dead time was less than 30%. Sam's Micro Analysis Toolkit (SMAK) (Sam's Microprobe Analysis Kit, 2006) was used for the XRF data analyses.

2.4.6 Geochemical Modelling

Geochemical modelling was performed using PHREEQC software (Parkhurst, 2013). Speciation calculations were used to study U complex formation and the saturation index of major species present in the groundwater. Special attention was given to C, S, and Fe species because of their known capabilities in U mobilization. Saturation indices obtained will help assess the potential minerals that are controlling U mobility. The WATEQ4F thermodynamic database (Ball & Nordstrom, 1991) embedded in PHREEQC was used in this work. The WATEQ4F thermodynamic database contains data for aqueous species, gases and mineral phase of elements that includes U. This database was modified by Janet Schramke (Environmental Consultant working on the Smith Ranch-Highland projects) with updated U speciation constants from Guillaumont et al. (2003), Dong and Brooks (2006) and Dong and Brooks (2008). Other studies (Salmon & Malmström, 2004; Luo et al., 2007; Jacques et al., 2008) used similar databases in modelling U and other contaminant in groundwater. Modelling used pH, Eh, temperature and aqueous concentration data (Table 2-1) from 2 monitoring boreholes approximately 1.5 m from the location where the ore was obtained. Parameters such as pH and Eh were varied to simulate different scenarios occurring at the mine site. The pH of the groundwater is 8 - 8.5 (lab measurement). The site model was tested under different pH conditions: alkaline, acidic and neutral. In addition, the groundwater Eh is approximately +80 mV (J. Clay, personal communication). The Eh was varied between +80 mV and -200 mV to study the effect of redox conditions on U mobility.

Table 2-1: Ion chemistry of waters used in PHREEQC modelling. Data provided by Cameco Resources, analyses performed by Inter-Mountain labs.

Constituents	Borehole M20	Borehole M39
pH*	8.3	8.2
pe	1.4	1.4
Temp	13	13
Al (mg/l)	0.05	0.05
Alkalinity ((mg/l of $CaCO_3$)	176	173
Ca (mg/l)	45	61
Cl (mg/l)	7	10
F (mg/l)	0.2	0.2
Fe (total) (mg/l)	0.49	0.42
K (mg/l)	6	7
Mg (mg/l)	10	12
Mn (mg/l)	0.04	0.04
Na (mg/l)	61	58
SO_4^{2-} (mg/l)	86	125
Si (mg/l of SiO_2)	16	16
U (mg/l)	0.0105	0.0131

* based on lab measurement

3 RESULTS AND DISCUSSION

3.1 Sample description

The samples from the two cores were dominated by sand, with coal lenses and clay. The sandy samples were mostly reddish to grey in colour suggesting the presence of oxidised Fe minerals. The clayey zones of the core were mostly grey; an indication of reduced conditions. Table 3-1 lists selected samples, their descriptions, and depths.

Table 3-1: Description of U core samples from MUB; Smith Ranch-Highland Mine, Wyoming.

Sample ID	Core	Depth (feet)	Depth (m)	Description
353.5	MUB-S1	353 - 353.5	107.7	Sandy, clay-like, grey
355.5L	MUB-S1	355.5 – 356	108.4	Sandy, clay-like, black coal lenses
355.5R	MUB-S1	355.5 – 356	108.4	Sandy, clay-like
358.5	MUB-S1	358- 358.5	109.3	Sandy, red
362.5	MUB-S1	362 - 362.5	110.5	Sandy, red
498.5L	MUB-N1	498 – 498.5	151.9	Clayey, black coal lenses
498.5R	MUB-N1	498 – 498.5	151.9	Grey clayey
500.5L	MUB-N1	500.5 – 501	152.6	Grey, black coal lenses
500.5R	MUB-N1	500.5 – 501	152.6	Grey sand
504.5	MUB-N1	504.5 – 505	153.8	Grey sand
509.5	MUB-N1	509.5 – 510	155.3	Grey sand
514.5	MUB-N1	514.5 – 515	156.8	Grey sand
519.5	MUB-N1	519.5 – 520	158.3	Grey sand
524.5	MUB-N1	524.5 – 525	159.9	Grey clayey

3.2 Elemental concentrations

Bulk elemental analysis of the core samples using digestion followed by ICP-MS, combustion and IC revealed that the ore is composed of Al, Fe, organic and inorganic C, Ti, Mn, K, Na V, Ni, Be, B, Cl, Se, Sr and Zn (Figure 3-1, Table A-1). There was no general trend of elemental concentration with respect to depth (Figure 3-1). Note that the sample ID corresponds to the sample depth below the ground in feet. In general, elemental concentrations of some elements (U, V, Ti, and Ca) were

higher in samples with coal lenses (samples 355.5L, 498.5L and 500.5L) than in samples containing just sandy materials.

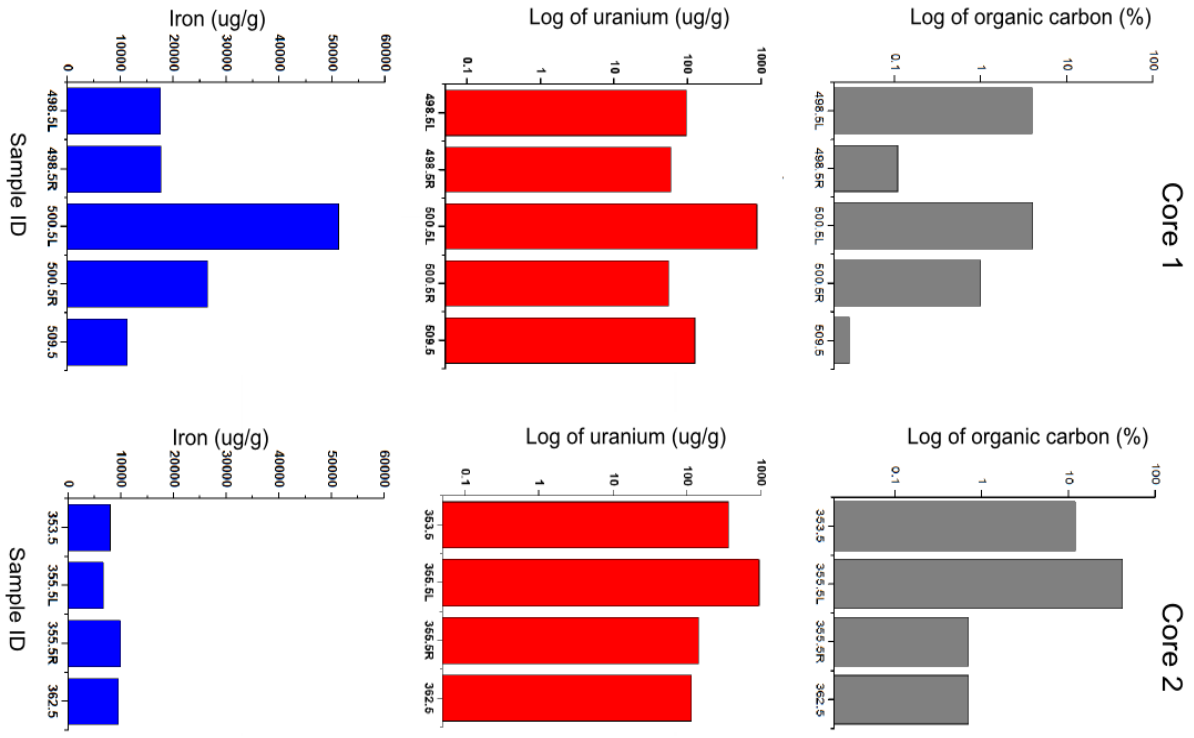

Figure 3-1: Elemental concentrations of U, Fe and organic C from core 1 and core 2. Note the sample ID is the same as the sample depth in feet.

The U concentrations ranged between 954 and 1.4 µg/g in all the samples from the two cores (Figure 3-1). The highest U concentration was associated with a sample containing coal lenses. Iron concentrations were on the order of thousands of µg/g in all the samples. Carbon was primarily present as organic C that accounted for 0.03 - 42.5 w/w % as compared with inorganic carbon which accounted for 0.01 - 0.32 w/w % of the core (Table A-1).

3.3 Mineralogical characteristics

Synchrotron X-ray diffraction patterns of core samples showed the presence of quartz [SiO_2], feldspar (albite [$Na(AlSi_3O_8)$]), muscovite [$KAl_2(AlSi_3O_{10})(OH)_2$], iron minerals including pyrite [FeS_2], vivianite [$Fe^{2+}{}_3(PO_4)_2 \cdot 8H_2O$] and goethite [α-FeO(OH)] and clay minerals (kaolinite [$Al_2Si_2O_5(OH)_4$], illite [$(K,H_3O)(Al,Mg,Fe)_2(Si,Al)_4O_{10}((OH)_2(H_2O))$] and chlorite

[$(Mg,Al,Fe)_3(Si,Al)_4O_{10}(OH)_2$ $(Mg,Al,Fe)_3(OH)_6$]) (Figures 3-2 and 3-3). Because the PXRD patterns only accounted for crystalline phases, amorphous phases that may be present in the samples are not identified. The detection limit of U mineral phases depends on crystallinity factors (e.g. crystal size) and whether there is overlap between the strongest peak of U and that of other elements within the ore matrix (Gallegos et al., 2015b). In these samples, the proportion of U minerals in the XRD analyses were mostly below detection, but traces of schoepite were observed in samples containing coal lenses. The samples containing coal lenses also contained pyrite, which is comprised of reduced iron and sulfur. Its presence is indicated by peaks at 17.881˚ 2Θ and 24.295˚ 2Θ in samples containing coal lenses (500.5L and 498.5L) (Figure 3-2). This result is similar to published results from the Smith Ranch-Highlands Mine Unit 4 (WoldeGabriel et al., 2014).

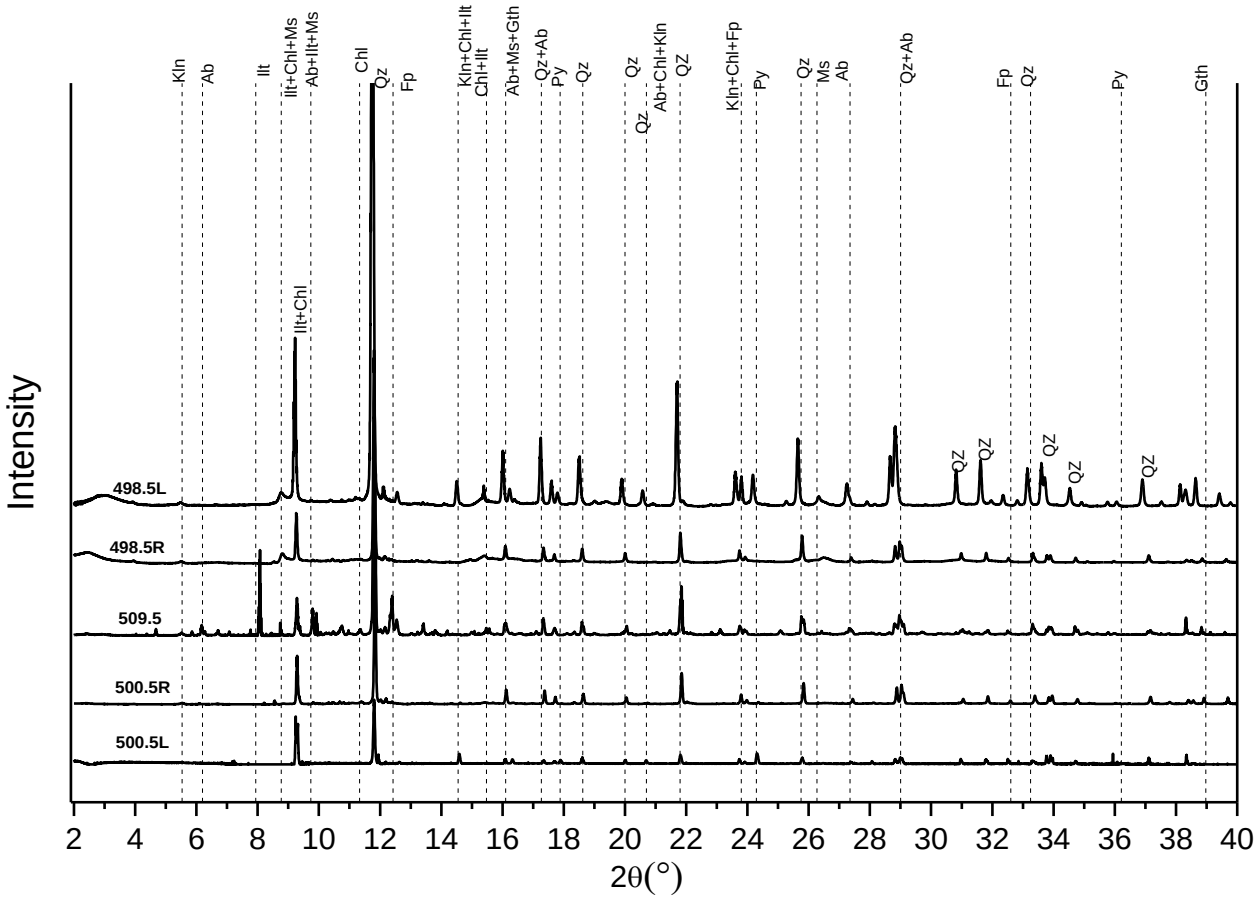

Figure 3-2: Synchrotron X-ray diffraction patterns of samples from core 1 (MUB-N1). Mineral phases that were identified (2θ range 2 – 40 degrees) (Qz=quartz, Kln=kaolinite, Gth=goethite, Py=pyrite, Ms=muscovite, Chl=chlorite, Ilt= illite, Fp=iron phosphate (vivianite) and Ab=albite.

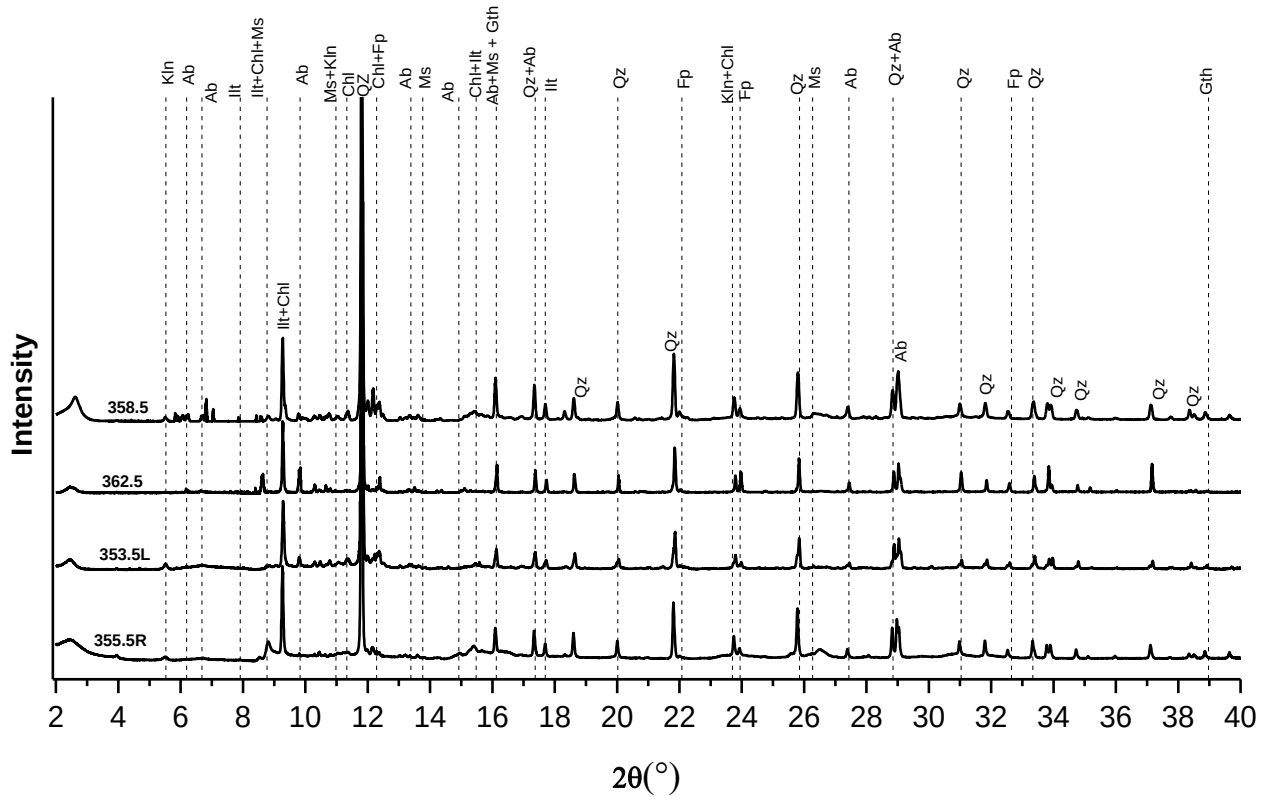

Figure 3-3: Synchrotron X-ray diffraction patterns of samples from core 2 (MUB-S1). Mineral phases that were identified (2θ range 2 – 40 degrees) include Qz=quartz, Kln=kaolinite, Gth =goethite, Py=pyrite, Ms=muscovite, Chl=chlorite, Ilt=illite, Fp=iron phosphate (vivianite) and Ab=albite.

Semi-quantitative analysis of the ore samples was performed using PDF-4 software to determine the approximate abundance of the crystalline minerals present in the core samples. The core was dominated by quartz (50 – 72 %), albite feldspar (1 – 13 %), iron minerals including goethite (0.1 - 6.8 %) and pyrite (0.4 - 13.7 %), clay (3 – 20 %) and smaller amounts of the secondary U mineral schoepite (Table 3-2). The abundance of clay throughout the aquifer materials was highly variable, with the highest clay concentration observed in samples containing coal lenses. The abundance of

pyrite was high (1 - 13 %) in samples containing coal lenses. Iron phosphate was also present in the sample and ranged from 0.3 - 9.3 % of the mineral component of the core samples.

Table 3-2: Semi-quantitative analysis of the crystalline phases present in the core sample.

Samples	**Core 2 (MUB-S1)**				**Core 1 (MUB-N1)**				
	362.5	**358.5**	**355.5L**	**355.5R**	**509.5**	**500.5L**	**500.5R**	**498.5L**	**498.5R**
Quartz	66.2	66.1	52.9	82	68.1	61.7	84.5	50.2	72.5
Albite	9.1	13.1	10.3	5.6	10.2	4.8	2.6	1.0	0.1
Kaolinite	7.2	0.5	7.9	3.6	2.5	5.1	3.3	9.9	2.6
Chlorite	4.7	4.8	6.3	1.5	0.0	5.7	2.6	0.5	6.5
Illite	0.5	5.4	0.9	0.0	0.0	2.2	0.7	11.2	3.4
Muscovite	10.3	0.8	13	3.8	4.7	0.8	0.2	14.3	7.3
Iron phosphate	0.6	9	6.5	2.2	9.3	0	0.4	0.3	5.3
Pyrite	0.0	0.0	1.1	0.0	0.4	13.7	1.0	4.6	0.5
Goethite	1.4	0.1	0.5	1.1	4.0	5.2	4.0	6.8	1.1
Schoepite	0.0	0.0	0.5	0.0	0.8	0.8	0.7	1.1	0.7

The PXRD results indicated the presence of Fe minerals including goethite and pyrite. Goethite in the ore samples may provide surface area and sorption sites for U adsorption, thereby retarding aqueous U transportation. The adsorption of U onto mineral surfaces is highly pH dependent (Dong et al., 2011). Dong et al. (2011) confirmed a strong adsorption of U onto goethite at pH > 4 in the presence of aqueous carbonate, thus in this study where the pH of the system is between 8.2 and 8.3, goethite is likely to provide sites for U sorption. Pyrite observed in samples containing coal lenses might be contributing to the high U content of these samples as pyrite has been reported to favor the precipitation of insoluble U minerals (Dahlkamp, 2010). For example, laboratory-based experiment using U(VI) reaction with pyrite crystals followed by XANES analyses have confirmed U(VI) adsorption and partial reduction to U(IV) (Aubriet et al., 2006; Eglizaud et al., 2006).

Sorption of U on to clay minerals has been described as essential in controlling U mobility in groundwater (Pabalan & Turner, 1996; Sylwester et al., 2000). Clay minerals (kaolinite, illite and chlorite) present in the core samples can provide surface area for U adsorption. The activity of carbonates in groundwater can greatly influence adsorption of U onto minerals (Jerden Jr & Sinha, 2003). Jerden Jr and Sinha (2003) reported the presence of carbonate complexes ($UO_2(CO_3)_2^{-2}$ and $UO_2(CO_3)$ dominating the total dissolved U at pH 7 in groundwater containing carbonates and U.

In the presence of Ca, ternary Ca-uranyl-carbonates complexes ($CaUO_2(CO_3)_3^{2-}$ and $Ca_2UO_2(CO_3)_3$) are reported to dominate aqueous U species (Kalmykov & Choppin, 2000; Brooks et al., 2003). These complexes greatly decrease the adsorption of U on clay minerals and soils (Zheng et al., 2003) because of their high solubility and negative charge surfaces. Brooks et al. (2003) also reported ternary-uranyl-carbonate complexes limit biotic reduction of uranyl minerals.

Feldspar present in the ore samples may be altered into clay. Alteration of feldspars into clay minerals followed by precipitation of secondary U mineral uranophane has been speculated in the work of Hamdy (2009) who studied the role of argillic alteration (hydrothermal alteration of rock to produce clay and other minerals) in U precipitation. The alteration of feldspar into clay has also been reported by Swapp (2015) in her work on analysing cores from the Smith Ranch-Highlands MUB.

3.4 Electron Microprobe Analysis and Scanning Electron Microscopy

To study the morphology and the chemical composition of the core samples, EMPA and SEM were performed. The results from the SEM and EMPA analyses showed the presence of quartz, feldspar, clay minerals, pyrite, and several trace elements which included V, U, Se, Ca, Ti and Mg (Figure 3-4). Mineral identifications were based on compositional information from EDS spectra. Examination of the SEM images and EMPA EDS data confirmed that the core is a heterogeneous mixture of minerals with grain sizes that are poorly sorted (Figure 3-4A). The results from these analyses are consistent with those observed in PXRD and ICP-MS analysis.

In BSE images, the elements with higher atomic numbers (e.g. U) are brighter while those of low atomic numbers are darker. Uranium-bearing minerals appear as brighter spots in Figure 3-4D. The EDS of the brighter spot shows the presence of U, Ti, Fe and Ca (Figure 3-5). Uranium and pyrite in the core samples were associated with coal lenses. The coal lenses also contained higher concentrations of V, Ti, Ca, and Cl. The existence of U, Fe, and other elements in close association to coal lenses suggest that coal lenses have high affinity for metal binding, thus coal lenses present in the core sample can play an essential role in concentrating U and Fe. The role of organic matter in concentrating U has been reported in a review paperby Cumberland et al. (2016).

Coal lenses have been reported to be associated with sandstone-type U deposit (Levnthial, 1979; WoldeGabriel et al., 2014) and are responsible for U formation, U concentration, U reduction and U preservation (Levnthial, 1979). Oxidised U in close contact with organic matter can be reduced to the insoluble U minerals uraninite and coffinite (Nagy et al., 1991). Organic matter can also intimately mix with the reduced U, enclosing the reduced U and preventing U oxidation (Levnthial, 1979).

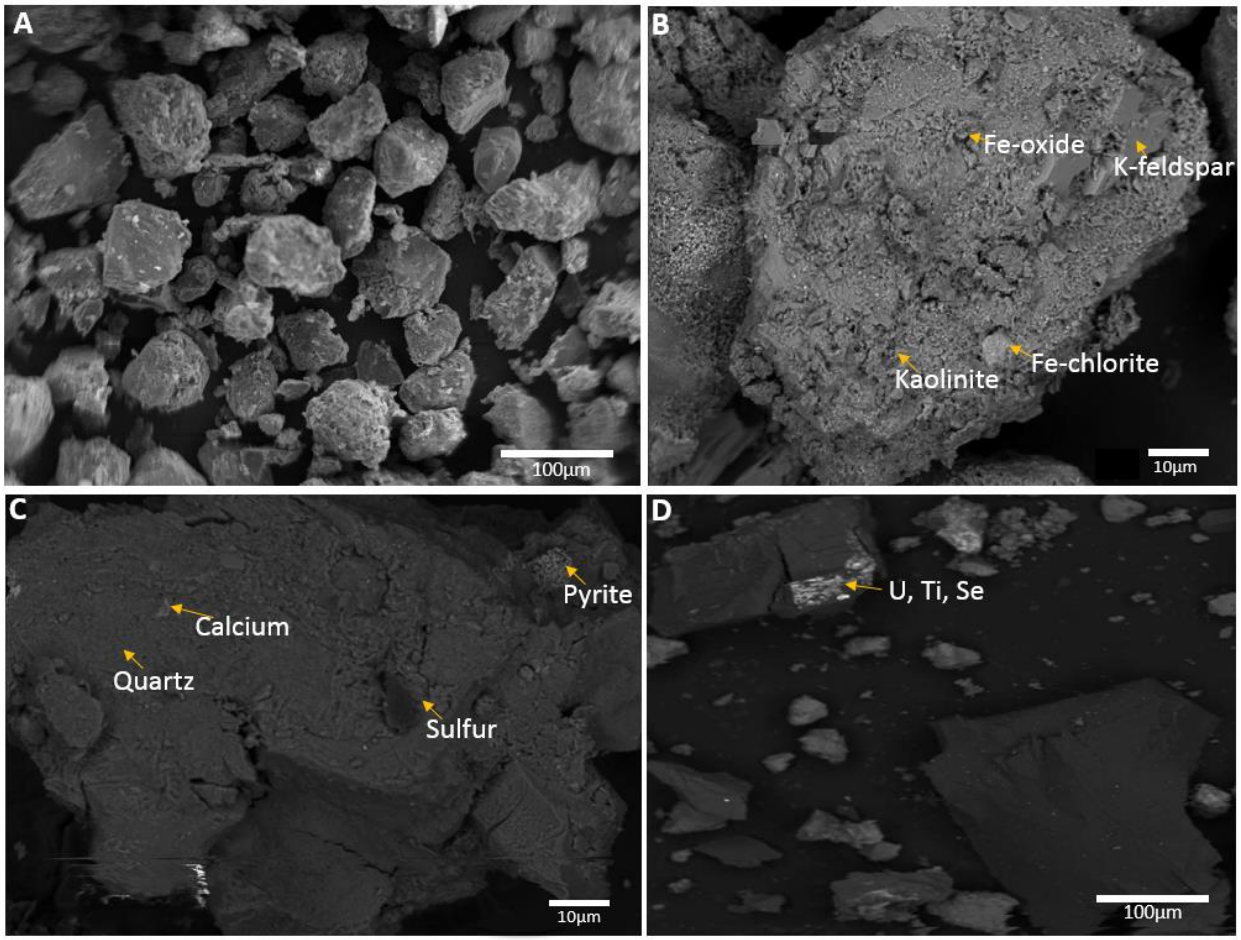

Figure 3-4: Backscattered electron images of (A) sample 500R illustrating grain sizes and shapes (B) sample 362.5 showing the presence of kaolinite, feldspar, chlorite and iron oxide (C) sample

498R showing the presence of quartz, pyrite and some calcium (D) sample 355.5L (a coal lens sample) displays the close association of U and other elements.

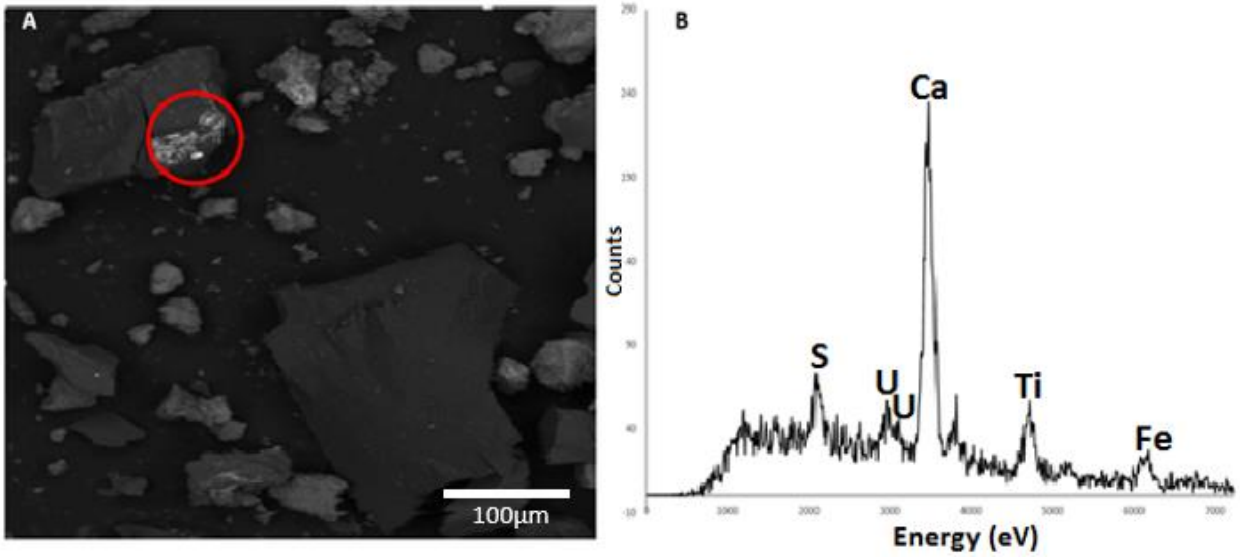

Figure 3-5: Backscattered electron image and EDS spectrum from sample 362.5 (Core 2) showing elemental distribution on selected mineral grains (S, U, Ti, and Fe).

Electron microprobe images and EDS also show pyrite in association with quartz and clay minerals in the coal lenses (Figure 3-6 and 3-7). Pyrite was observed on the surfaces of the clay and quartz and also in cracks and fractures in the clay minerals (Figure 3-7). Pyrite has also been observed around coal lenses and sometimes as partially recrystallized framboids (Figure 3-6).

The EMPA and EDS results showed U occurring with Fe, S, Ca and other elements. Sulfide minerals can contribute immensely to the immobilization of U by reducing oxidised U to insoluble U minerals (Qafoku et al., 2009). Framboidal pyrite observed in our samples is believed to form from microbially-mediated sulfate reduction (Suzuki et al., 2005). Qafoku et al. (2009) reported framboidal pyrite in alluvial sediment from a U-contaminated site and concluded that the framboidal pyrite can adsorb and retain U in its structure thus serving as a possible storage site for oxidised-soluble U species. They added that in the presence of oxygen, oxidative dissolution of the framboidal pyrite can desorb or release the U and subsequently increase the concentration of U in groundwater.

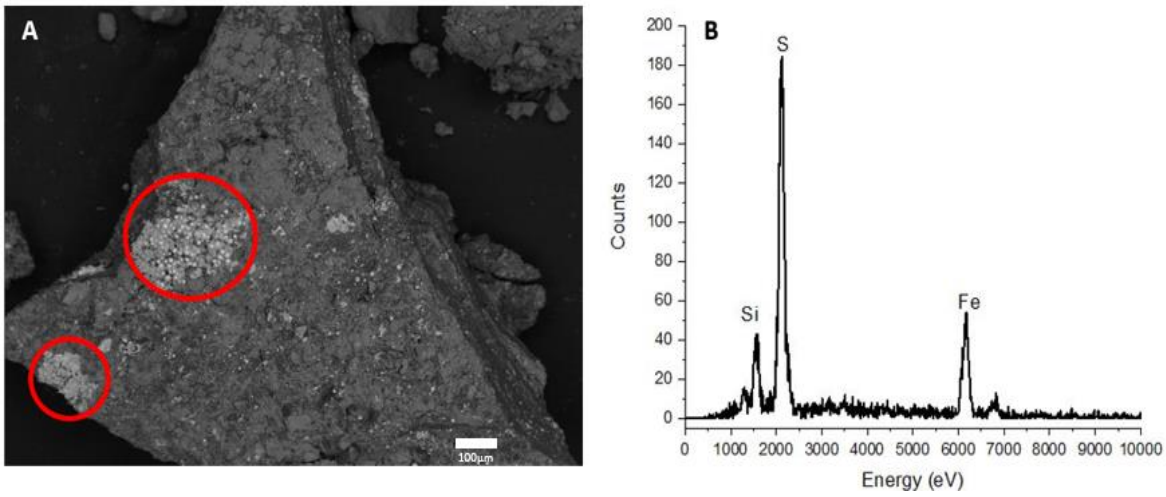

Figure 3-6: Backscattered electron image and EDS spectrum of sample 498L showing the presence of framboidal pyrite on quartz.

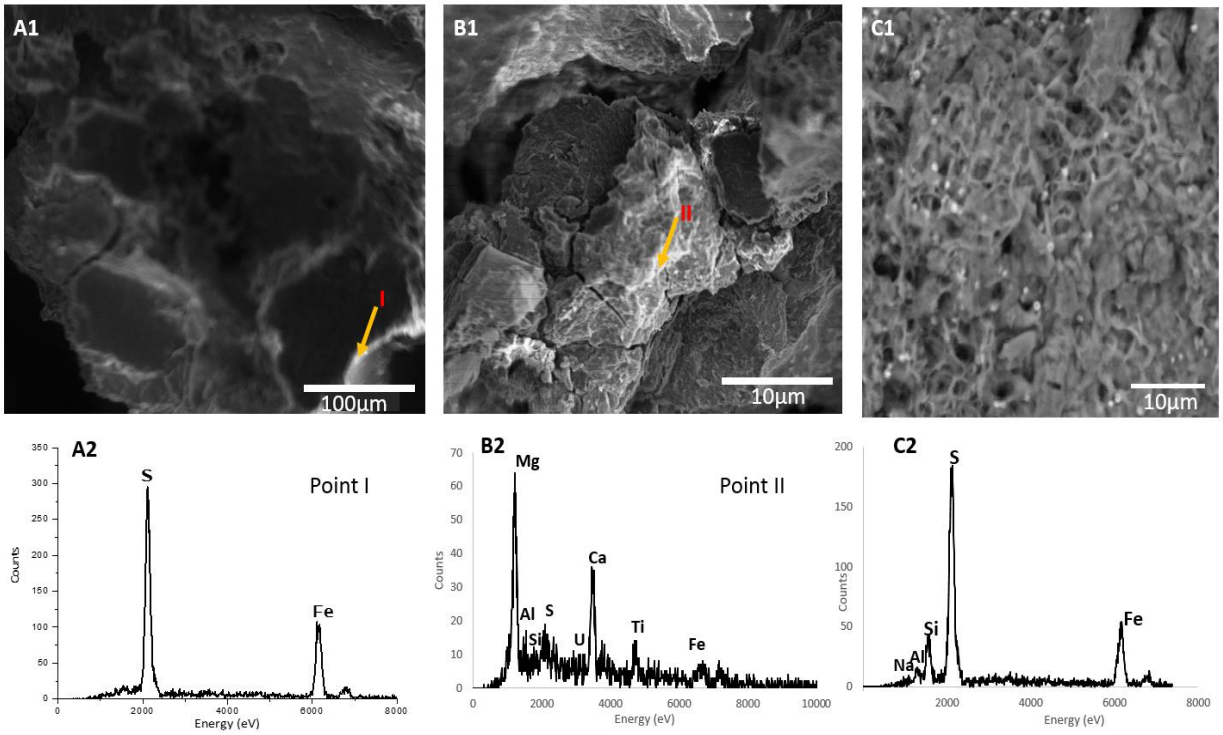

Figure 3-7: Scanning electron images and EDS showing pyrite occurring along the edges of clay at (A1 and A2), in holes and fractures of clay and rock fragments (B1 and B2) and on surface of clay minerals (CI and C2). C2 is an integrated spectrum for the whole C1 map area.

3.5 Solid-phase geochemistry

Understanding speciation and chemistry of elements within the ore matrix is important to determine the mobility, reactivity and toxicity of elements in such environments. In this study, characterization of C, Fe, S and U phases were performed using synchrotron XANES. Phosphorus XANES was attempted but the concentration of P was too low for us to get data of acceptable quality in the available beamtime. This XANES analysis using LCF helps in defining the proportion of the different solid phases present in the core samples. Table 3-3 shows a summary of the elemental XANES analysis, and sections 3.5.1 - 3.5.4 detail XANES analyses for each element analysed.

Table 3-3: XANES analyses: summary of valence, phase and carbon functional group information for cores 1 and 2 Sample

	S	**Fe**	**U**	**C**
Core 1	Valences: S(-1), S(-2), S(+6) Phases: Gypsum (0 - 22 ± 2 %) Anhydrite (36 ± 2 – 78 ± 2 %) Pyrite (13 ± 3 – 40 ± 5 %) Thianthrene (3 ± 1 – 40 ± 2%)	Valences: Fe(+2), Fe(+3) Phases: Goethite (1 ± 2 - 90 ± 1 %) Pyrite (1±1 - 53 ± 1 %) Vivianite (0 - 29 ± 1 %) Illite (0 – 43 ± 5 %) Chlorite (0 – 50 ± 1 %)	below detection limit	Organic C: aromatic carboxylic alkyl inorganic C: not present
Core 2	Valences: S(-1), S(-2), S(+6) Phases: Gypsum (22 ± 2– 40 ± 2 %) Anhydrite (32 ±1 –58 ± 1 %) Pyrite (8±3– 23 ± 2 %) Thianthrene (2 ±1 – 45 ± 2 %)	Valences: Fe(+2), Fe(+3) Phases: Goethite (9 ±3 – 65 ± 7 %) Pyrite (0 – 7 ± 1 %) Vivianite (0 - 41 ± 2 %) Illite (33 ± 5 - 69 ± 5%) Chlorite (0 – 32± 2 %)	Valences: U(+4), U(+6) Phases: Uraninite (40 ± 3%) Carnotite (60 %)	Organic C: aromatic carboxylic alkyl inorganic C: not present

3.5.1 Sulfur XANES

The S K-edge XANES spectra measured for all the samples showed the presence of two major absorption peaks, the first is a broad peak over the energy range of 2471 to 2475 eV and the second at 2482.8 eV (Figure 3-8). An additional broad band in the energy range of 2485 to 2487 eV was

observed in some samples. The observed absorption bands indicate the presence of multiple oxidation state of S in the samples. The absorption band energy peaks can be assigned to oxidation states of S according to literature data (Table 3-3; ESRF database; Zeng et al., 2013). The first absorption band (2471eV to 2475 eV) may be assigned to reduced S species, such as iron sulfide minerals (e.g. pyrite), and organic sulfur (e.g. thiol groups). The second major absorption band (2482.8 eV) may be due to oxidised S species, for example sulfate or sulfonate (Solomon et al., 2003; Zeng et al., 2013). Other intermediate S species might also be present as minor components that cannot be resolved from the major features in these spectra; thus, to identify these minor components a principal component analysis (PCA) target transform was performed.

Table 3-4: First derivative of edge maximum energy positions and oxidation numbers for some S compounds based on literature (ESRF database; Zeng et al., 2013).

Sulfur compounds	**Energy positions (eV)**	**Oxidation state**
Iron monosulfide	2468.9 – 2471.1	-2
Iron disulfide	2470.8 – 2472.5	-1
Elemental sulfur	2471.7 -2472.8	0
Inorganic sulfate	2482 - 2483	+6
Organic sulfide	2472.9	0 & +6

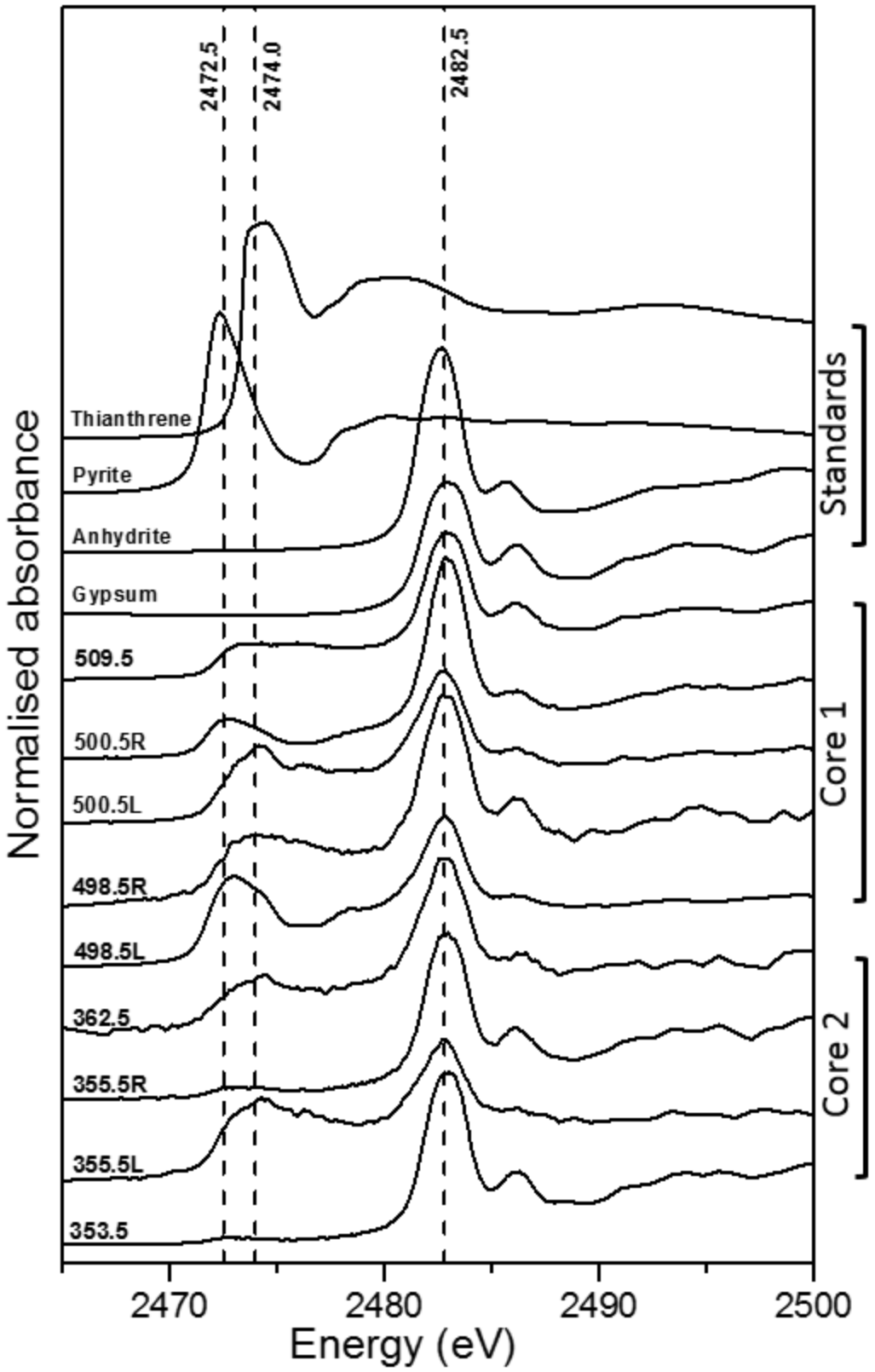

Figure 3-8: Sulfur XANES spectra for core 1 and core 2 samples and reference spectra.

Results from PCA showed the presence of four principal components. These components were based on the indicator function (IND of Malinowski) values and variance which indicate major components in the spectra (Malinowski, 1978). A target transform analysis comparing the principal component spectra to reference standard spectra showed a match for pyrite, gypsum, anhydrite and organic sulfur thianthrene ($C_{12}H_8S_2$). The surety of these S species was assessed using their spoil values (Table B-1). Spoil values between 0 and 6 are generally considered acceptable for linear combination fitting (LCF) analysis (Malinowski, 1978). As expected, the reduced sulfur phase pyrite had a spoil value of 1.07, and is an excellent candidate for quantification analysis. The sulfate minerals gypsum and anhydrite had spoil values of 1.90 and 1.78 respectively, and are also good for quantitative analysis (Table B-1). The presence of pyrite in the core samples was also confirmed in the PXRD analysis.

Quantification of the different S species present in the core were obtained using LCF. Results from the LCF analysis (Table 3-5) show that the samples are comprised of reduced and oxidised S species. Figure 3-9 shows LCF plots from core 1 (sample 500.5R) and core 2 (sample 353.5) showing the contribution of the different S species in the core samples. The LCF results from the samples indicated that sulfate minerals (gypsum and anhydrite) were approximately 30 - 70 % w/w of the S K-edge spectra while organic S species thianthrene accounted for about 3 - 40% w/w of S K-edge spectra. The sulfide phase pyrite on the other hand was found to account for almost 5 - 20% w/w of the S K-edge spectra except in the coal lens sample 495.5 L from core 1, where it was 41% w/w of the S K-edge spectra. In general, observed percentages of pyrite were higher in samples containing coal lenses than samples containing just sandy materials.

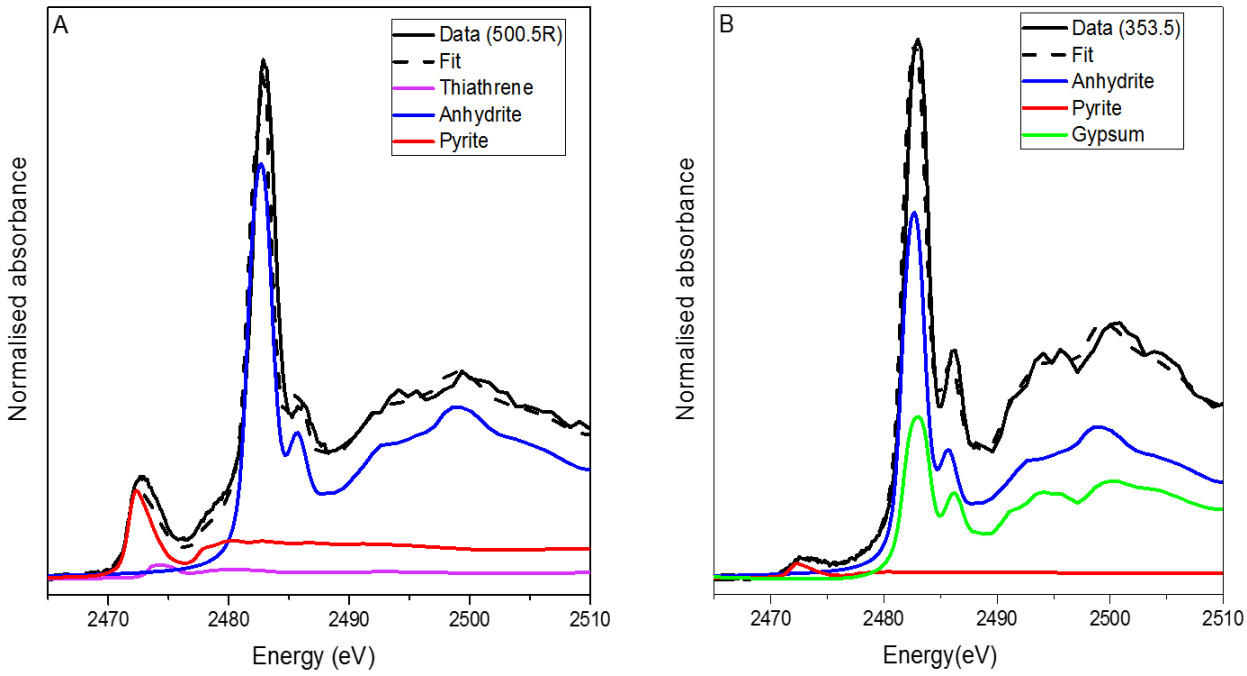

Figure 3-9: Experiment and linear combination fit for S K-edge XANES spectra for (A) 500.5R (core 1) and (B) 353.5 (core 2) together with spectra for three standards scaled according to their functional contributions to the fitted spectra.

Table 3-5: Weight of components from bulk S K-edge XANES LCF in core 1 and core 2. The sum of the components was forced to 1.

	Sample ID	Anhydrite	Gypsum	Pyrite	Thianthrene	Sum	R-factor
Core 1	498.5L	0.36± 0.01	0.00	0.41±	0.23 ±0.02	1.00	0.060
	498.5R	0.55± 0.03	0.00	0.13±	0.32 ± 0.05	1.00	0.025
	500.5L	0.44 ± 0.01	0.00	0.15 ±	0.42 ±0.02	1.00	0.058
	500.5R	0.78 ± 0.01	0.00	0.19 ±	0.03 ± 0.01	1.00	0.016
	509.5	0.44 ± 0.04	0.22 ±	0.13 ±	0.21 ± 0.01	1.00	0.015
Core 2	353.5	0.57 ± 0.01	0.39 ±	0.08 ±	0.21 ± 0.01	1.00	0.003
	355.5L	0.32 ± 0.01	0.00	0.23 ±	0.45 ± 0.05	1.00	0.090
	355.5R	0.50 ± 0.01	0.40 ±	0.05±0.01	0.05 ± 0.01	1.00	0.003
	362.5	0.58 ± 0.01	0.00	0.13 ±	0.29 ± 0.029	1.00	0.071

Migration and retardation of U in groundwater are control by processes that include sorption (Langmuir, 1978; Hsi & Langmuir, 1985). Sorption of U on mineral surfaces depends on pH and availability of complexing agents such as sulfate (Bachmaf et al., 2008). At pH values greater than 6, sulfate has barely any impact on U sorption on the clay mineral bentonite, and hydroxide- uranyl complexes are observed to dominate the total dissolved U (Bachmaf et al., 2008). Therefore, at the current pH of the site (8.2-8.3), we expect the presence of sulfate minerals in our core samples may not necessary affect sorption of U onto the clay minerals. However, pyrite present in the core may favour the reduction and precipitation of reduced U minerals thereby controlling the concentration of soluble U minerals in the core samples.

3.5.2 Iron XANES

Normalised Fe K-edge spectra of the samples from core 1 and core 2 with reference standards are shown in Figure 3-10. The spectra are characterised by a broad pre-edge peak centered at 7113.6 eV (consistent with reduced iron phases) and a white line at 7130 eV (consistent with Fe (III) minerals e.g. goethite, hematite and lepidocrocite) (Prietzel et al., 2007) (Figure 3-10). A secondary broad peak at approximately 7142 eV was also observed in some of the samples. The secondary peaks were smaller than the white line peak located at 7130 eV. Spectra for core 1 and

core 2 were compared to a set of Fe reference standards, shown in Figure 3-10. The spectra could not be fitted to a single standard reference spectrum of Fe, indicating the presence of multiple oxidation states of Fe.

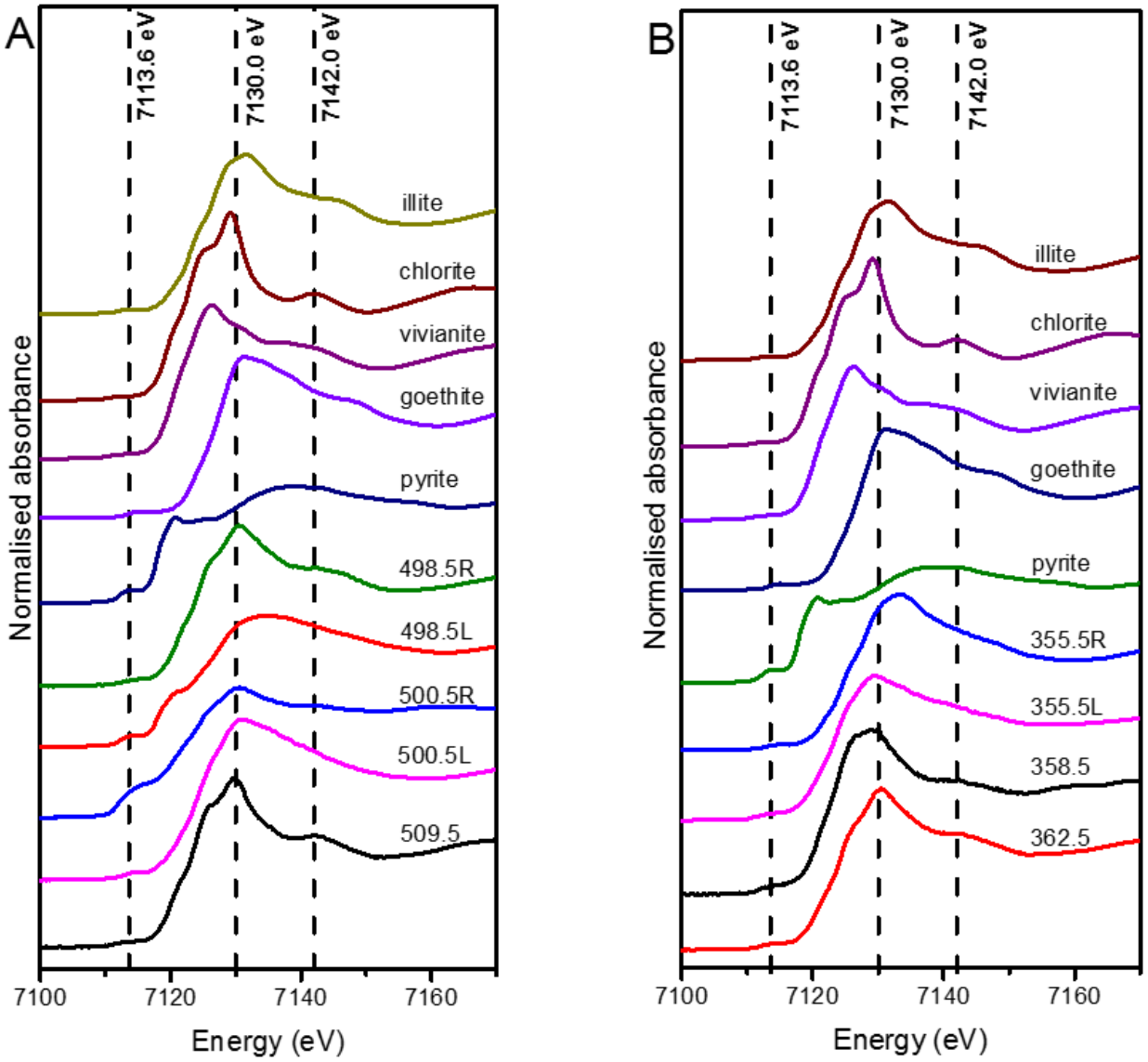

Figure 3-10: Iron K-edge XANES spectra of samples from (a) core 1 (b) core 2 with Fe reference minerals. The broken dashed lines represent K-edge energies for the different oxidation states of Fe.

Principal component analysis was used to determine the major Fe minerals present in the ore. The PCA target transform using reference Fe standards showed pyrite, goethite, illite, vivianite and chlorite as the major Fe phases present in the ore. These minerals had spoil values which are acceptable and in a range suitable for LCF analysis (Table B-2). Pyrite and goethite were chosen because they were also confirmed present in the PXRD and XANES analysis. Addition of the clay minerals in the LCF analysis was based on the observation of clay minerals in our PXRD analysis and that fact that the goodness of fit value was better when the clay minerals were used in the model. Vivianite was added based on observed iron phosphate in our PXRD analysis. The LCF was performed using the combination of five reference iron standards (pyrite, goethite, illite, vivianite and chlorite) obtained from the PCA target transform analysis. The combination of these reference standards adequately explains the contribution of each reference minerals to the spectra of the core. The residual values (R-factor), which measures the goodness of fit, was less than 0.009 (0.0002 - 0.008) and thus indicated a good fit.

The results of the LCF analysis including the goodness of fit parameter (R-factor) are shown in Table 3-6. The fitted Fe K-edge spectra for sample 498.5L (core 1) and 355L (core 2) are also shown in Figure 3-11. The LCF results indicate the presence of pyrite accounting for less than 10 % w/w of the Fe present in the core except in samples from core 1 (498.5L and 500.5R) where pyrite accounts for almost 50 % of the Fe in the core sample (Table 3-6). Goethite accounted for 1 - 60 % w/w of the Fe present. Vivianite also accounted for 5 - 30 % w/w of the Fe while clay minerals (chlorite and illite) accounted for 1 - 60 % w/w of the Fe present in the ore.

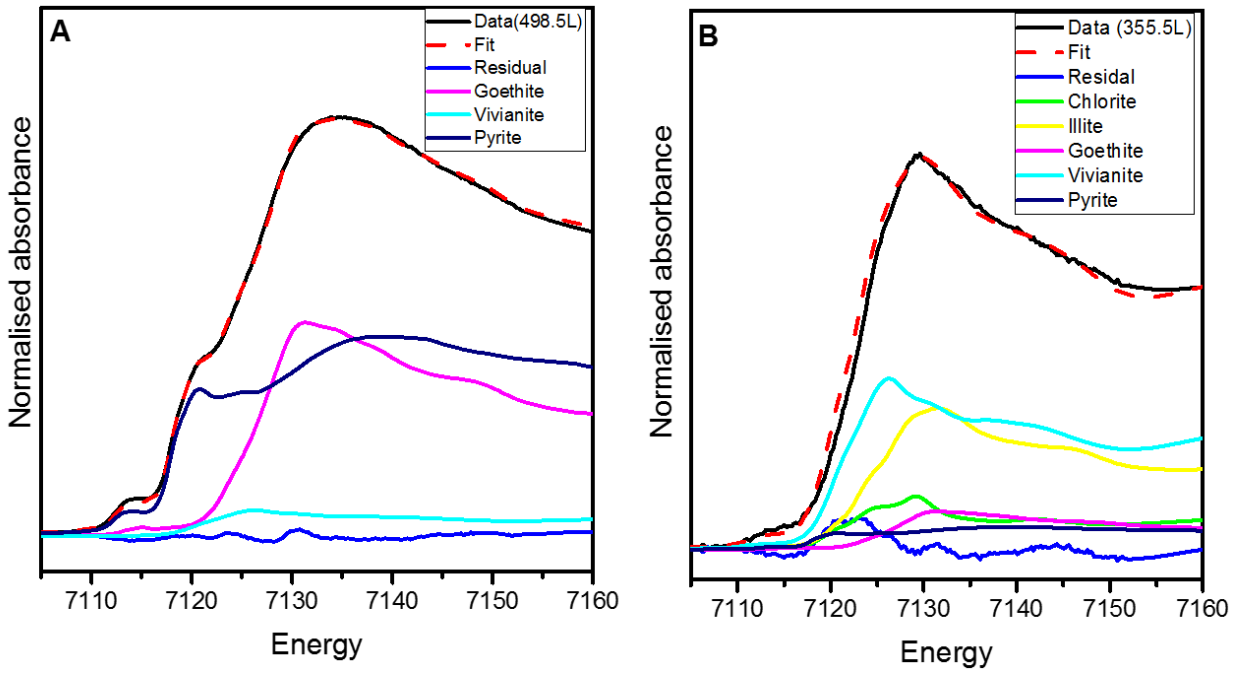

Figure 3-11: Experimental and linear combination fits for the Fe K-edge near-edge spectra for two examples: (A) core 1 (498.5L) (B) core 2 (355.5L) along with spectra representing the fractional contributions of the components used to generate the fitted spectrum.

Table 3-6: Results LCF for Fe K-edge XANES spectra for core 1 and core 2. ± is the estimated standard deviation from the fit.

	Borehole	Pyrite	Goethite	Vivianite	Illite	Chlorite	Sum	R-factor
Core 1								
	498.5L	0.53±0.01	0.42±0.01	0.05±0.01	0.00	0.00	1.00	0.0002
	498.5R	0.01±0.01	0.18±0.04	0.17±0.07	0.43±0.06	0.21±0.03	1.00	0.0024
	500.5L	0.07±0.01	0.93±0.01	0.00	0.00	0.00	1.00	0.0057
	500.5R	0.54±0.02	0.24±0.04	0.00	0.22±0.01	0.00	1.00	0.0019
	509.5	0.00	0.01±0.02	0.29±0.01	0.24±0.03	0.55±0.01	1.00	0.0004
Core 2	355.5L	0.07±0.01	0.09±0.03	0.41±0.02	0.33±0.05	0.11±0.06	1.00	0.0009
	355.5R	0.01±0.01	0.17±0.03	0.13±0.02	0.69±0.05	0.00	1.00	0.0012
	358.5	0.00	0.65±0.07	0.00	0.35±0.09	0.01±0.10	1.00	0.0089
	362.5	0.02±0.01	0.15±0.04	0.15±0.01	0.36±0.03	0.32±0.02	1.00	0.0007

The presence of pyrite in the core samples was confirmed with Fe S K-edge XANES analysis, EMPA results and PXRD analysis. The occurrence of pyrite is supported by published data from the Smith Ranch–Highlands Mine Unit 4 (WoldeGabriel et al., 2014). The appearance of vivianite confirms the presence of phosphate which is essential in understanding U chemistry. Uranium has been found to bond to phosphate in low pH environment resulting in the precipitation of uranyl phosphate minerals such as autunite and meta-autunite (Fomina et al., 2007; Ray et al., 2011). Phosphate activity has also been demonstrated to control U mobility under a range of aerobic and anaerobic conditions at low to neutral pHs (Beazley et al., 2011).

The iron oxide mineral goethite was present in the Fe K-edge XANES data and this is consistent with the PXRD results, and with previous reports (WoldeGabriel et al., 2014). The presence of goethite may provide surface area for U sorption. Observed clay minerals associated with Fe phases (illite and chlorite) can greatly enhance U uptake from the system. Uranium has been

confirmed to adsorb directly on chlorite surface by inner-sphere complexation and the adsorption is even greater in the presence of Ca and CO_3 minerals (Singer et al., 2009).

3.5.3 Uranium XANES

Attempts were made to collect U L(III)-edge XANES spectra on all the samples, however spectra were only obtained in one sample; sample 355.5L (core 2). This may be explained by the fact that U concentrations were below the detection limit of the beamline. The ICP-MS analysis showed 954 µg/g of U in sample 355.5L but less than 30 µg/g of U in each of the remaining samples (Table A-1). Another reason why we could not detect the U on HXMA may be due to how U was distributed in the ore samples; whether U was uniformly distributed or found in localised spots within the core samples. The HXMA beamline is used for bulk measurements thus it is difficult to obtain measurements on localised spots because the beam cannot be focussed on a very small region of the sample.

Uranium L-edge XANES spectra from sample 355.5L together with four reference U standards are shown in Figure 3-12. The spectra exhibited mixed peak position characteristics; an indication of mixed reduced and oxidised U phases in the sample. Uranium L(III)-edge XANES spectra of core samples from the Smith Ranch-Highland Mine Unit 4 also confirms the presence of oxidised and reduced forms of U (WoldeGabriel et al., 2014; Gallegos et al., 2015b).The U standards were chosen to reflect the two [(U(IV) and U(VI)] most common oxidation state of U in environmental samples. The increase in valence charge of U is associated with an increase in energy position of the U peak (Kosog et al., 2012); U(IV) minerals have their white line at an edge energy lower than that observed in U(VI) minerals (Kosog et al., 2012). The bulk U L-edge spectrum of sample 355.5L is characterised by a peak at 17169 eV and a post-edge oscillation at approximately 17210 eV. The spectrum resembles that of uraninite (UO_2); because both spectra have an intense white line at 17169 eV. The spectrum also has a small shoulder feature at around 17178 eV (Figure 3-12). The presence of the shoulder feature is reported to be from a multiple scattering effect that indicates the existence of oxidised U species (Crean et al., 2014).

Linear combination fitting results indicated that the U L-edge XANES spectra was dominated by carnotite ($K_2(UO_2)_2(VO_4).3H_2O$) that accounted for 60 ± 2 % w/w of the U L-edge spectra and uraninite also accounted for 40 ± 3 % w/w of U L-edge spectra (Figure 3-13). The use of carnotite

and uraninite is to represent the percentage of U(VI) and U(IV) species present in the core samples, respectively. The analysis reported a goodness of fit (R-factor) of 0.0049 and a reduced chi square value of 0.00103, thus indicating a good fit for the spectrum. Uraninite and carnotite are among the U minerals previously identified at the Smith Ranch-Highlands mine (Dahlkamp, 2010), thus confirming the presence of oxidised and reduced U phases associated with the MUB samples.

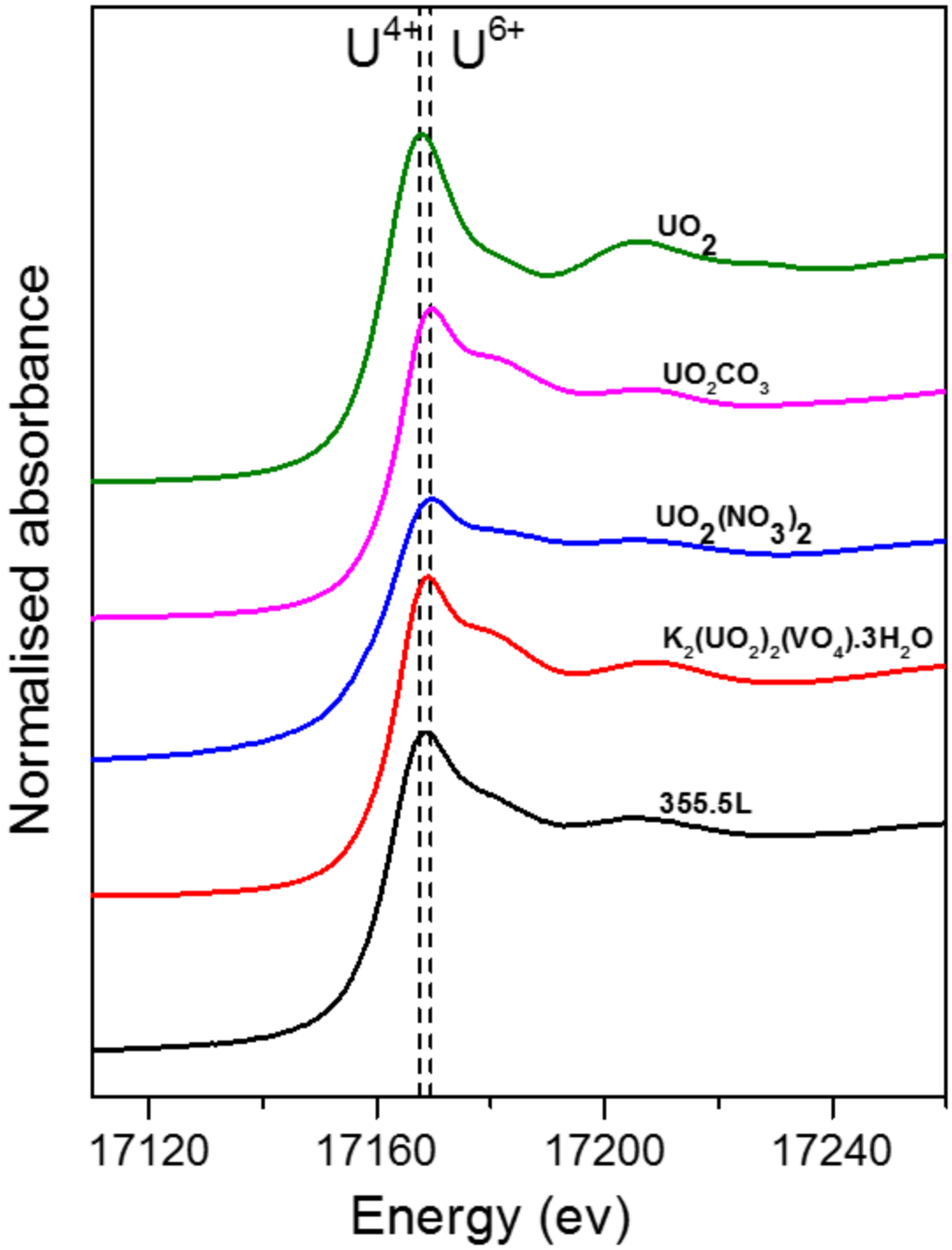

Figure 3-12: Uranium L-edge XANES of sample 355.5L together with reference standards representing U(IV) and U(VI) phases.

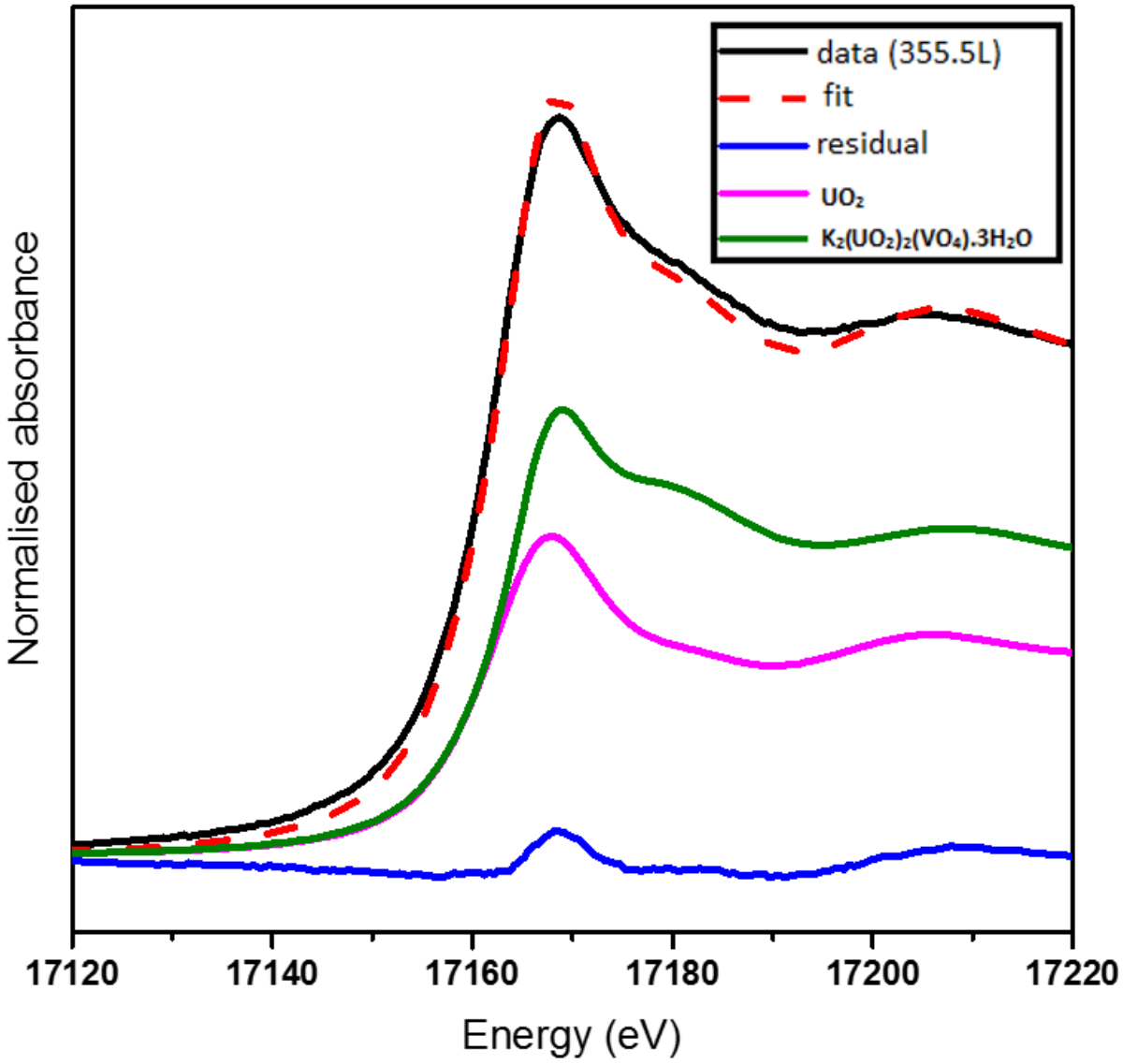

Figure 3-13: Experimental and linear combination fits for the U L-edge XANES spectra of sample 355.5 along with spectra representing the fractional contributions of the components used to generate the fitted spectrum.

3.5.4 Carbon XANES

Carbon K-edge XANES anaysis was performed to determine the functional groups of C in the core sample. Organic C can reduce solube U(VI) to insolube U(IV) while inorganic C can also co-precipitate and form complexes with U. Bulk C K-edge XANES spectra for the samples and a reference compound (lignite) are shown in Figure 3-14. The spectra exhibited the presence and

abundance of several organic functional groups, characterised by features in the near-edge region. The peak features at 285.1, 288.1, and 289.2 eV correspond to aromatic, carboxylic and alkyl groups, respectively. The C funtional groups were assigned based on published spectra (Hitchcock et al., 1986; Hitchcock & Ishii, 1987; Francis & Hitchcock, 1992; Urquhart & Ade, 2002) (Table 3-7). The C K-edge spectrum of the lignite standard sample showed similarities to that of the samples; thus the spectra are consistent with the presence of lignite in the core samples. The occurance of lignite in cores from the Wyoming Basin has been reported in many studies (Dahlkamp, 2010).

Inorganic and organic C content in cores were relatively low based on combustion data, with both accounting for < 10 wt % of the core except in the coal lens sample 355.5L where organic C alone accounted for 42.5 wt % of the core (Appendix A-1). Organic C concentrations were higher in samples containing coal lenses than in samples containing just sandy materials. The C K-edge spectrum of sample 355.5L also shows an intense peak feature at 283.5 eV representing quinone C. The peak at 283.5 eV was also observed in coal lens sample 500.5L which contained 4.01 wt % of organic C from the combustion analysis.

The C1s – π* transition is caused by the promotion of core electrons from the lowest lying orbital to a bound state unoccupied molecular orbital) (Brandes et al., 2004; Cooney & Urquhart, 2004). The peak feature corresponding to C1s – π* transition normally occurs at higher energies in carbonate minerals (Blanchard et al., 2016). Blanchard et al. (2016) reported a peak energy of 290.4 eV for C1s – π* transition in calcite while Urquhart and Ade (2002) reported 290.5 eV for the C1s – π* transition in carbonates m nerals. This peak position for carbonate minerals is represented by a red dotted line in Figure 3-15. From the figure, it is obvious that the characteristic feature of a carbonate peak (C1s – π* transition) is absent in all the samples, thus organic C are the major forms of C-containining phases in this system. This is consistent with with results from the Smith Ranch-Highlands Mine Unit 4 (Gallegos et al., 2015b).The presence of broad peaks around 285 eV in most of the spectra may be due to the overlapping of the functional groups as observed in the work of Brandes et al. (2004).

The samples containing sandy material have peaks at 296.9 eV and at 299.5 eV corresponding to potassium (K) $L_{2,3}$–edges. This was not surprising because the PXRD data has confirmed the presence of K-feldspars and muscovite in the core samples. The presence of muscovite and

feldspars in U core samples was also observed in the earlier work of WoldeGabriel et al (2014) at Smith Ranch-Highlands Mine Unit 4.

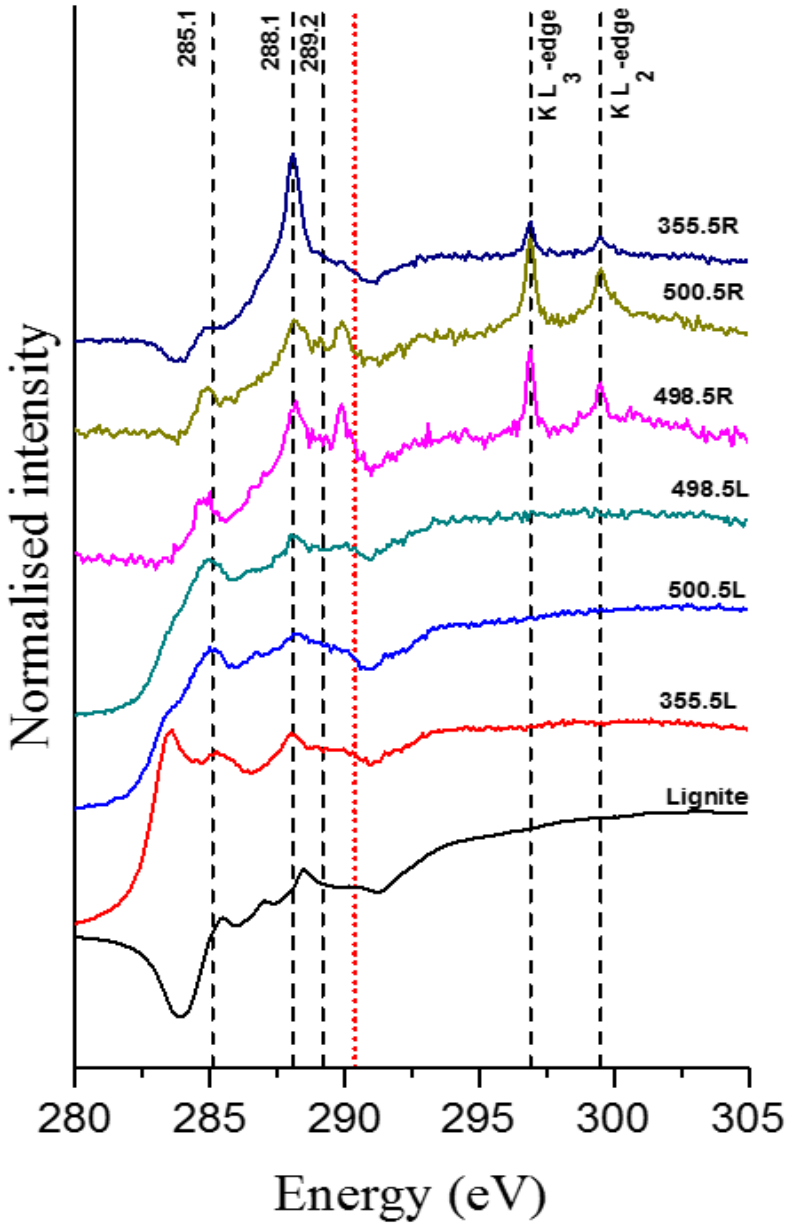

Figure 3-14: Bulk C K-edge XANES spectra for sample containing coal lenses (500.5L, 355.5L, and 498.5L) and sandy material (500.5R, 355.5R, and 498.5R). Characteristic peaks for potassium (K) L2,3-edges were observed in the sandy materials samples. The vertical red dotted line marks the location of the most distinguishable feature for inorganic C K-edge spectra.

Table 3-7: Carbon K-edge energy positions based on reported data (Hitchcock et al., 1986; Hitchcock and Ishii, 1987; Francis and Hitchcock, 1992; Urquhart and Ade, 2002).

Peak energy (eV)	Organic carbon forms
283.0-284.5	Aromatic /quinone C=O
284.9–285.5	Unsaturated/aromatic C=C
286.0–287.4	Aromatic C=OH
287.0–288.5	Aliphatic C-H
287.7–288.6	Carboxylic C-COOH
289.3–289.5	Alcohol
290.3–290.6	Carbonate

3.6 Micro XRF results

To determine the distribution of elements within the ore matrix and whether U is co-occuring with other element, µXRF analysis was performed. High energy synchrotron µXRF maps (Figures 3 - 15, C-1, C-2, and C-3) illustrate the distribution of Fe, Se, Ti, Mn, As, Ca, U, Pb and V in the core samples. It is important to note that the emission peaks for some elements overlap. For instance, the emission peak for U Lα1 and Rb Kα1 partially overlap, therefore U could be masked by co-occurring Rb, or it could appear as a false positive if Rb is present but U is not. Furthermore the emission peaks for V Kα1 and Ti Kβ1 as well as that of As Kα1 and Pb Lα1 also overlap.

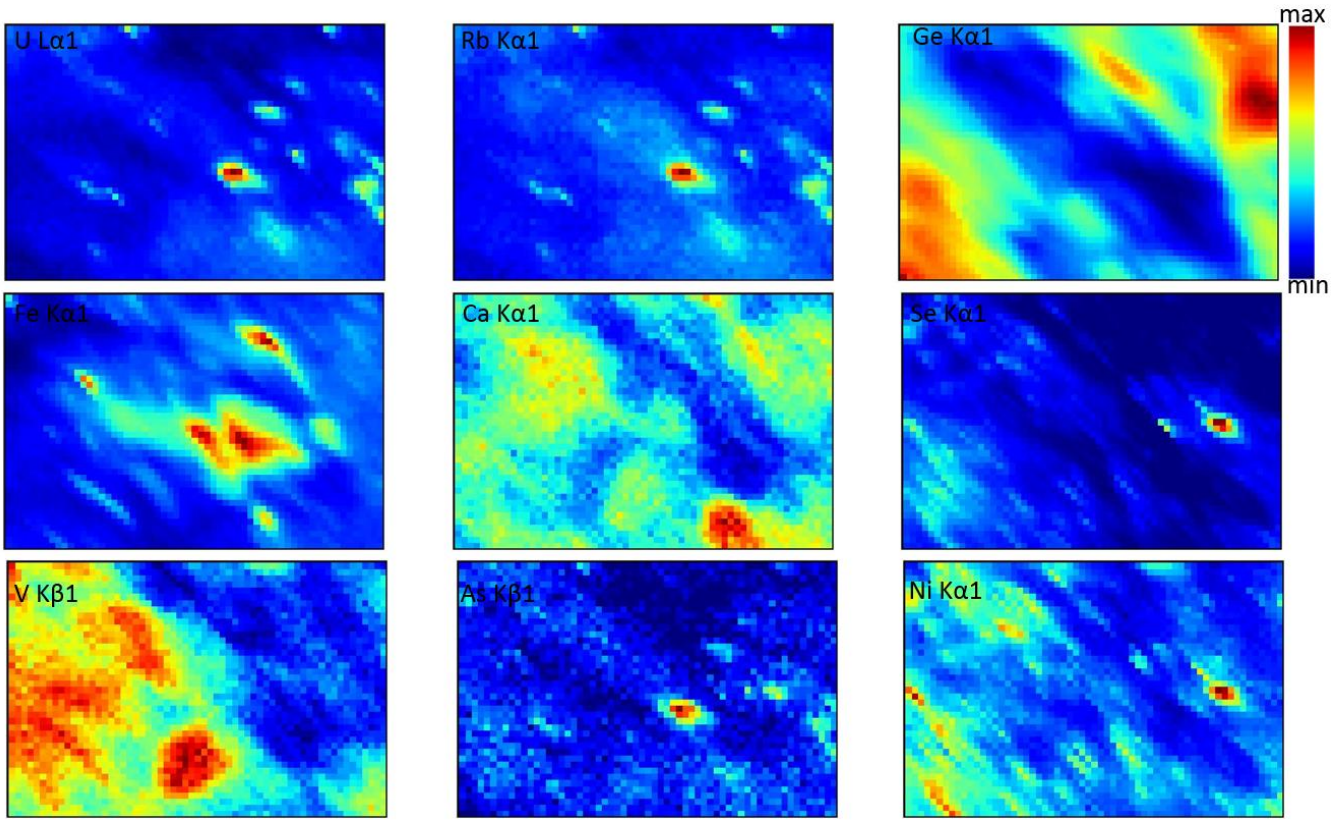

Figure 3-15: X-ray fluorescence elemental distribution map for sample 355.5L (coal lens). The size of each map is 300 µm x 200 µm. X-ray fluorescence intensities of the element are scale between maximum (red) and minimum (blue).

Potential U hotspot regions were manually inspected to confirm emission peak positions representing U were not false positives (Figure 3-16 and 3-17). All the samples were examined and true U hotspots were detected in only one sample, 355.5L sample, which was the coal lens sample, and contained a high percentage of organic matter (42.5 wt %). The absence of detectable U in the rest of the samples could be due to the low concentration of U or how U was distributed in these samples.

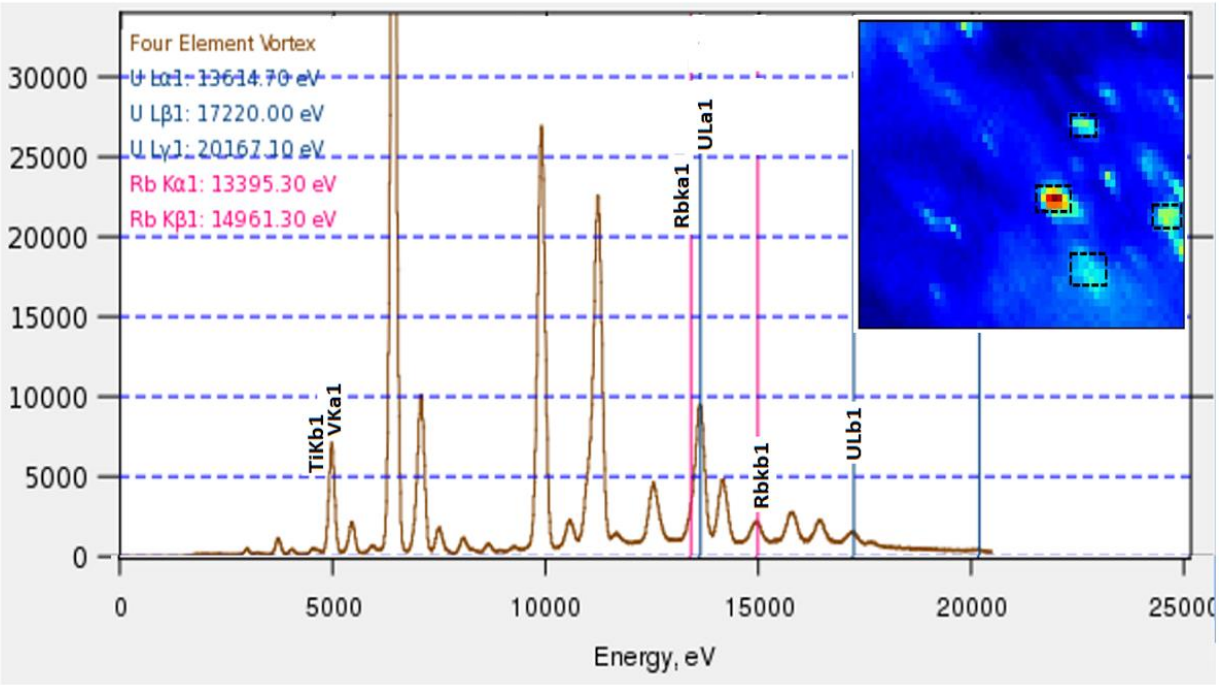

Figure 3-16: Verified U hotspots (inset, in boxes) correspond to U emission spectra in sample 355.5L (coal lenses). Scale of the image is 300 x 200 µm.

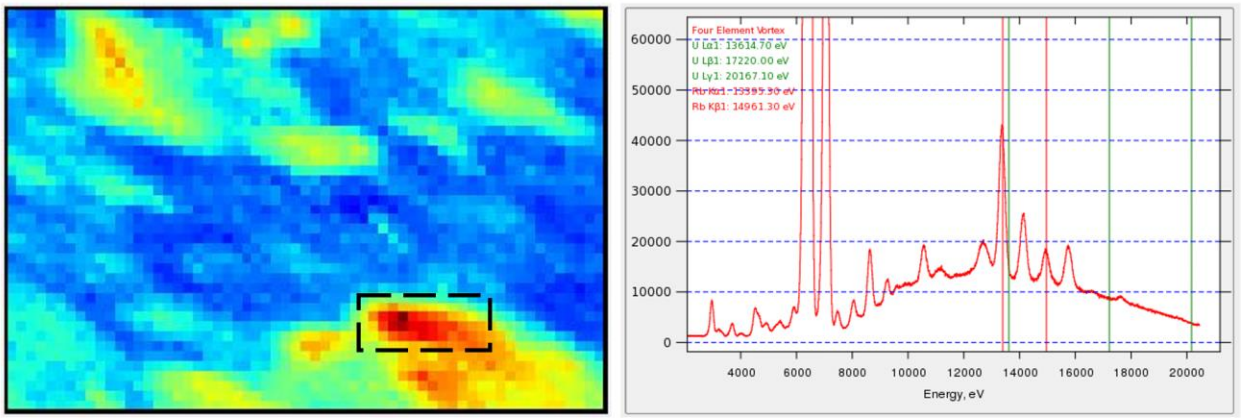

Figure 3-17: U/Rb hotspot (in black box) from sample 500.5R showing the presence of RbKα1 and RbKβ1 without any U. Image size is 300 x 200 µm

In order to investigate the co-occurance of U with other elements (e.g., Fe, Ca, Mn, V), colour overlap maps were constructed for sample 355.5L (Figure 3-18). The region of the plot where U overlaps with other element are shown in purple. Figure 3-19 shows U co-occuring with Fe, Ca, Mn, As and V, indicated by the presence of purple colour on the maps.

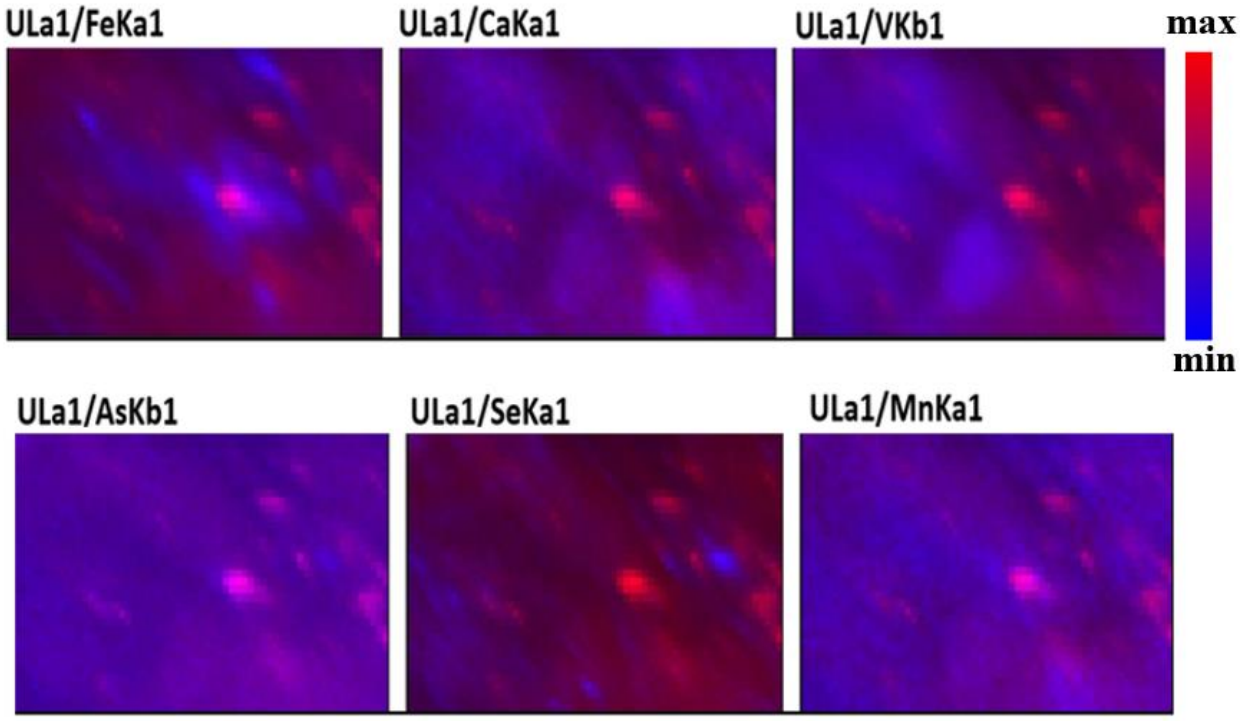

Figure 3-18: Colour overlap maps of sample 355.5L (coal lenses) showing the co-occurrence of U with Fe, Ca, V, Mn, Se, and As. Uranium are represented by red in all the maps while the other elements are represented by blue. The size of the map was 300 x 200 µm.

Tri-colour plots were also constructed to show the relationship between: U, Fe, and Ca (Figure 3-19A); U, Fe and V (Figure 3-19B); U, Ca and Mn (Figure 3-19C); and as U, Ca and V (Figure 3-19D). The presence of a pale to light yellow colour indicates a co-localization of all three elements. The strong correlation between U-V and U-Ca is consistent with the presence of the secondary U minerals carnotite ($K_2(UO_2)_2(VO_4)_2\ 3H_2O$), uranophane ($Ca(UO_2)_2(SiO_3OH)_2.5H_2O$), autunite ($Ca(UO_2)_2(PO_4)_2.11H_2O$) and/or tyuyamunite ($Ca(UO_2)_2(VO_4)_2.5\text{-}8H_2O$). These secondary U minerals have been reported to occur in the Powder River Basin within which the Smith Ranch-Highland mine lies (Dahlkamp, 2010).

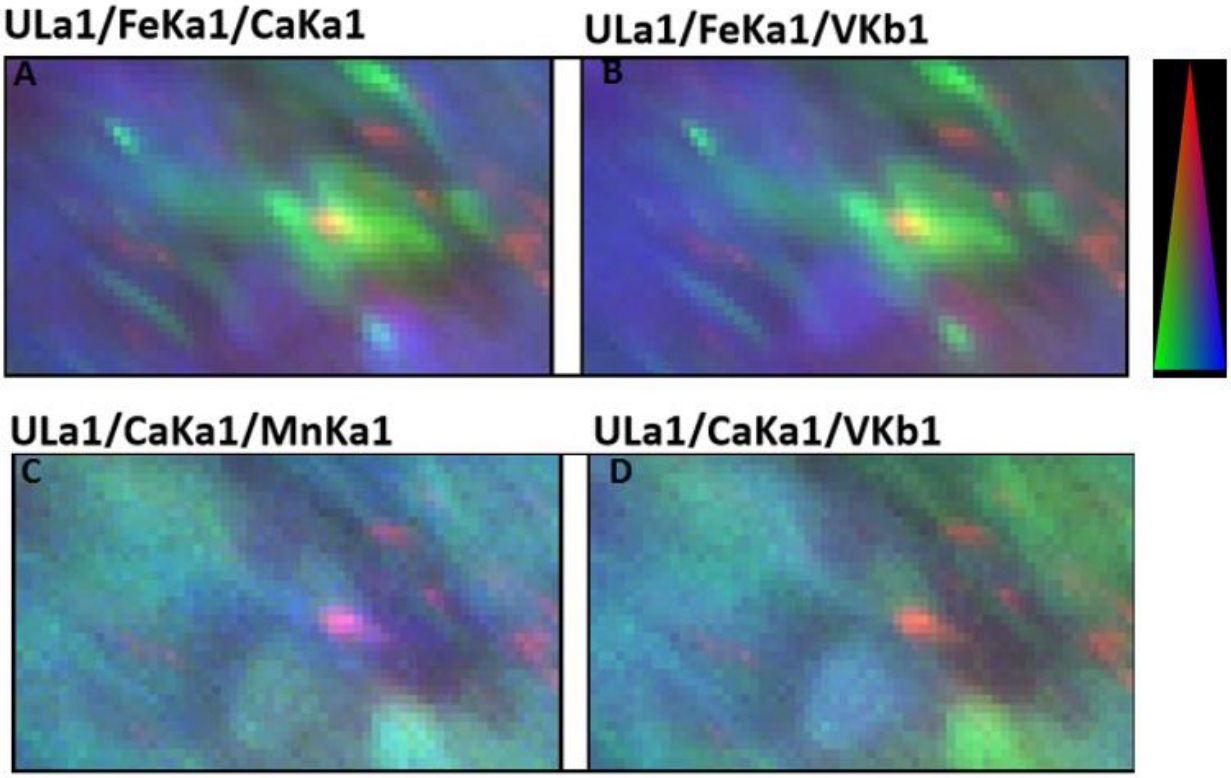

Figure 3-19: Tri-colour maps (300 x 200 µm) for sample 355.5L (coal lenses) showing the co-locations of elements with U. (A) Red=U, green=Fe and blue=Ca (B) Red=U, green = Fe and blue = V, (C) Red=U, green =Ca and blue=Mn, (D) Red=U, green =Ca and blue=V.

The cooccurance of U with other elements within the ore matrix was confirmed using correlation plots. Figure 3-20 shows a selected region of the ULa1/FKa1 correlation plot in the 355L (coal lenses) sample corresponding to areas of high Fe and high U. The co-occurance of U with Ca was also confirm and a selected portion of their correlation plot (Figure 3-21) showed region of high Ca with low U concentration.

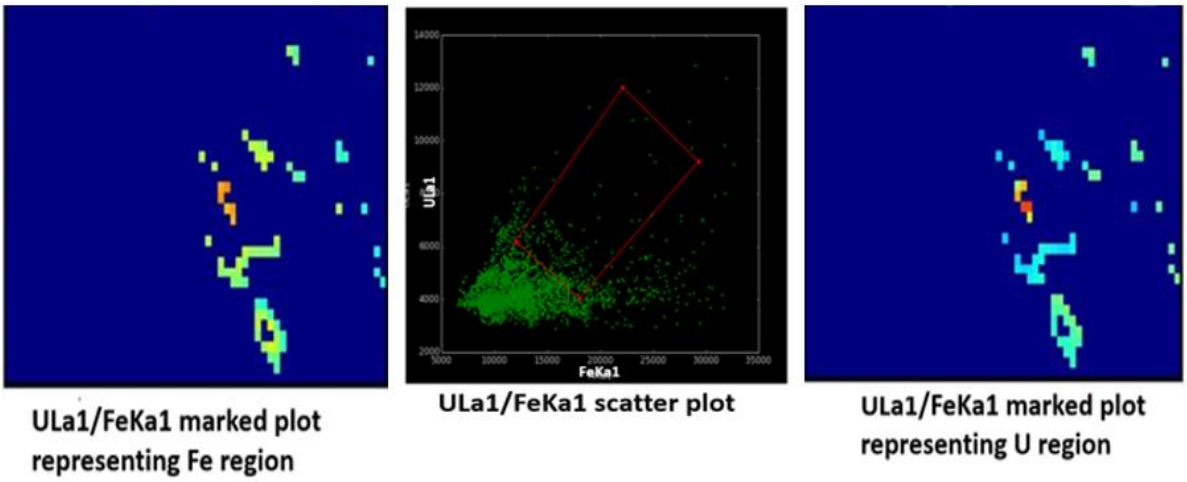

Figure 3-20: Scatter plot and colour maps plot from sample 355.5L illustrating regions of high U and Fe content. (Red=high, blue = low). Map size was 300 x 200 µm.

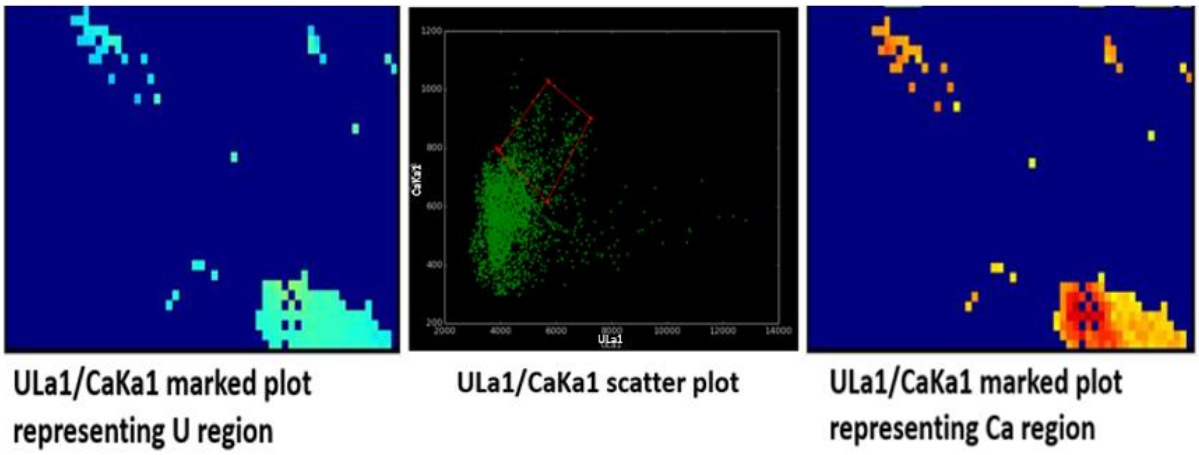

Figure 3-21: Scatter plot and colour maps plot from sample 355.5L illustrating regions of low U and high Fe content. (Red=high, blue = low). Map size was 300 x 200 µm.

3.7 Aqueous geochemistry

3.7.1 Modelling results

The solubility and mobility of U are controlled by the formation and precipitation of primary and secondary U minerals and the presence of other minerals including carbonates, Fe-oxyhydroxides, clays and organic matter (Abdelouas, 2006; Gómez et al., 2006; Gavrilescu et al., 2009). In groundwater, carbonates can serve as complexing agents and decrease adsorption of U onto minerals by forming uranyl-carbonates complexes (Langmuir, 1997). Clay minerals provide surfaces for U adsorption (Dong et al., 2011) and Fe oxyhydroxides serves as strong sorbents for U. Uranium adsorption on Fe oxyhydroxides as well as U and Fe oxyhydroxides co-precipitating have been reported to control U mobility in groundwater (Duff et al., 2002). In this study, geochemical modelling was performed to confirm the saturation state of aqueous species and minerals that may control the mobility of U at the Smith Ranch–Highlands MUB.

Results of PHREEQC geochemical modelling (using parameters from Table 2-1) from boreholes M20 and M39 (located near core sites 1 and 2, respectively) showed the groundwater is supersaturated with calcite, aragonite, siderite, dolomite, ferrihydrite, goethite, hematite, magnetite, quartz, tremolite and undersaturated with gypsum, uraninite, coffinite, fluorite, halite, and rhodochrosite (Table D-1). Figure 3-22 shows the saturation state of some common minerals in the core samples. These common minerals were chosen because of their known importance in U mobility. Note that clays are not included in this table because Aluminum (Al) concentrations were below detection in the groundwater.Phosphorus concentrations were also not reported for the groundwater data.

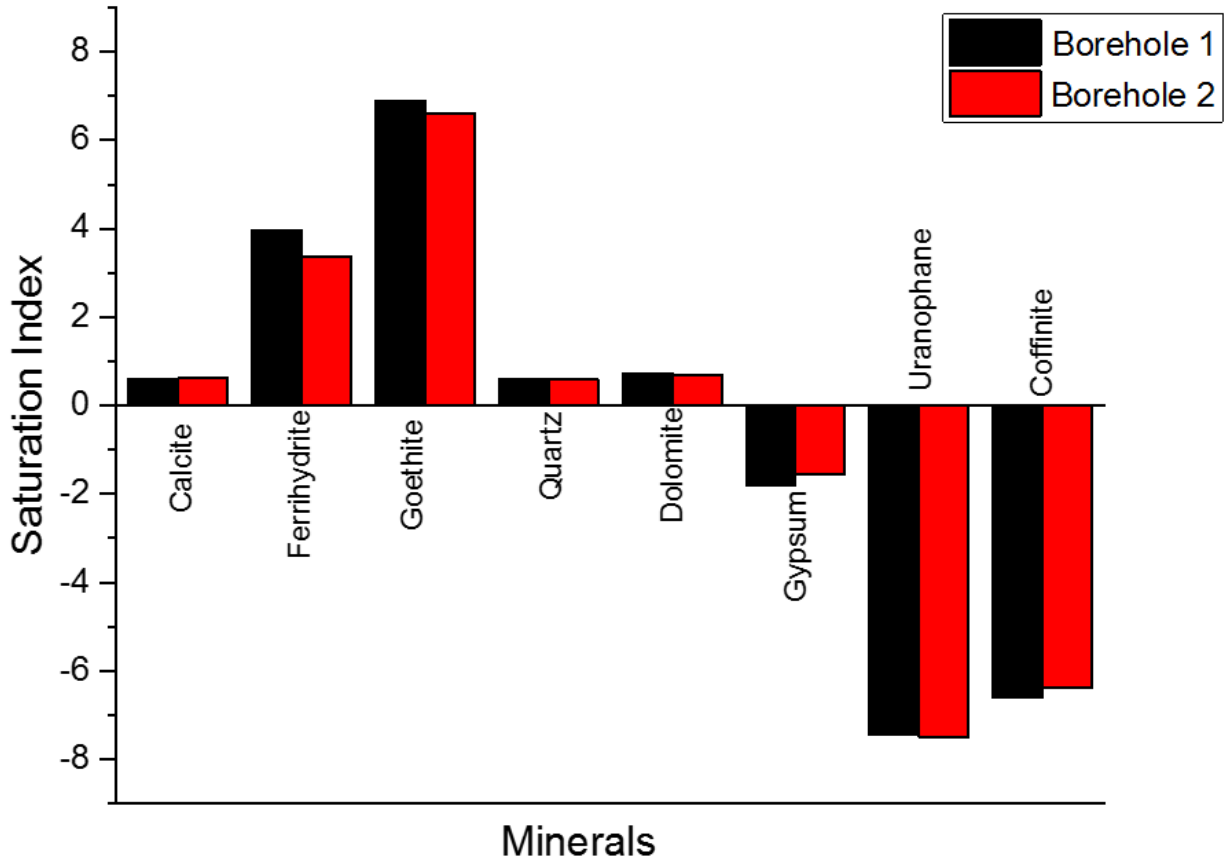

Figure 3-22: Saturation indices of selected major minerals phases for M20 (black) and M39 (red) borehole samples from the Smith Ranch-Highlands Mine Unit B.

To determine if secondary U mineral phases were controlling U concentrations in groundwater from both boreholes at current pH, Eh and temperature conditions, SI were calculated for the secondary U minerals rutherfordine (UO_2CO_3), uranophane ($Ca(UO_2)_2(SiO_3OH)_2{:}5H_2O$), uranium hydroxide ($UO_2(OH)_2$) and metaschoepite ($UO_3{:}2H_2O$). The results (Table D-1) indicate that the groundwater is undersaturated with respect to these secondary U minerals. Hence, these secondary U mineral phases may not control U concentrations in the groundwater. Calculated SI for primary U minerals uraninite (UO_2) and coffinite ($USiO_4$) (Figure 3-22 and Table D-1) also indicate undersaturation with respect to the groundwater. However, modelling results (Figure 3-22, Table D-1) showed that the groundwater is supersaturated with ferrihydrite, goethite, hematite, magnetite, dolomite, aragonite and calcite. This suggests that these mineral phases may act as sinks (geochemical controls) for dissolved U through sorption or co-precipitation. Although the groundwater is supersaturated with carbonate minerals, PXRD analyses did not show the presence

of carbonate minerals. This could be because the carbonate minerals are present in proportions below the detection limit of PXRD technique. This is likely the case, because proportions of inorganic C (0.01 - 0.32 w/w %) in the combustion analyses for the core samples were low. Furthermore, the carbonates may have been masked by the presence of other prominent peaks in the PXRD analyses.

The uranyl ion (UO_2^{2+}) can readily adsorb onto calcite and dolomite due to its high affinity for carbonates (Elless & Lee, 1998; Rihs et al., 2004; Kelly et al., 2006). Calcite is known for its buffering capabilities in soil solution and can adsorb U onto its surface at neutral pH (Zheng et al., 2003) and therefore can act as a geochemical control on U in sediments. The precipitation of calcite from Ca-rich groundwater in contact with carbonate minerals will result in lower concentrations of Ca^{2+} and CO_3^{2-} in the groundwater leading to diminished activities of ternary-uranyl-carbonates complexes. At the current pH (average pH 8.25) of the groundwater at MUB, geochemical modelling results showed the groundwater is supersaturated with respect to calcite, thus, calcite should precipitate out of the groundwater. The precipitation of calcite implies removal of Ca^{2+} and CO_3^{2-} from the groundwater thereby diminishing the activities of carbonates complexes and ternary-uranyl-carbonates complexes. The near absence of these uranyl complexes may create favourable conditions for U to adsorb onto clay surfaces.

Other studies have highlighted the importance of Fe oxyhydroxides in controlling U mobility (Murphy et al., 1999; Giammar & Hering, 2001; Wazne et al., 2003). Gabriel et al. (1998) reported adsorption of U on goethite-coated sands. Adsorption and co-precipitation of U with ferrihydrite has also been reported by Bruno et al. (1995); however, the subsequent transformation of the ferrihydrite to more crystalline goethite and haematite results in less sorption of U as compared to U sorption on a freshly prepared ferrihydrite. Although the groundwater was supersaturated with Fe oxyhydroxides including goethite, ferrihydrite, magnetite, and haematite, only goethite was observed in both the Fe XANES and PXRD analyses of the solid samples.

Because aluminum (Al) was below detection in all samples, I assumed a maximum concentration of 0.05 mg/L (half the DL of 0.1 mg/L) of Al in the groundwater in order to incorporate Al concentrations into the PHREEQC model. The model results showed that the groundwater is supersaturated with clay minerals illite, chlorite, kaolinite and other Al-containing minerals

(Figure 3-23, Table D-1). The presence of illite, chlorite, and kaolinite were also confirmed from PXRD and EMPA analysis of the solid core samples.

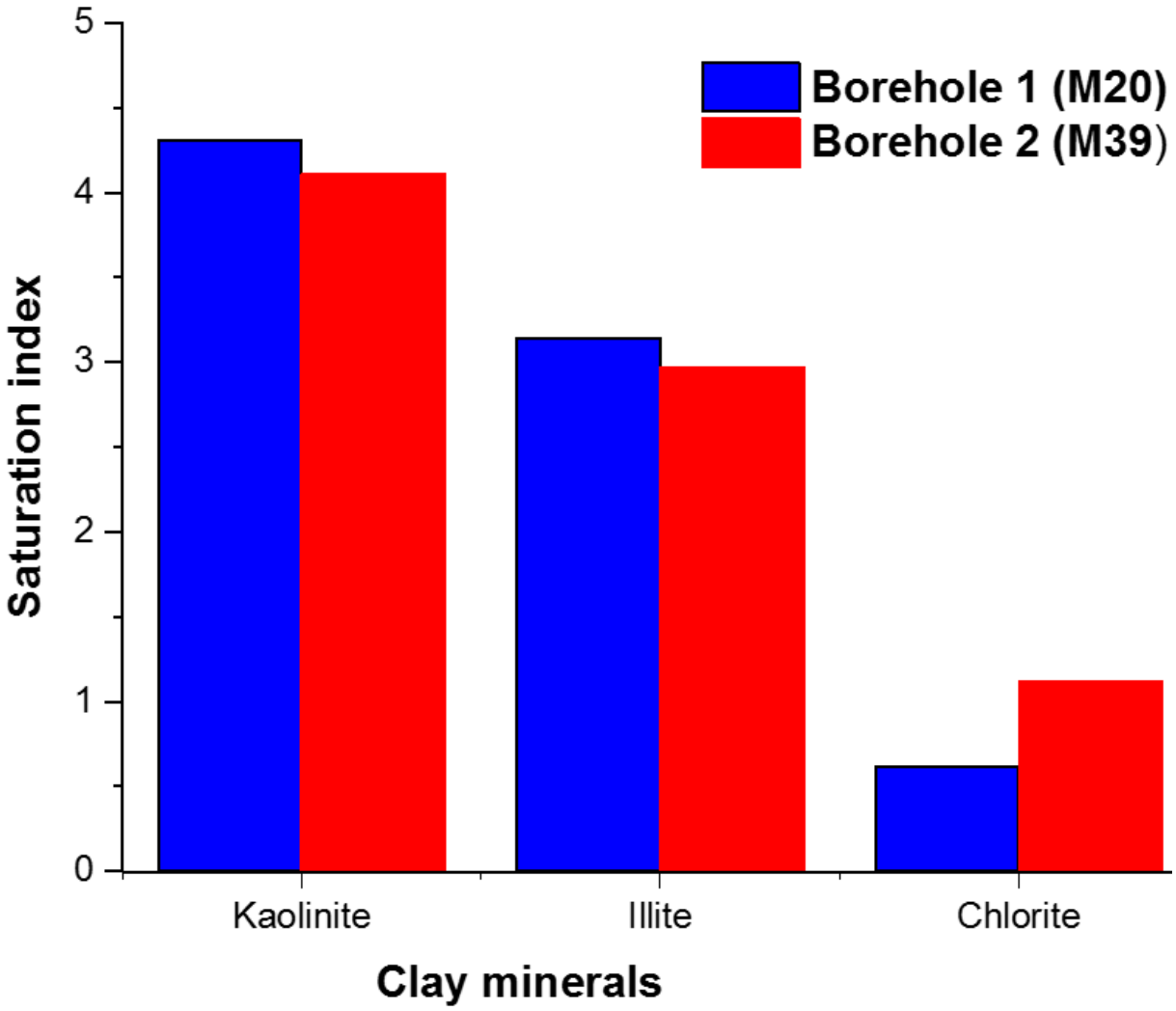

Figure 3-23: Saturation state of clay minerals at the Smith Ranch-Highland MUB in groundwater from two boreholes (M29 and M30) located near the core positions.

The master variables Eh and pH are important parameters that contribute to U speciation and mobility in groundwater (Jerden Jr & Sinha, 2003). To study the effect of pH on the saturation states of minerals that can control U mobility, a PHREEQC simulation was performed using a range in pH values (3, 5, 7, 9, and 11) at the same groundwater Eh (+80 mV). The results showed that the groundwater samples from both boreholes (M20 and M39) were undersaturated with respect to carbonate minerals (calcite, dolomite, aragonite) and iron minerals (ferrihydrite,

goethite, haematite, and magnetite) at pH below 7, near saturated (i.e. equilibrium) at circumneutral pH and supersaturated above pH 8. The silicate mineral quartz was supersaturated at pH 7 and 9 but slightly undersaturated at very alkaline pH (pH=11). Gypsum on the other hand, was undersaturated at all pH values tested. The trend was similar for the two boreholes (Figure 3-24, Tables E-1 and E-2).

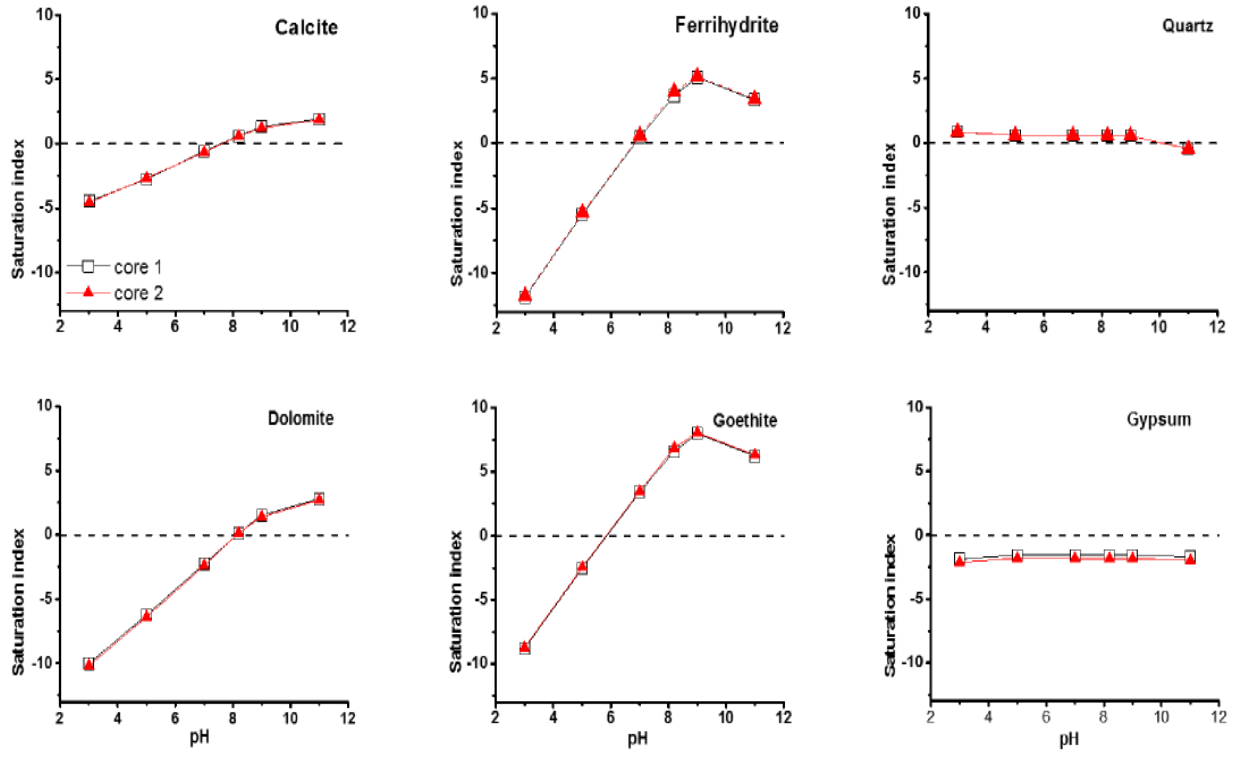

Figure 3-24: Saturation index of some important mineral phases in MUB groundwater, at varying pH conditions (Eh = +80 mV). The data points for both M39 and M20 overlaps.

The effect of different pH conditions on secondary U mineral phases were tested in the PHREEQC model. The simulation results (Figure 3-25) indicate that the groundwater is undersaturated with respect to secondary U mineral phases (rutherfordine, metaschoepite, paulscherrerite, and uranophane) at the different pH conditions tested. On the other hand, the groundwater samples from both boreholes were found to be undersaturated at pH > 5, but supersaturated at pH 3 and 5 with respect to primary U minerals (uraninite, coffinite). This implies that a change in the current pH of the groundwater to pH ≤ 5 at the current redox potential of the groundwater (Eh =+80 mV)

may result in the precipitation of primary U minerals. This could help to control the concentration of U in the groundwater. However, this is unrealistic considering the current conditions at the site.

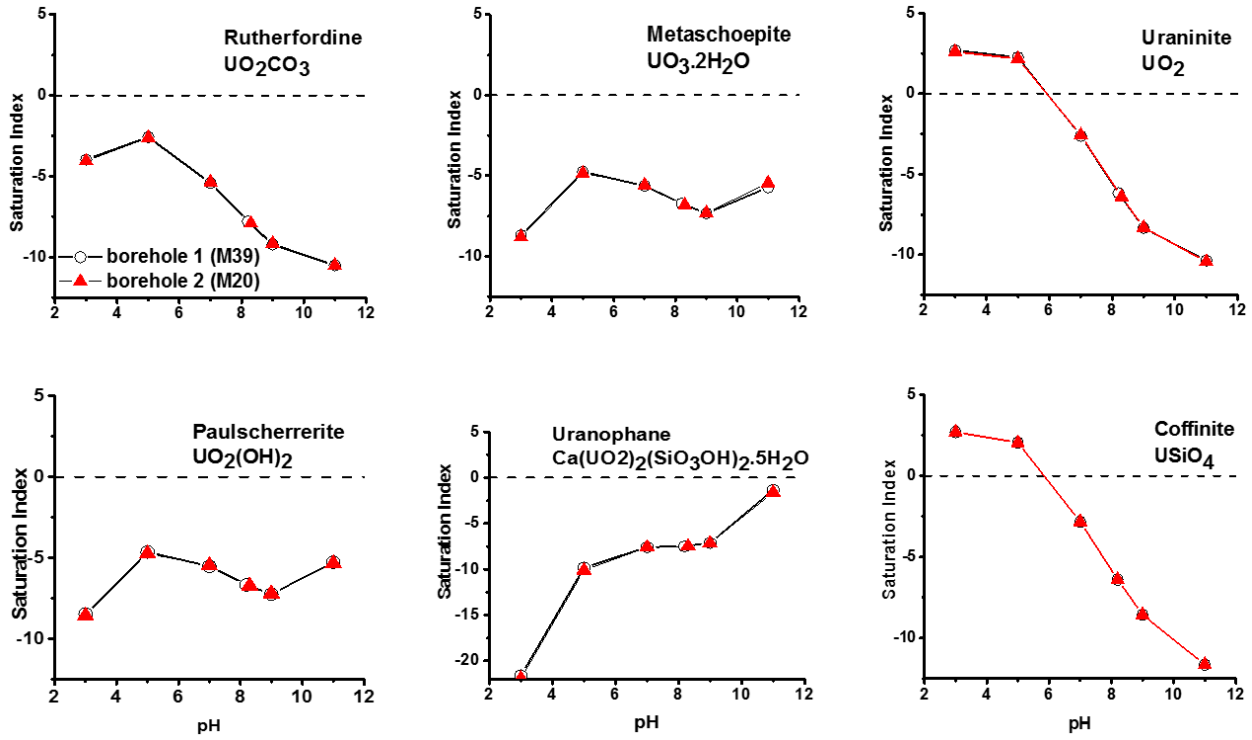

Figure 3-25: Saturation indices for secondary and primary U minerals for borehole M39 and borehole M20 under different pH conditions and Eh of 80 mV using PHREEQC. The data points for both M39 and M20 overlaps. The vertical dashed line represent saturation at zero (equilibrium).

To determine the effect of redox conditions on the minerals that control U mobility, a range of redox potentials were tested in the PHREEQC model. The model used Eh values of -100, -150, -200, +80, +100, +150, +200, +300 mV, at the current groundwater pH (8.2 for borehole M39 and 8.3 for borehole M20). The Eh values were converted to pE (-1.7, -2.5, -3.4, +1.3, +1.7, +2.5, +3.4, +5.1V) using the equation below because the PHREEQC model requires input for pE instead of Eh.

$$pE = \frac{F}{2.3RT} \text{ x Eh (mV)} \quad (5)$$

Where R = The universal gas constant = 8.31 JK^{-1} mol^{-1}
T = Temperature in Kelvin
F = Faraday constant =23.1 kcal V^{-1} $equiv^{-1}$

The results of the simulation are presented in Figure 3-26, Table F-1 and Table F-2. The results showed that the groundwater is supersaturated with carbonate minerals (calcite, dolomite) under the current pH conditions and the saturation state of these minerals is unaffected by changes in the redox potential of the groundwater. The results also show that the groundwater is supersaturated with the Fe mineral goethite over the range of the redox potential values tested. The SI for goethite also increases with an increase in redox potential of the groundwater (Figure 3-26). This implies that goethite can likely precipitate out of the groundwater and provide a surface for U adsorption over the range of redox potentials tested. Ferrihydrite was also calculated to remain in solution at negative Eh values, but it begins to precipitate when Eh values approach a positive value. The tested range of Eh values did not show any effect on quartz as it remains supersaturated and reported no change in SI values throughout the simulations. The results show that for gypsum and quartz, the SI values did not change with changes in the Eh. The SI values for gypsum remained negative while those for quartz remained positive over the Eh range tested. This implies that groundwater is undersaturated with respect to gypsum and supersaturated with quartz over the range of Eh tested.

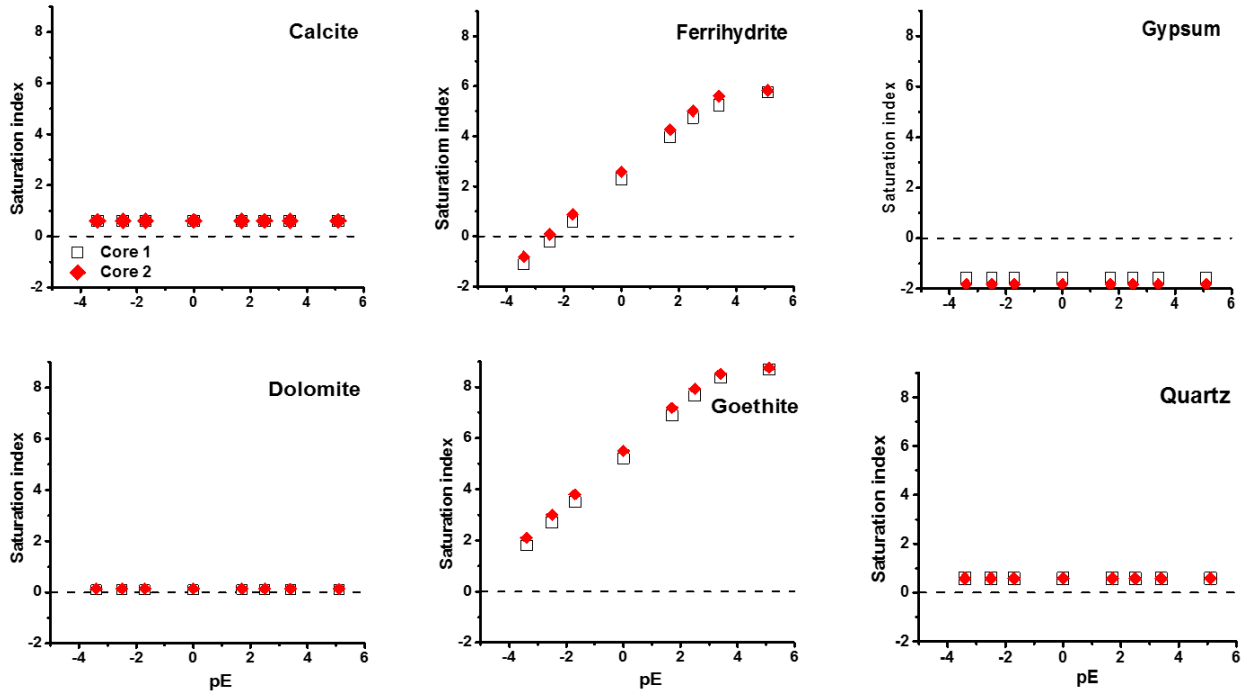

Figure 3-26: Geochemical modelling results with varying Eh from M20 (red pyramid, pH 8.3) and M39 (square plain box, pH 8.2). The data points for both M39 and M20 overlaps. The horizontal dashed line represents SI = 0.

To determine the effects of varying redox conditions on primary and secondary U mineral phases in the groundwater, SI was calculated for secondary U minerals (uranophane, rutherfordine) (Figure 3-27). The model results indicate undersaturation of the groundwater with respect to the secondary U minerals under the different redox conditions tested. The groundwater showed supersaturation with the primary U minerals, uraninite and coffinite (Figure 3-27) only at negative Eh values. The tested redox potentials did not have any effect on clay minerals because they remain supersaturated and maintain the same saturation index values. These trends are similar for both borehole M20 and M39.

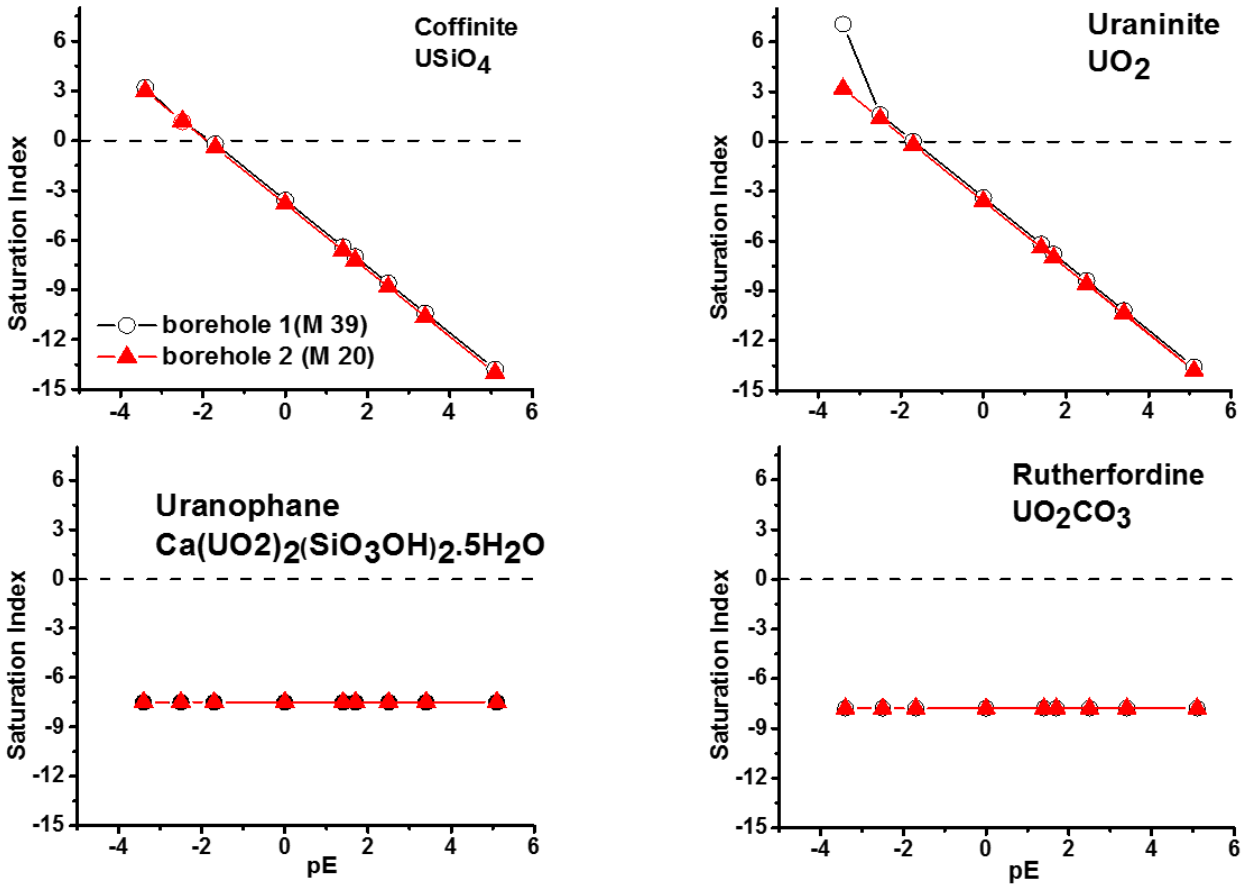

Figure 3-27: Saturation indices of U mineral at different Eh condition for borehole 1 (M39) at pH 8.2 and borehole 2 (M20) at pH 8.3. The vertical dashed line represent saturation at zero.

Pourbaix diagrams were generated using Geochemist's Workbench (Bethke & Yeakel, 2017) for the groundwater system and are shown in Figure 3-28. The diagrams depict the stability fields and mineral phases for Fe, C, S, and U species in the groundwater at 13˚C (the groundwater temperature). The activities for Fe, C, S and U were obtained from the modelling results (8.061 x 10^{-4} M, 3.463 x10^{-3} M, 1.099 x10^{-3} M and 4.389 x10^{-22} M, respectively). Samples from borehole M20 and M39 were plotted from measured pH and Eh values. The Eh-pH diagram for aqueous U in the presence of carbonate, iron and sulfate ions at 13˚C is shown in Figure 3-29. The sample plot from the M20 and M39 groundwater pH and Eh values falls in the region dominated by $UO_2(CO_3)_3^{4-}$. Therefore $UO_2(CO_3)_3^{4-}$ is the likely form of U-carbonate complexes in the Smith Ranch-Highland MUB groundwater.

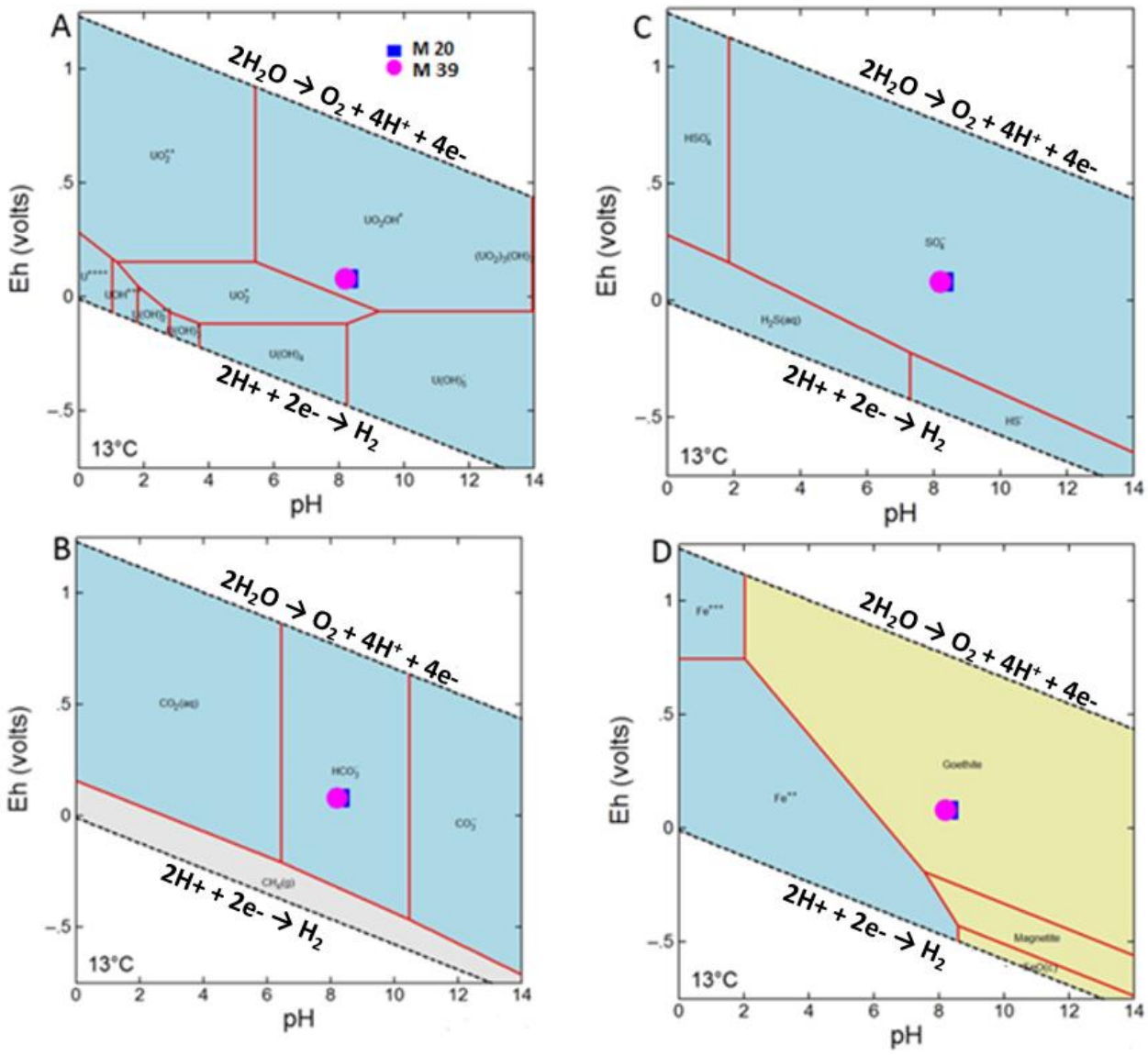

Figure 3-28: Pourbaix diagram illusstrating the stability fields of (A) U species, (B) carbonates species (C) S species and (D) Fe species. Sample plot (purple circle for M20 and blue squares for M39) from measured Eh and pH values of the boreholes.

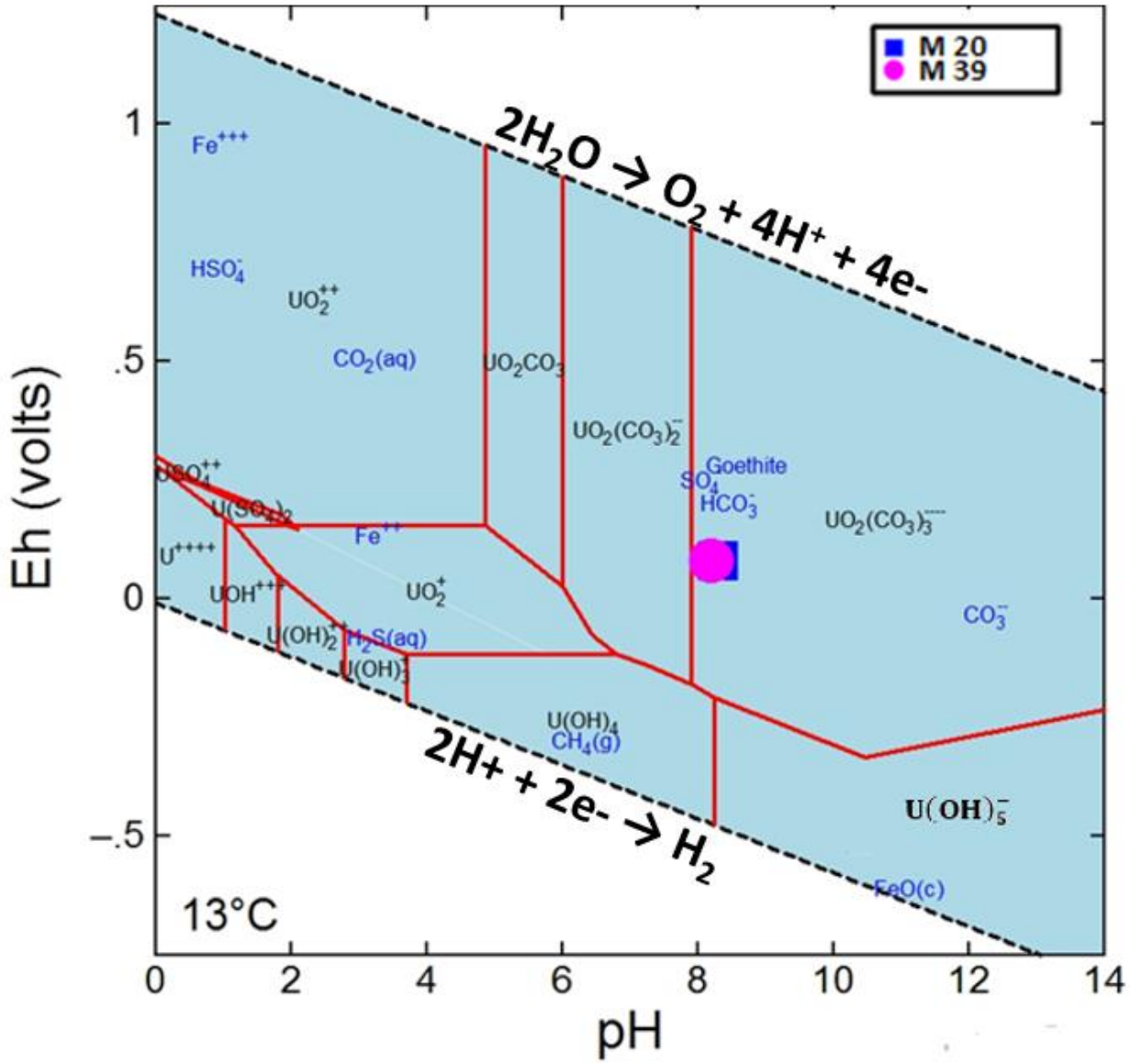

Figure 3-29: pH-Eh diagram of UO_2-C-S-Fe-H_2O system at 13˚C and 1 bars. [Fe]= 8.061 x 10^{-4} M, [C] = 3.463 x10^{-3} M, [S] =1.099 x10^{-3} M and [U] = 4.389 x10^{-22} M.

The modelling results suggest that secondary U minerals do not control the mobility of U in the groundwater but the primary U minerals may act as a possible sink for dissolved U at low pH (3 – 5). However, such low pH values are unrealistic at this mine site. At pH > 5, dissolved U concentrations in the groundwater are dominated by U(VI) species. These U(VI) species are soluble and may form complexes in the presence of ligands such as carbonate ions. The model identifies the presence of ternary aqueous uranyl complex ($Ca_2UO_2(CO_3)_3$ and $CaUO_3(CO_3)_3^{-2}$)

and other complexes including $UO_2(CO_3)_3^{-4}$ and $MgUO_2(CO_3)_3^{-2}$). The formation of these complexes results from carbonate, Mg and Ca present in the groundwater.

At pH values greater than 4, $Ca_2UO_2(CO_3)_3$ and $CaUO_3(CO_3)_3^{-2}$ species dominate U in the groundwater and become the major species controlling dissolved U(VI) concentrations in the groundwater followed by other complexes $UO2(CO_3)_3^{-4}$ and $UO_2(OH)_3^-$. Uranyl and related complexes have been found to adsorb on surfaces of iron hydroxide, clay minerals and organic matter (Hsi & Langmuir, 1985; Bachmaf et al., 2008; Cumberland et al., 2016) thereby decreasing U solubility in groundwater. The observed $Ca_2UO_2(CO_3)_3$ and $CaUO_3(CO_3)_3^{-2}$ may affect the adsorption of U onto mineral surface. $Ca_2UO_2(CO_3)_3$ and $CaUO_3(CO_3)_3^{-2}$ has been reported to decrease uranyl adsorption onto mineral surface and also limit biotic reduction of U minerals (Wazne et al., 2003; Neiss et al., 2007). From this model, we can predict that at the current pH and Eh condition of the site, primary and secondary U minerals may not be responsible for controlling U concentrations in the groundwater. However, the presence of carbonates, clays, and Fe-oxyhydroxides which are all supersaturated in the groundwater may control U concentrations and mobility in groundwater.

3.8 Conceptual model

A Conceptual model of the aquifer solids downgradient of Smith Ranch-Highlands MUB include considerations of the mineralogical and geochemical data from cores and the groundwater that surrounds the mine unit. The aquifer materials consist of arkosic sandstone containing clays, Fe oxides, pyrite and carbonates; all of which are likely important in controlling U mobility. Figure 3-30 shows a simple model that depicts the mineralogy and its importance in U mobility at the current pH and Eh conditions of the groundwater. The presence of minerals such as clays and goethite are likely to act as controls on U concentrations through precipitation and adsorption. Uranium can also incorporate into Fe mineral structures thereby decreasing U availability in groundwater. Reduction of soluble U(VI) to insoluble U(IV) can also occur in the presence of microbes, reduced iron in minerals (e.g. pyrite), and organic matter.

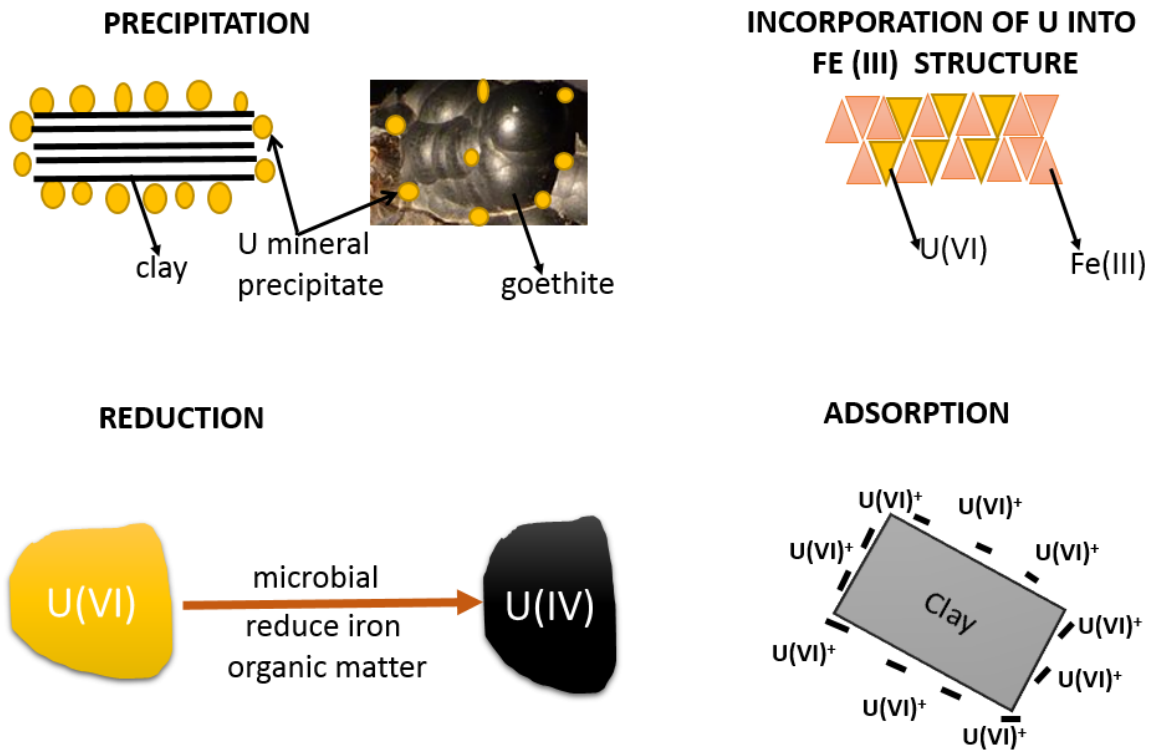

Figure 3-30: Conceptual model of U immobilization mechanism at pH of 8.2 and Eh of +80 mV. Illustration is not to scale.

At different pH and Eh conditions, the saturation states of minerals can be useful in predicting how natural attenuation processes such as precipitation and adsorption can help in U immobilization. Figure 3-31 is a simple model that shows the saturation state of important minerals (calcite, kaolinite, goethite, uranophane and uraninite) and their relationship to pH and Eh. Uraninite and uranophane were chosen to represent primary and secondary U minerals, respectively. The solid black lines represent a plot at constant positive Eh (+80 mV) and varying pHs while the green dash lines represent plot at a constant negative Eh (-200 mV) and varying pHs. Each coloured column in the figure represent a mineral and its saturation state at a range of pHs; hashed regions represent pH conditions where the mineral is supersaturated. The uraninite and uranophane model (grey column) shows undersaturation of the secondary and primary U minerals uraninite and uranophane between pH 7-11, at an Eh of +80 mV. Thus, these U minerals will likely not control U concentrations in the groundwater at the current pH and Eh conditions. At Eh of -200 mV and varying pH conditions, uranophane remains undersaturated with respect to groundwater while uraninite appears supersaturated between pH 5 to 10, thus if the system undergo reduction

processes resulting in low Eh, precipitation of uraninite is likely to occur that could result in lowering the concentration of U in the groundwater.

Goethite (orange column), which is a strong sorbent, is supersaturated at pH 6-11 and Eh 80 mV, thus between pH 6 and 11 we expect that goethite will precipitate under these conditions and U will sorb to goethite in the aquifer thereby the goethite will influence U mobility in the groundwater. Under reducing conditions (Eh of -200 mV), goethite is supersaturated at pHs from 7.5-11; thus, even in low redox potential conditions, goethite is likely to influence U concentrations through adsorption and precipitation. Carbonates (calcite, white column) also showed supersaturation at pH > 8 and at both Ehs of +80 and -200 mV, thus the change in the redox condition of the system did not affect the saturation state of calcite. The clays model (kaolinite, purple column) showed super saturation with respect to the groundwater at pH 6-10 and Eh of +80 and -200 mV respectively. The different redox potentials modelled did not affect the saturation state of the clay, thus in this system clay minerals are likely to influence U concentrations and availability by adsorption. From this model we can predict that natural attenuation processes such as sorption, reduction and precipitation will influence U mobility over the long term.

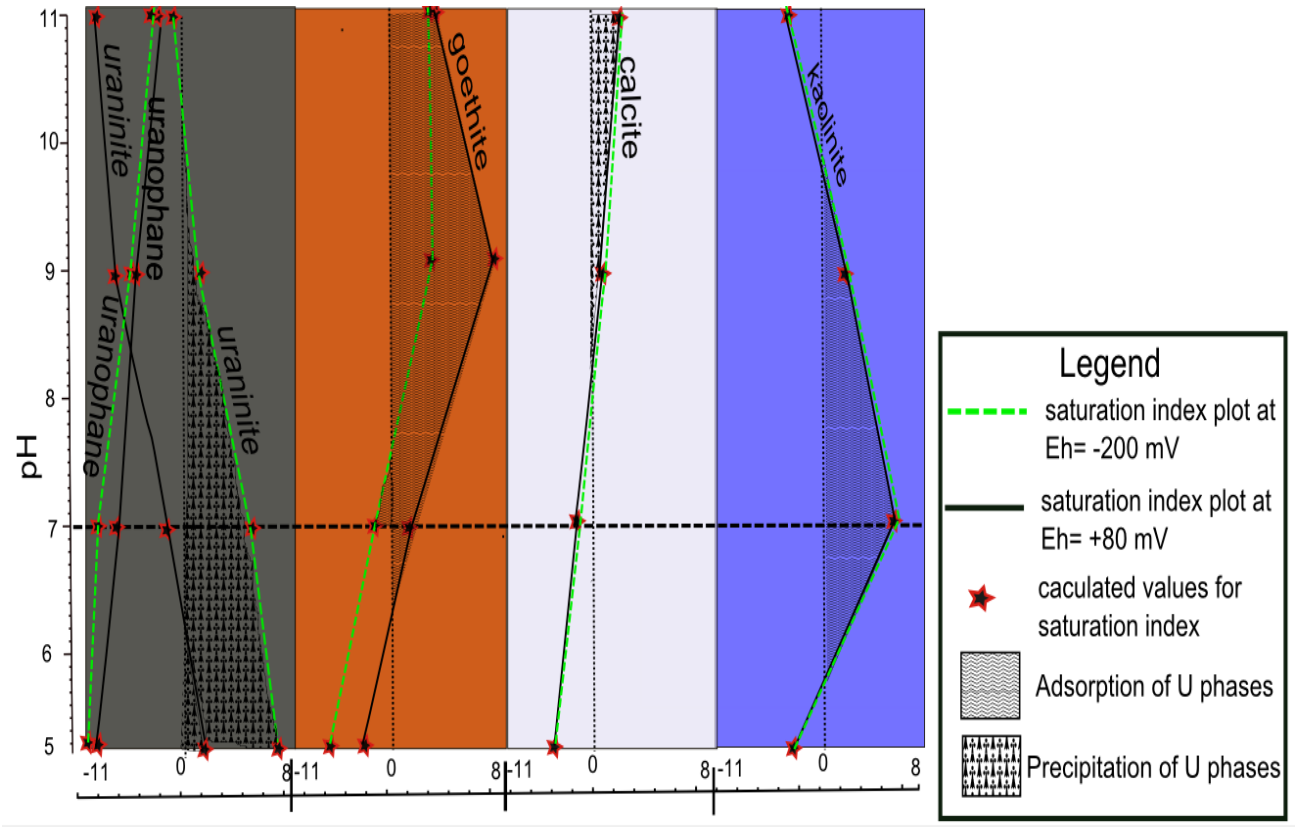

Figure 3-31: A conceptual model of the state of U under different pH conditions and Ehs of +80 mV and -200 mV.

4 CONCLUSION AND FUTURE DIRECTIONS

4.1 Summary and conclusion

The objective of this research was to characterise core taken down-gradient of an ISR mine unit at the Smith Ranch-Highlands mine located in Wyoming, USA. This characterization aims to provide information on the capacity of down-gradient aquifer solids to attenuate U. This question was examined by assessing the mineralogy, elemental concentrations and elemental distribution in the core samples. Eleven core samples from two boreholes and groundwater data from two monitoring boreholes were used in this work. Carbon, S, Fe and U solid phase speciation as well as aqueous phase geochemistry were assessed, and a conceptual model of the site was also generated.

Bulk elemental analysis confirmed that the cores are composed of Fe, Al, Cl, Mg, V, Ti, U, Cu, Co, Mn, Be and Ca. Phase identification of the PXRD pattern revealed that the cores' mineralogy were dominated by quartz, clays, feldspars, albite, goethite and pyrite. These minerals are important for understanding U chemistry. Electron microprobe analysis and SEM confirmed the presence of minerals observed in the PXRD and also showed the heterogeneous nature of the grains that make up the core samples. The clays and goethite observed are likely to play crucial role in U mobility by providing surface area for U to adsorb thereby controlling U concentrations and mobility in groundwater (Sylwester et al., 2000; Dong et al., 2011). Bulk U L-edge XANES showed U occurring as both U(VI) and U(IV) in samples that contain coal lenses. Uranium also co-occurred with other elements such as Fe, Ca and V. The co-occurrence of U with other elements can promote the formation and precipitation of secondary U minerals thereby controlling U concentrations in the groundwater. Bulk C K-edge XANES had functional groups that were characteristics of organic C. This observation supports the combustion data that showed organic C is the main form of C in the core samples. Organic C is known to reduce soluble U(VI) to insoluble U(IV) (Campbell et al., 2012). Sulfur K-edge XANES showed the presence of sulfide and sulfate minerals in the sample while Fe K-edge XANES showed peaks that are characteristic of Fe(II) and Fe(III) minerals. Fe(II) can bind with sulfides and produce pyrite which is an important reductant in U chemistry (Qafoku et al., 2009).

Geochemical modelling predicted undersaturation of the groundwater with primary and secondary U minerals but supersaturation with respect to clays, carbonates and Fe oxyhydroxides at the

current pH and Eh of the site. These minerals can control U mobilization through sorption and co-precipitation (Duff et al., 2002).

The occurrence of U in close association with other elements such as Fe and Ca in samples with coal lenses suggests that coal lenses have a high affinity for metal binding. Thus, the presence of coal lenses in the samples may play an important role in concentrating U thereby reducing U concentrations in groundwater. Secondary and primary U minerals are not predicted to form under current aquifer conditions, and thus should offer no control on U mobility. The fact that U occurs with pyrite is consistent with a reduction of soluble U(VI) to less soluble U(IV) by the pyrite; thus, pyrite may retard U movement in groundwater. Observed clays minerals, carbonates and goethite present may play a crucial role in controlling U mobility in groundwater by either adsorbing U or co-precipitating with U. More work is needed to determine the long–term stability of U associated with coal lenses and U occurring in the presence of pyrite.

4.2 Recommendations

Leaching experiments on the core samples are recommended to investigate soluble elements associated with the core samples such as U, Ca, and Fe. This experiment could be important to understand how susceptible U is to remobilization if geochemical conditions change with time. Such data can be used in geochemical modelling to predict the saturation state of minerals in the deposit. In addition to leaching, hydrological investigations of the nature of flow in the aquifer are essential to understand the current and long-term fate of U and other dissolved elements in the aquifer. The rate and direction of groundwater flow are important to estimate the risk of downgradient contamination in a fate and transport model formulation.

Microcosm experiments are also recommended on the core samples to establish and study the microbes associated with the downgradient aquifer solids and their possible role in U sequestration.

Sulfur minerals and their chemical species are important in U chemistry. Reduced S species can reduce oxidised U to more stable U species that can precipitate out of the groundwater thereby decreasing U concentrations and mobility. Determining S concentrations in the core samples could be useful to identify how much S is present in the core samples. Knowing how much S is present

in the core samples is important when planning S K-edge XANES analysis. Sulfur K-edge XANES could be of value to determine the speciation of S in the core samples. Knowing the species of S will help identify the forms of S present and their role in U immobilization.

The distribution and association of U with other elements are important in studying the nature of U in downgradient aquifers. To study the micro-scale spatial distribution of U and other elements, thin sections of the core samples could be prepared and used to obtain information from SEM, EMPA, and micro XRF-mapping. Lab-based column experiments are also recommended to test the rate at which the clays, pyrite and organic matter present in the core samples can reduce U concentration and mobility. This will help in estimating how natural attenuation process can help in controlling U mobility.

The importance of modelling as a predictive tool in determining the current and future fate of U in groundwater cannot be overlooked, thus additional geochemical modelling using data from additional boreholes is recommended to predict the saturation state of minerals at the site. Surface complexation modelling can also be performed to predict how sorption and complexation affect U mobility. A holistic picture of the site should include hydrological data and models as well as bio-geochemical data in describing U attenuation at the site.

REFERENCES

Abdelouas, A. (2006). Uranium Mill Tailings: Geochemistry, Mineralogy, and Environmental Impact. *Elements, 2*(6), 335-341. doi: 10.2113/gselements.2.6.335

Abdelouas, A., Lu, Y., Lutze, W., & Nuttall, H. E. (1998a). Reduction of U(VI) to U(IV) by indigenous bacteria in contaminated ground water. *Journal of Contaminant Hydrology, 35*(1–3), 217-233. doi: http://dx.doi.org/10.1016/S0169-7722(98)00134-X

Abdelouas, A., Lutze, W., & Nuttall, E. (1998b). Chemical reactions of uranium in ground water at a mill tailings site. *Journal of Contaminant Hydrology, 34*(4), 343-361. doi: http://dx.doi.org/10.1016/S0169-7722(98)00097-7

Alan, M. H., & George, W. H. (2007). *Nuclear Energy Now: Why the time has come for the world's most misunderstood energy source*. New Jersey: John Wiley & Sons Inc,.

Aubriet, H., Humbert, B., & Perdicakis, M. (2006). Interaction of U(VI) with pyrite, galena and their mixtures: a theoretical and multitechnique approach *Radiochimica Acta* (Vol. 94, pp. 657).

Bachmaf, S., Planer-Friedrich, B., & Merkel Broder, J. (2008). Effect of sulfate, carbonate, and phosphate on the uranium(VI) sorption behavior onto bentonite *Radiochimica Acta* (Vol. 96, pp. 359).

Ball, J. W., & Nordstrom, D. K. (1991). User's manual for WATEQ4F, with revised thermodynamic data base and text cases for calculating speciation of major, trace, and redox elements in natural waters *Open-File Report* (Version 2.0. ed.).

Barnes, C. E., & Cochran, J. K. (1993). Uranium geochemistry in estuarine sediments: Controls on removal and release processes. *Geochimica et Cosmochimica Acta, 57*(3), 555-569. doi: http://dx.doi.org/10.1016/0016-7037(93)90367-6

Beazley, M. J., Martinez, R. J., Webb, S. M., Sobecky, P. A., & Taillefert, M. (2011). The effect of pH and natural microbial phosphatase activity on the speciation of uranium in subsurface soils. *Geochimica et Cosmochimica Acta, 75*(19), 5648-5663. doi: https://doi.org/10.1016/j.gca.2011.07.006

Bethke, C., & Yeakel, S. (2017). *Geochemist's Workbench Reference Manual*. Aqueous Solutions, LLC. Champaign, Illinois.

Beyenal, H., Sani, R. K., Peyton, B. M., Dohnalkova, A. C., Amonette, J. E., & Lewandowski, Z. (2004). Uranium Immobilization by Sulfate-Reducing Biofilms. *Environmental Science & Technology, 38*(7), 2067-2074. doi: 10.1021/es0348703

Bhattacharyya, A., Campbell, K. M., Kelly, S. D., Roebbert, Y., Weyer, S., Bernier-Latmani, R., et al. (2017). Biogenic non-crystalline U(IV) revealed as major component in uranium ore deposits. *8*, 15538. doi: 10.1038/ncomms15538

Blanchard, P. E. R., Grosvenor, A. P., Rowson, J., Hughes, K., & Brown, C. (2016). Identifying calcium-containing mineral species in the JEB Tailings Management Facility at McClean Lake, Saskatchewan. *Applied Geochemistry, 73*, 98-108. doi: http://dx.doi.org/10.1016/j.apgeochem.2016.08.001

Borch, T., Kretzschmar, R., Kappler, A., Cappellen, P. V., Ginder-Vogel, M., Voegelin, A., et al. (2010). Biogeochemical Redox Processes and their Impact on Contaminant Dynamics. *Environmental Science & Technology, 44*(1), 15-23. doi: 10.1021/es9026248

Borch, T., Roche, N., & Johnson, T. E. (2012). Determination of contaminant levels and remediation efficacy in groundwater at a former in situ recovery uranium mine. *Journal of Environmental Monitoring, 14*(7), 1814-1823. doi: 10.1039/C2EM30077J

Bostick, B. C., Fendorf, S., Barnett, M. O., Jardine, P. M., & Brooks, S. C. (2002). Uranyl Surface Complexes Formed on Subsurface Media from DOE Facilities. *Soil Science Society of America Journal, 66*(1), 99-108. doi: 10.2136/sssaj2002.9900

Brandes, J. A., Cody, G. D., Rumble, D., Haberstroh, P., Wirick, S., & Gelinas, Y. (2008). Carbon K-edge XANES spectromicroscopy of natural graphite. *Carbon, 46*(11), 1424-1434. doi: http://dx.doi.org/10.1016/j.carbon.2008.06.020

Brandes, J. A., Lee, C., Wakeham, S., Peterson, M., Jacobsen, C., Wirick, S., et al. (2004). Examining marine particulate organic matter at sub-micron scales using scanning transmission X-ray microscopy and carbon X-ray absorption near edge structure spectroscopy. *Marine Chemistry, 92*(1–4), 107-121. doi: http://dx.doi.org/10.1016/j.marchem.2004.06.020

Brooks, S. C. (2001). Waste characteristics of the former S-3 ponds and outline of uranium chemistry relevant to NABIR field research center studies.

Brooks, S. C., Fredrickson, J. K., Carroll, S. L., Kennedy, D. W., Zachara, J. M., Plymale, A. E., et al. (2003). Inhibition of Bacterial U(VI) Reduction by Calcium. *Environmental Science & Technology, 37*(9), 1850-1858. doi: 10.1021/es0210042

Bruno, J., De Pablo, J., Duro, L., & Figuerola, E. (1995). Experimental study and modeling of the U(VI)-$Fe(OH)_3$ surface precipitation/coprecipitation equilibria. *Geochimica et Cosmochimica Acta, 59*(20), 4113-4123. doi: http://dx.doi.org/10.1016/0016-7037(95)00243-S

Cameco. (2013). Annual Report: http://www.cameco.com/annual_report/2013/mda/operations-development-projects/uranium/operating-properties/smith-ranch-highland/.

Cameco Resources Inc. (2013). Application for Alternate Concentration Limits for the Smith Ranch-Highland Mine Unit-B In Situ Leach Uranium Mine, Converse County, WY.

Campbell, K. M., Kukkadapu, R. K., Qafoku, N. P., Peacock, A. D., Lesher, E., Williams, K. H., et al. (2012). Geochemical, mineralogical and microbiological characteristics of sediment

from a naturally reduced zone in a uranium-contaminated aquifer. *Applied Geochemistry, 27*(8), 1499-1511. doi: https://doi.org/10.1016/j.apgeochem.2012.04.013

Canadian Nuclear Association. (2015). The Canadian Nuclear Factbook. https://cna.ca/downloads/ms_13753.pdf

Carter, M. R. (1993). Soil sampling and methods of analysis: CRC Press.

Casas, I., de Pablo, J., Giménez, J., Torrero, M. E., Bruno, J., Cera, E., et al. (1998). The role of pe, pH, and carbonate on the solubility of UO2 and uraninite under nominally reducing conditions. *Geochimica et Cosmochimica Acta, 62*(13), 2223-2231. doi: https://doi.org/10.1016/S0016-7037(98)00140-9

Cheng, T., Barnett, M. O., Roden, E. E., & Zhuang, J. (2004). Effects of Phosphate on Uranium(VI) Adsorption to Goethite-Coated Sand. *Environmental Science & Technology, 38*(22), 6059-6065. doi: 10.1021/es040388o

Clark, D. L., Hobart, D. E., & Neu, M. P. (1995). Actinide Carbonte Complexes and Their Importance in Actinide Environmental Chemistry. *Chemical Reviews, 95*(1), 25-48. doi: 10.1021/cr00033a002

Cooney, R. R., & Urquhart, S. G. (2004). Chemical Trends in the Near-Edge X-ray Absorption Fine Structure of Monosubstituted and Para-Bisubstituted Benzenes. *The Journal of Physical Chemistry B, 108*(47), 18185-18191. doi: 10.1021/jp046868j

Crawford, J. (1999). *Geochemical Modelling–A Review of Current Capabilities and Future Directions.* PhD thesis, Royal Institute of Technology (KTH), Stockholm.

Crean, D. E., Livens, F. R., Stennett, M. C., Grolimund, D., Borca, C. N., & Hyatt, N. C. (2014). Microanalytical X-ray Imaging of Depleted Uranium Speciation in Environmentally Aged Munitions Residues. *Environmental Science & Technology, 48*(3), 1467-1474. doi: 10.1021/es403938d

Cumberland, S. A., Douglas, G., Grice, K., & Moreau, J. W. (2016). Uranium mobility in organic matter-rich sediments: A review of geological and geochemical processes. *Earth-Science Reviews, 159*, 160-185. doi: http://dx.doi.org/10.1016/j.earscirev.2016.05.010

Dahlkamp, F. J. (2010). *Uranium Deposits of the World*: Springer-Verlag Berlin Heidelberg.

Dong, W., & Brooks, S. C. (2006). Determination of the Formation Constants of Ternary Complexes of Uranyl and Carbonate with Alkaline Earth Metals (Mg2+, Ca2+, Sr2+, and Ba2+) Using Anion Exchange Method. *Environmental Science & Technology, 40*(15), 4689-4695. doi: 10.1021/es0606327

Dong, W., & Brooks, S. C. (2008). Formation of Aqueous MgUO2(CO3)32− Complex and Uranium Anion Exchange Mechanism onto an Exchange Resin. *Environmental Science & Technology, 42*(6), 1979-1983. doi: 10.1021/es0711563

Dong, W., Tokunaga, T. K., Davis, J. A., & Wan, J. (2011). Uranium(VI) Adsorption and Surface Complexation Modeling onto Background Sediments from the F-Area Savannah River Site. *Environmental Science & Technology, 46*(3), 1565-1571. doi: 10.1021/es2036256

Dong, W., Tokunaga, T. K., Davis, J. A., & Wan, J. (2012). Uranium(VI) Adsorption and Surface Complexation Modeling onto Background Sediments from the F-Area Savannah River Site. *Environmental Science & Technology, 46*(3), 1565-1571. doi: 10.1021/es2036256

Du, X., Boonchayaanant, B., Wu, W.-M., Fendorf, S., Bargar, J., & Criddle, C. S. (2011). Reduction of Uranium(VI) by Soluble Iron(II) Conforms with Thermodynamic Predictions. *Environmental Science & Technology, 45*(11), 4718-4725. doi: 10.1021/es2006012

Duff, M. C., Coughlin, J. U., & Hunter, D. B. (2002). Uranium co-precipitation with iron oxide minerals. *Geochimica et Cosmochimica Acta, 66*(20), 3533-3547. doi: http://dx.doi.org/10.1016/S0016-7037(02)00953-5

Edwards, C. R., & Oliver, A. J. (2000). Uranium processing: A review of current methods and technology. *Journal of The Minerals, Metals & Materials Society 52*(9), 12-20. doi: 10.1007/s11837-000-0181-2

Eglizaud, N., Miserque, F., Simoni, E., Schlegel, M., & Descostes, M. (2006). Uranium(VI) interaction with pyrite (FeS_2): Chemical and spectroscopic studies *Radiochimica Acta* (Vol. 94, pp. 651).

Elias, A. D., Krumholz, R. L., Wong, D., Long, E. P., & Suflita, M. J. (2003). Characterization of Microbial Activities and U Reduction in a Shallow Aquifer Contaminated by Uranium Mill Tailings. *Microbial Ecology, 46*(1), 83-91. doi: 10.1007/s00248-002-1060-x

Elless, M. P., & Lee, S. Y. (1998). Uranium Solubility of Carbonate-Rich Uranium-Contaminated Soils. *Water, Air, and Soil Pollution, 107*(1), 147-162. doi: 10.1023/a:1004982515941

EPA. (Last updated December, 2016). Effluent Guidelines. from https://www.epa.gov/eg/learn-about-effluent-guidelines

ESRF database. Database for organic and inorganic sulfur compouds. from http://www.esrf.eu/home/UsersAndScience/Experiments/XNP/ID21/php/Database-SOrganic.html

Essilfie-Dughan, J., Hendry, M. J., Warner, J., & Kotzer, T. (2012). Microscale mineralogical characterization of As, Fe, and Ni in uranium mine tailings. *Geochimica et Cosmochimica Acta, 96*(0), 336-352. doi: http://dx.doi.org/10.1016/j.gca.2012.08.005

Essilfie-Dughan, J., Hendry, M. J., Warner, J., & Kotzer, T. (2013). Arsenic and iron speciation in uranium mine tailings using X-ray absorption spectroscopy. *Applied Geochemistry, 28*, 11-18. doi: http://dx.doi.org/10.1016/j.apgeochem.2012.10.022

Fomina, M., Charnock, J. M., Hillier, S., Alvarez, R., & Gadd, G. M. (2007). Fungal transformations of uranium oxides. *Environmental Microbiology, 9*(7), 1696-1710. doi: 10.1111/j.1462-2920.2007.01288.x

Fox, M. H. (2014). *Why We Need Nuclear Power: The Environmental Case*: OUP USA.

Francis, J. T., & Hitchcock, A. P. (1992). Inner-shell spectroscopy of p-benzoquinone, hydroquinone, and phenol: distinguishing quinoid and benzenoid structures. *The Journal of Physical Chemistry, 96*(16), 6598-6610. doi: 10.1021/j100195a018

Frank, A. J. (1954). Summary of Carbonate Leaching of Uranium Ores *Other Information: Decl. Sept. 23, 1955. Orig. Receipt Date: 31-DEC-56* (pp. Medium: X; Size: Pages: 34).

Freeman, M. D., & Stover, D. E. (1999). The Smith Ranch Project: a 1990s in situ uranium mine. *The Uranium Institute 24th Annual Symposium, 8–10 September (1999)* (pp. 1-20).

Gabriel, U., Gaudet, J. P., Spadini, L., & Charlet, L. (1998). Reactive transport of uranyl in a goethite column: an experimental and modelling study. *Chemical Geology, 151*(1–4), 107-128. doi: http://dx.doi.org/10.1016/S0009-2541(98)00074-6

Gallegos, T. J., Bern, C. R., Birdwell, J. E., Haines, S. S., & Engle, M. A. (2015a). *The role of water in unconventional in situ energy resource extraction technologies: Chapter 7 in Food, energy, and water: The chemistry connection.*

Gallegos, T. J., Campbell, K. M., Zielinski, R. A., Reimus, P. W., Clay, J. T., Janot, N., et al. (2015b). Persistent U(IV) and U(VI) following in situ recovery (ISR) mining of a sandstone uranium deposit, Wyoming, USA. *Applied Geochemistry, 63*, 222-234. doi: http://dx.doi.org/10.1016/j.apgeochem.2015.08.017

Ganesh, R., Robinson, K. G., Reed, G. D., & Sayler, G. S. (1997). Reduction of Hexavalent Uranium from Organic Complexes by Sulfate- and Iron-Reducing Bacteria. *Applied and Environmental Microbiology, 63*(11), 4385-4391.

Gavrilescu, M., Pavel, L. V., & Cretescu, I. (2009). Characterization and remediation of soils contaminated with uranium. *Journal of Hazardous Materials, 163*(2–3), 475-510. doi: http://dx.doi.org/10.1016/j.jhazmat.2008.07.103

Geipel, G., Bernhard, G., Brendler, V., & Nitsche, H. (1998). Complex formation between UO2+2 and CO2-3: studied by laser-induced photoacoustic spectroscopy (LIPAS). *Radiochim. acta, 82*, 59-62.

Giammar, D. E., & Hering, J. G. (2001). Time Scales for Sorption−Desorption and Surface Precipitation of Uranyl on Goethite. *Environmental Science & Technology, 35*(16), 3332-3337. doi: 10.1021/es0019981

Giblin, A. M., Batts, B. D., & Swaine, D. J. (1981). Laboratory simulation studies of uranium mobility in natural waters. *Geochimica et Cosmochimica Acta, 45*(5), 699-709. doi: http://dx.doi.org/10.1016/0016-7037(81)90043-0

Gillespie, A. W., Phillips, C. L., Dynes, J. J., Chevrier, D., Regier, T. Z., & Peak, D. (2015). Chapter One - Advances in Using Soft X-Ray Spectroscopy for Measurement of Soil Biogeochemical Processes. In L. S. Donald (Ed.), *Advances in Agronomy* (Vol. Volume 133, pp. 1-32): Academic Press.

Golder Associates. (2010). Smith Ranch-Highland uranium project; Source Material License SUA-1548 Renewal Submittal.

Gomez, M. A., Hendry, M. J., Koshinsky, J., Essilfie-Dughan, J., Paikaray, S., & Chen, J. (2013). Mineralogical Controls on Aluminum and Magnesium in Uranium Mill Tailings: Key Lake, Saskatchewan, Canada. *Environmental Science & Technology, 47*(14), 7883-7891. doi: 10.1021/es400658f

Gómez, P., Garralón, A., Buil, B., Turrero, M. J., Sánchez, L., & de la Cruz, B. (2006). Modeling of geochemical processes related to uranium mobilization in the groundwater of a uranium mine. *Science of The Total Environment, 366*(1), 295-309. doi: http://dx.doi.org/10.1016/j.scitotenv.2005.06.024

Gorby, Y. A., & Lovley, D. R. (1992). Enzymic uranium precipitation. *Environmental Science & Technology, 26*(1), 205-207. doi: 10.1021/es00025a026

Granger, H. C., & Warren, C. G. (1969). Unstable sulfur compounds and the origin of roll-type uranium deposit. *Economic Geology, 64*, 160-171.

Granger, H. C., & Warren, C. G. (1979). The importance of dissolved free oxygen during formation of Sandstone-Type Uranium Deposits. Open-File Report 79-1603

Gu, B., Wu, W.-M., Ginder-Vogel, M. A., Yan, H., Fields, M. W., Zhou, J., et al. (2005). Bioreduction of Uranium in a Contaminated Soil Column. *Environmental Science & Technology, 39*(13), 4841-4847. doi: 10.1021/es050011y

Guillaumont, R., Fanghanel, T., Neck, V., Fuger, J., Palmer, D. A., Grenthe, I., et al. (2003). *Update on the Chemical Thermodynamics of Uranium, Neptumium, Plutonium, Americium, and Technetium*. Elsevier: Amsterdam, The Netherlands.

Haberstroh, P. R., Brandes, J. A., Gélinas, Y., Dickens, A. F., Wirick, S., & Cody, G. (2006). Chemical composition of the graphitic black carbon fraction in riverine and marine sediments at sub-micron scales using carbon X-ray spectromicroscopy. *Geochimica et Cosmochimica Acta, 70*(6), 1483-1494. doi: http://dx.doi.org/10.1016/j.gca.2005.12.001

Hall, S. (2009). Groundwater Restoration at Uranium In Situ Recovery Mines, South Texas Coastal Plains. : U.S. geological Survey Open-File report 2009—1143. (PP.32).

Hamdy, H. A. (2009). Role of Argillic Alteration in Uranophane Precipitation along Shear Zones of the Gattar Granites, Eastern Desert, Egypt *Earth Science, 20*(2), 45-69. doi: 10.4197/ear.20-2.4 .

Han, R., Zou, W., Wang, Y., & Zhu, L. (2007). Removal of uranium(VI) from aqueous solutions by manganese oxide coated zeolite: discussion of adsorption isotherms and pH effect. *Journal of Environmental Radioactivity, 93*(3), 127-143. doi: http://dx.doi.org/10.1016/j.jenvrad.2006.12.003

Harshman, E. N., & Adams, S. S. (1981). Geology and recognition criteria for roll-type uranium deposits in continental sandstones. United States Department of Energy, Grand Junction, Colorado.

Hitchcock, A. P. (2011). Axis is free for noncormercial use. it is written in interactive data language (IDL). http://unicorn.macmaster.ca/aXis2000.html

Hitchcock, A. P., Horsley, J. A., & Stöhr, J. (1986). Inner shell excitation of thiophene and thiolane: Gas, solid, and monolayer states. *The Journal of Chemical Physics, 85*(9), 4835-4848. doi: doi:http://dx.doi.org/10.1063/1.451718

Hitchcock, A. P., & Ishii, I. (1987). Carbon K-shell excitation spectra of linear and branched alkanes. *Journal of Electron Spectroscopy and Related Phenomena, 42*(1), 11-26. doi: http://dx.doi.org/10.1016/0368-2048(87)85002-8

Ho, C. H., & Miller, N. H. (1986). Adsorption of uranyl species from bicarbonate solution onto hematite particles. *Journal of Colloid and Interface Science, 110*(1), 165-171. doi: http://dx.doi.org/10.1016/0021-9797(86)90365-6

Hsi, C. K. D., & Langmuir, D. (1985). Adsorption of uranyl onto ferric oxyhydroxides: Application of the surface complexation site-binding model. *Geochimica et Cosmochimica Acta, 49*(9), 1931-1941. doi: http://dx.doi.org/10.1016/0016-7037(85)90088-2

Hu, K., Wang, Q., Tao, G., Wang, A., & Ding, D. (2011). Experimental Study on Restoration of Polluted Groundwater from in Situ Leaching Uranium Mining with Sulfate Reducing Bacteria and ZVI-SRB. *Procedia Earth and Planetary Science, 2*(0), 150-155. doi: http://dx.doi.org/10.1016/j.proeps.2011.09.025

Hua, B., Xu, H., Terry, J., & Deng, B. (2006). Kinetics of Uranium(VI) Reduction by Hydrogen Sulfide in Anoxic Aqueous Systems. *Environmental Science & Technology, 40*(15), 4666-4671. doi: 10.1021/es051804n

Hyun, S. P., Cho, Y. H., Hahn, P. S., & Kim, S. J. (2001). Sorption mechanism of U(VI) on a reference montmorillonite Binding to the internal and external surfaces. Journal of Radioanalytical and Nuclear Chemistry, 250(1), 55-62.

IAEA. (2001). *Manual of acid in situ leach uranium mining technology. (Forward, p.1).* Retrieved from http://www-pub.iaea.org/mtcd/publications/pdf/te_1239_prn.pdf.

IAEA. (2016). In situ leach uranium mining: An overview of operations: IAEA Nuclear Energy Series No. NF-T-1.4. http://www-pub.iaea.org/MTCD/Publications/PDF/P1741_web.pdf.

Jacques, D., Šimůnek, J., Mallants, D., & van Genuchten, M. T. (2008). Modeling Coupled Hydrologic and Chemical Processes: Long-Term Uranium Transport following Phosphorus Fertilization All rights reserved. No part of this periodical may be reproduced or transmitted in any form or by any means, electronic or mechanical, including photocopying, recording, or any information storage and retrieval system, without permission in writing from the publisher. *Vadose Zone Journal, 7*, 698-711. doi: 10.2136/vzj2007.0084

Jamieson, B., & Frost, S. (1997). *The McArthur River Project: High grade uranium mining.* Paper presented at the The Uranium Institute, 22nd Annual Symposium., London.

Jerden Jr, J. L., & Sinha, A. K. (2003). Phosphate based immobilization of uranium in an oxidizing bedrock aquifer. *Applied Geochemistry, 18*(6), 823-843. doi: http://dx.doi.org/10.1016/S0883-2927(02)00179-8

Kalmykov, S. N., & Choppin, G. R. (2000). Mixed Ca2+/UO22+/CO32- complex formation at different ionic strengths. *Radiochimica Acta, 88(9-11), 603-606.*

Kaufman, D. G., & Franz, C. M. (2000). *Biosphere 2000 : protecting our global environment* (3rd ed.). Dubuque, Iowa: Kendall/Hunt Pub. Co.

Kelly, S. D., Kemner, K. M., Carley, J., Criddle, C., Jardine, P. M., Marsh, T. L., et al. (2008). Speciation of Uranium in Sediments before and after In situ Biostimulation. *Environmental Science & Technology, 42*(5), 1558-1564. doi: 10.1021/es071764i

Kelly, S. D., Rasbury, E. T., Chattopadhyay, S., Kropf, A. J., & Kemner, K. M. (2006). Evidence of a Stable Uranyl Site in Ancient Organic-Rich Calcite. *Environmental Science & Technology, 40*(7), 2262-2268. doi: 10.1021/es051970v

Kosog, B., La Pierre, H. S., Denecke, M. A., Heinemann, F. W., & Meyer, K. (2012). Oxidation State Delineation via U LIII-Edge XANES in a Series of Isostructural Uranium Coordination Complexes. *Inorganic Chemistry, 51*(14), 7940-7944. doi: 10.1021/ic3011234

Langen, R. E., & Kidwell, A. L. (1974). Geology and geochemistry of the highlands uranium deposits. *Sci. bull, 6*, 41-48.

Langmuir, D. (1978). Uranium solution-mineral equilibria at low temperatures with applications to sedimentary ore deposits. *Geochimica et Cosmochimica Acta, 42*(6), 547-569. doi: http://dx.doi.org/10.1016/0016-7037(78)90001-7

Langmuir, D. (1997). *Aqueous Environmental Geochemistry*. Prentice Hall, Inc. New York.

Larson, B. A. (2008). *X-ray Spectromicroscopy Analysis and Its Applications to Bacterial Interactions in the Environment.* (PhD PhD), Stony Brook University. Retrieved from http://xray1.physics.sunysb.edu/research/pdf_papers/dissertations/larson_phd_2008.pdf

LECO Corporation. (2008). Carbon/Sulfur Determinator Specification Sheet. St. Joseph,MI. Retrieved from http://www.usbioecuador.com/descargas/leco-inorganica/CS230-ht.pdf.

Levnthial, J. S. (1979). Organic matter and sandstone-type uranium deposits: A Primer: United State Department of Interior Geological Survey.

Livens, F. R., Jones, M. J., Hynes, A. J., Charnock, J. M., Mosselmans, J. F. W., Hennig, C., et al. (2004). X-ray absorption spectroscopy studies of reactions of technetium, uranium and neptunium with mackinawite. *Journal of Environmental Radioactivity, 74*(1–3), 211-219. doi: http://dx.doi.org/10.1016/j.jenvrad.2004.01.012

Lovley, D. R., Phillips, E. J. P., Gorby, Y. A., & Landa, E. R. (1991). Microbial reduction of uranium. *Nature, 350*(6317), 413-416.

Luo, J., Weber, F.-A., Cirpka, O. A., Wu, W.-M., Nyman, J. L., Carley, J., et al. (2007). Modeling in situ uranium(VI) bioreduction by sulfate-reducing bacteria. *Journal of Contaminant Hydrology, 92*(1–2), 129-148. doi: http://dx.doi.org/10.1016/j.jconhyd.2007.01.004

Maehata, K., Idemitsu, K., & Tanaka, K. (2011). X-ray energy dispersive spectroscopy of uranium ore using a TES microcalorimeter mounted on a field-emission scanning electron microscope. *Nuclear Instruments and Methods in Physics Research Section A: Accelerators, Spectrometers, Detectors and Associated Equipment, 648*(1), 285-289. doi: http://dx.doi.org/10.1016/j.nima.2011.06.005

Malinowski, E. R. (1978). Theory of error for target factor analysis with applications to mass spectrometry and nuclear magnetic resonance spectrometry. *Analytica Chimica Acta, 103*(4), 339-354. doi: http://dx.doi.org/10.1016/S0003-2670(01)83099-3

Mays, W. M. (1992). Restoration of groundwater at three in situ mines in Texas. Paper presented at the IAEA Technical Committee Meeting, Vienna Austria, Oct. 5–8, 1992

Mays, W. M. (1994). *Restoration of groundwater at three in situ mines in Texas.* Paper presented at the IAEA Technical Committee Meeting, Vienna Austria, Oct. 5–8, 1992 as reviewed in Nuexco Review, May 1994, Groundwater Restoration of In-Situ Uranium Mines (1994).

McBeth, J. M. (2015). Protocol for handling uranium ore and wastes [V 3.1].

Merkel, B. (2008). *Uranium, mining and hydrogeology*: Berlin, Springer.

Merritt, R. C. (1971). *The Extractive Metallurgy of Uranium*: Colorado School of Mines Research Institute, Library of Congress Catalog No. 71-157076, p 252-254

Monreal, M. J., & Diaconescu, P. L. (2010). The riches of uranium. *Nat Chem, 2*(5), 424-424. doi: doi:10.1038/nchem.642

Morrison, S. J., Metzler, D. R., & Dwyer, B. P. (2002). Removal of As, Mn, Mo, Se, U, V and Zn from groundwater by zero-valent iron in a passive treatment cell: reaction progress

modeling. *Journal of Contaminant Hydrology*, *56*(1–2), 99-116. doi: http://dx.doi.org/10.1016/S0169-7722(01)00205-4

Moyes, L. N., Parkman, R. H., Charnock, J. M., Vaughan, D. J., Livens, F. R., Hughes, C. R., et al. (2000). Uranium Uptake from Aqueous Solution by Interaction with Goethite, Lepidocrocite, Muscovite, and Mackinawite: An X-ray Absorption Spectroscopy Study. *Environmental Science & Technology, 34*(6), 1062-1068. doi: 10.1021/es990703k

Murphy, R. J., Lenhart, J. J., & Honeyman, B. D. (1999). The sorption of thorium (IV) and uranium (VI) to hematite in the presence of natural organic matter. *Colloids and Surfaces A: Physicochemical and Engineering Aspects, 157*(1–3), 47-62. doi: http://dx.doi.org/10.1016/S0927-7757(99)00115-6

Nagy, B., Gauthier-Lafaye, F., Holliger, P., Davis, D. W., Mossman, D. J., Leventhal, J. S., et al. (1991). Organic matter and containment of uranium and fissiogenic isotopes at the Oklo natural reactors. *Nature, 354*(6353), 472-475.

Nash, J. T., Granger, H. C., & Adams, S. S. (1981). Geology and concepts of genesis of important types of uranium deposits. *Econ. Geol. 75th anniversary volume (1981), pp. 63–116*.

Neiss, J., Stewart, B. D., Nico, P. S., & Fendorf, S. (2007). Speciation-Dependent Microbial Reduction of Uranium within Iron-Coated Sands. *Environmental Science & Technology, 41*(21), 7343-7348. doi: 10.1021/es0706697

Norris, J. D., & Drummond, p. (2000). Uranium recovery by in situ leaching: The Smith Ranch Project Uranium 2000. *Proccesses Matallurgy of uranium*, 311-319.

Ortiz-Bernad, I., Anderson, R. T., Vrionis, H. A., & Lovley, D. R. (2004). Resistance of solid-phase U(VI) to microbial reduction during in situ bioremediation of uranium-contaminated groundwater. *Appl Environ Microbiol, 70*(12), 7558-7560. doi: 10.1128/aem.70.12.7558-7560.2004

Pabalan, R. T., Bertetti, F. P., Prikryl, J. D., & Turner, D. R. (1996). *Uranium (VI) sorption onto selected mineral surfaces: Key geochemical parameters*: American Chemical Society, Washington, DC (United States).

Pabalan, R. T., & Turner, D. R. (1996). Uranium(6+) sorption on montmorillonite: Experimental and surface complexation modeling study. *Aquatic Geochemistry, 2*(3), 203-226. doi: 10.1007/bf01160043

Page, L. R., Stocking, H. E., & Smith, H. B. (1956). *Contributions to the Geology of Uranium and Thorium: By the United States Geological Survey and Atomic Energy Commission for the United Nations International Conference on Peaceful Uses of Atomic Energy, Geneva, Switzerland, 1955*: U.S. Government Printing Office.

Parkhurst, D. L., and C.A.J. Appelo. (2013). Description of input and examples for PHREEQC version 3—A computer program for speciation, batch-reaction, one-dimensional transport,

and inverse geochemical calculations: U.S. Geological Survey Techniques and Methods, book 6, chap. A43, 497 p., available only at http://pubs.usgs.gov/tm/06/a43/

Pelizza, M. S., & Bartels, C. S. (2016). 7 - Introduction to uranium in situ recovery technology A2 - Hore-Lacy, Ian *Uranium for Nuclear Power* (pp. 157-213): Woodhead Publishing.

Phillips, E. J. P., Landa, E. R., & Lovley, D. R. (1995). Remediation of uranium contaminated soils with bicarbonate extraction and microbial U(VI) reduction. *Journal of Industrial Microbiology, 14*(3), 203-207. doi: 10.1007/bf01569928

Powder Diffraction File. (2012). International Centre for Diffraction Data. Newtown Square, Pennsylvania, USA.

Prietzel, J., Thieme, J., Eusterhues, K., & Eichert, D. (2007). Iron speciation in soils and soil aggregates by synchrotron-based X-ray microspectroscopy (XANES, μ-XANES). *European Journal of Soil Science, 58*(5), 1027-1041. doi: 10.1111/j.1365-2389.2006.00882.x

Qafoku, N. P., Kukkadapu, R. K., McKinley, J. P., Arey, B. W., Kelly, S. D., Wang, C., et al. (2009). Uranium in Framboidal Pyrite from a Naturally Bioreduced Alluvial Sediment. *Environmental Science & Technology, 43*(22), 8528-8534. doi: 10.1021/es9017333

Quinton, E. G., Ronald, J., Buchanan, J., Ellis, E. D., & Shoemaker, H. S. (1997). A method to compare groundwater cleanup technologies. *Remediation Journal, 7*(16), 7-16. doi: 10.1002/rem.3440070403

Rackley, R. I. (1972). The Environment of Wyoming Tertiary Uranium Deposits. AAPG Bulletin, v. 56, n. 4, pp. 755-774.

Ravel, B., & Newville, M. (2005). ATHENA, ARTEMIS, HEPHAESTUS: data analysis for X-ray absorption spectroscopy using IFEFFIT. *Journal of Synchrotron Radiation, 12*(4), 537-541. doi: doi:10.1107/S0909049505012719

Ray, A. E., Bargar, J. R., Sivaswamy, V., Dohnalkova, A. C., Fujita, Y., Peyton, B. M., et al. (2011). Evidence for multiple modes of uranium immobilization by an anaerobic bacterium. *Geochimica et Cosmochimica Acta, 75*(10), 2684-2695. doi: https://doi.org/10.1016/j.gca.2011.02.040

Reynolds, H. S., Ram, R., Charalambous, F. A., Antolasic, F., Tardio, J., & Bhargava, S. (2010). Characterisation of a uranium ore using multiple X-ray diffraction based methods. *Minerals Engineering, 23*(9), 739-745. doi: http://dx.doi.org/10.1016/j.mineng.2010.05.006

Rihs, S., Sturchio, N. C., Orlandini, K., Cheng, L., Teng, H., Fenter, P., et al. (2004). Interaction of Uranyl with Calcite in the Presence of EDTA. *Environmental Science & Technology, 38*(19), 5078-5086. doi: 10.1021/es049847b

Salmon, S. U., & Malmström, M. E. (2004). Geochemical processes in mill tailings deposits: modelling of groundwater composition. *Applied Geochemistry, 19*(1), 1-17. doi: http://dx.doi.org/10.1016/S0883-2927(03)00129-X

Sam's Microprobe Analysis Kit. (2006). Webb Sam. Software and documentation. available at: http://www.sams-xrays.com/#!smak/n44a5.

Sani, R. K., Peyton, B. M., Smith, W. A., Apel, W. A., & Petersen, J. N. (2002). Dissimilatory reduction of Cr(VI), Fe(III), and U(VI) by Cellulomonas isolates. *Appl Microbiol Biotechnol, 60*(1-2), 192-199. doi: 10.1007/s00253-002-1069-6

Schnohr, C. S., & Ridgway, M. C. (2015). *Introduction to X-Ray Absorption Spectroscopy* Vol. 190. *X-Ray Absorption Spectroscopy of Semiconductors, Springer Series in Optical Sciences 190* (pp. 1-26). Retrieved from http://hdl.handle.net/1885/14671 doi:DOI 10.1007/978-3-662-44362-0_1

Shchetochkin, V. N., & Kislyakov, Y. M. (1993). Exogenic-epigenetic uranium deposits of the Kyzylkums and adjacent regions. *Geol Ore Deposits, 35*(3), 100-220.

Singer, D. M., Maher, K., & Brown Jr, G. E. (2009). Uranyl–chlorite sorption/desorption: Evaluation of different U(VI) sequestration processes. *Geochimica et Cosmochimica Acta, 73*(20), 5989-6007. doi: http://dx.doi.org/10.1016/j.gca.2009.07.002

Solomon, D., Lehmann, J., & Martínez, C. E. (2003). Sulfur K-edge XANES Spectroscopy as a Tool for Understanding Sulfur Dynamics in Soil Organic Matter. *Soil Science Society of America Journal, 67*(6), 1721-1731. doi: 10.2136/sssaj2003.1721

Spirakis, C. S. (1996). The roles of organic matter in the formation of uranium deposits in sedimentary rocks. *Ore Geology Reviw, 11*(1-3), 53-69. doi: 10.1016/0169-1368(95)00015-1

Stefaniak, E. A., Alsecz, A., Frost, R., Máthé, Z., Sajó, I. E., Török, S., et al. (2009). Combined SEM/EDX and micro-Raman spectroscopy analysis of uranium minerals from a former uranium mine. *Journal of Hazardous Materials, 168*(1), 416-423. doi: http://dx.doi.org/10.1016/j.jhazmat.2009.02.057

Stewart, B. D., Amos, R. T., & Fendorf, S. (2011). Effect of Uranium(VI) Speciation on Simultaneous Microbial Reduction of Uranium(VI) and Iron(III) All rights reserved. No part of this periodical may be reproduced or transmitted in any form or by any means, electronic or mechanical, including photocopying, recording, or any information storage and retrieval system, without permission in writing from the publisher. *Journal of Environmental Quality, 40*(1), 90-97. doi: 10.2134/jeq2010.0304

Stewart, B. D., Mayes, M. A., & Fendorf, S. (2010). Impact of Uranyl−Calcium−Carbonato Complexes on Uranium(VI) Adsorption to Synthetic and Natural Sediments. *Environmental Science & Technology, 44*(3), 928-934. doi: 10.1021/es902194x

Stewart, C. L. (2002). *The mineralogy of uranium rollfront deposits and its significance to in situ carbonate leach mining.* (MSc), University of Wyoming, Laramie, WY.

Stewart, C. L., Reimann, L. J., & Swapp, S. M. (2000). Mineralogic Considerations for Uranium In Situ Leach Mining: A Preliminary Study of Uranium and Associated Mineralogy of Roll-Front Uranium Deposits in Wyoming and Nebraska. *Can. Inst. Min. Bull*(93), 89-96.

Stout, R. M., & Stover, D. E. (1997). *The Smith Ranch uranium project.* Paper presented at the Uranium and nuclear energy 1997, London, pp 105-118.

Susini, J. (2008). Uranium speciation in mine tailings: ESRF.

Suzuki, Y., Kelly, S. D., Kemner, K. M., & Banfield, J. F. (2005). Direct Microbial Reduction and Subsequent Preservation of Uranium in Natural Near-Surface Sediment. *Applied and Environmental Microbiology, 71*(4), 1790-1797. doi: 10.1128/AEM.71.4.1790-1797.2005

Swanson, V. E. (1956). *Uranium in marine black shales of the United States.* Paper presented at the Geological Survey Prof. paper 300, Contributions to the Geology of Uranium and Thorium by the USA Geological Survey and the Atomic energy commission for UN,Geneva, Switzerlannd. 300 : 451- 456.

Swapp, M. S. (2015). MUB source term core analysis and description.

Sylwester, E. R., Hudson, E. A., & Allen, P. G. (2000). The structure of uranium (VI) sorption complexes on silica, alumina and montmorillonite. *Geochimica et Cosmochimica Acta, 64*, 2431-2438. doi: 10.1016/S0016-7037(00)00376-8

Toby, B. H., & Von Dreele, R. B. (2013). GSAS-II: the genesis of a modern open-source all purpose crystallography software package. *Journal of Applied Crystallography, 46*(2), 544-549. doi: doi:10.1107/S0021889813003531

Tsui, T. F. (1984). Mineralogical Characterization Uranium Ore To Evaluate In Situ Leaching Prospects. doi: 10.2118/11045-PA

Uhrie, J. L., Drever, J. I., Colberg, P. J. S., & Nesbitt, C. C. (1996). In situ immobilization of heavy metals associated with uranium leach mines by bacterial sulfate reduction. *Hydrometallurgy, 43*(1), 231-239. doi: http://dx.doi.org/10.1016/0304-386X(95)00087-W

Um, W., Serne, R. J., Brown, C. F., & Rod, K. A. (2008). Uranium(VI) sorption on iron oxides in Hanford Site sediment: Application of a surface complexation model. *Applied Geochemistry, 23*(9), 2649-2657. doi: http://dx.doi.org/10.1016/j.apgeochem.2008.05.013

United States Nuclear Regulatory Commission. (Last updated August 22, 2013). ISR Wellfield Ground Water Quality Data. from http://www.nrc.gov/info-finder/materials/uranium/licensed-facilities/smith-ranch/isr-wellfield-ground-water-quality-data.html

United States Nuclear Regulatory Commission. (Last updated January 3, 2017). Appendix A to Part 40—Criteria Relating to the Operation of Uranium Mills and the Disposition of Tailings or Wastes Produced by the Extraction or Concentration of Source Material From Ores Processed Primarily for Their Source Material Content. *https://www.nrc.gov/reading-rm/doc-collections/cfr/part040/part040-appa.html*.

Urquhart, S. G., & Ade, H. (2002). Trends in the Carbonyl Core (C 1S, O 1S) → π*C=O Transition in the Near-Edge X-ray Absorption Fine Structure Spectra of Organic Molecules. *The Journal of Physical Chemistry B, 106*(34), 8531-8538. doi: 10.1021/jp0255379

Vivo, B., Ippolito, F., Capaldi, G. S., & Simpson, P. R. (1984). Uranium geochemistry, mineralogy, geology, exploration and resources. from http://public.eblib.com/choice/publicfullrecord.aspx?p=3103037

Waite, T. D., Davis, J. A., Payne, T. E., Waychunas, G. A., & Xu, N. (1994). Uranium(VI) adsorption to ferrihydrite: Application of a surface complexation model. *Geochimica et Cosmochimica Acta, 58*(24), 5465-5478. doi: http://dx.doi.org/10.1016/0016-7037(94)90243-7

Waite, T. D., Davis James, A., Fenton, B. R., & Payne Timothy, E. (2000). Approaches to modelling uranium(VI) adsorption on natural mineral assemblages *Radiochimica Acta International journal for chemical aspects of nuclear science and technology* (Vol. 88, pp. 687).

Wall, J., D. , & Krumholz, L. R. (2006). Uranium Reduction. *Annu. Rev. Microbiol. 60:149–66.*

Wan, J., Tokunaga, T. K., Brodie, E., Wang, Z., Zheng, Z., Herman, D., et al. (2005). Reoxidation of Bioreduced Uranium under Reducing Conditions. *Environmental Science & Technology, 39*(16), 6162-6169. doi: 10.1021/es048236g

Wazne, M., Korfiatis, G. P., & Meng, X. (2003). Carbonate Effects on Hexavalent Uranium Adsorption by Iron Oxyhydroxide. *Environmental Science & Technology*, *37*(16), 3619-3624. doi: 10.1021/es034166m

Webb, S. M. (2005). SIXpack: A graphical user interface for XAS analysis using IFEFFIT. *Phys. Scr, 115*, 1011−1014.

Wei-min, W., Carley, J., T. Gentry, Ginder-Vogel, M. A., Fienen, M., Mehlhorn, T., et al. (2006). Pilot-Scale in Situ Bioremedation of Uranium in a Highly Contaminated Aquifer. 2. Reduction of U(VI) andGeochemical Control of U(VI) Bioavailability. *Environ. Sci. Technol., 40*, 3986–3995.

Wersin, P., Hochella, M. F., Persson, P., Redden, G., Leckie, J. O., & Harris, D. W. (1994). Interaction between aqueous uranium (VI) and sulfide minerals: Spectroscopic evidence for sorption and reduction. *Geochimica et Cosmochimica Acta, 58*(13), 2829-2843. doi: http://dx.doi.org/10.1016/0016-7037(94)90117-1

WoldeGabriel, G., Boukhalfa, H., Ware, S. D., Cheshire, M., Reimus, P., Heikoop, J., et al. (2014). Characterization of cores from an in situ recovery mined uranium deposit in Wyoming: Implications for post-mining restoration. *Chemical Geology, 390*(0), 32-45. doi: http://dx.doi.org/10.1016/j.chemgeo.2014.10.009

Womble, T., Shu, W., & Savage, K. (2013). Uranium distribution in geochemically diverse sediments. *Journal of the South Carolina Academy of Science, 9*(2).

World Nuclear Association. (Last updated; September, 2016). In Situ Leach (ISL) mining of Uranium. from http://www.world-nuclear.org/information-library/facts-and-figures/world-nuclear-power-reactors-and-uranium-requireme.aspx

World Nuclear Association. (updated May 2017). World Uranium Mining Production. from http://www.world-nuclear.org/information-library/nuclear-fuel-cycle/mining-of-uranium/world-uranium-mining-production.aspx

Wright, K. E., Hartmann, T., & Fujita, Y. (2011). Inducing mineral precipitation in groundwater by addition of phosphate. *Geochemical Transactions, 12*(1), 8. doi: 10.1186/1467-4866-12-8

Wu, W.-M., Carley, J., Fienen, M., Mehlhorn, T., Lowe, K., Nyman, J., et al. (2006). Pilot-Scale in Situ Bioremediation of Uranium in a Highly Contaminated Aquifer. 1. Conditioning of a Treatment Zone. *Environmental Science & Technology, 40*(12), 3978-3985. doi: 10.1021/es051954y

Wu, W.-M., Carley, J., Luo, J., Ginder-Vogel, M. A., Cardenas, E., Leigh, M. B., et al. (2007). In Situ Bioreduction of Uranium (VI) to Submicromolar Levels and Reoxidation by Dissolved Oxygen. *Environmental Science & Technology, 41*(16), 5716-5723. doi: 10.1021/es062657b

Zeng, T., Arnold, W. A., & Toner, B. M. (2013). Microscale Characterization of Sulfur Speciation in Lake Sediments. *Environmental Science & Technology, 47*(3), 1287-1296. doi: 10.1021/es303914q

Zheng, Z., Tokunaga, T. K., & Wan, J. (2003). Influence of calcium carbonate on U(VI) sorption to soils. *Environ. Sci. Technol., 37*(24), 5603-5608. doi: 10.1021/es0304897

APPENDICES

Appendix A

Table A-1: Major and Trace element composition from MUB, Smith Ranch-Highlands Mine.

Sample	Chloride (µg/g)	Inorganic C (%)	Organic C (%)	Al (µg/g)	Sb (µg/g)	As (µg/g)	Ba (µg/g)	Be (µg/g)	B (µg/g)
Core 2 (MUB-S1)									
355.5L	<100	0.23	42.5	7900	28	6.2	74	11	34
355.5R	<50	0.01	0.07	14500	<0.2	2.4	34	0.5	5
353.5	<50	0.02	0.12	17000	<0.2	1.9	42	0.4	4
362.5	<50	0.02	0.07	18800	<0.2	2.3	200	0.5	3
Core 1 (MUB-N1)									
498.5L	<100	0.27	3.95	32600	0.5	48	61	1.3	13
498.5R	<50	0.10	0.11	37100	<0.2	4.8	70	1.0	12
500.5L	<100	0.31	4.01	10100	19	109	43	5.1	50
500.5R	<50	0.07	1.01	22600	0.2	19	46	0.8	7
509.5	<500	0.32	0.03	16800	<0.2	1.4	24	0.4	2

Sample	Cd (µg/g)	Ca (µg/g)	Cr (µg/g)	Co (µg/g)	Cu (µg/g)	Fe (µg/g)	Pb (µg/g)	Mg (µg/g)	Mn (µg/g)
Core 2 (MUB-S1)									
355.5L	28	700	220	120	30	6700	135	180	120
355.5R	<0.1	50	21	3.7	2.8	10000	4.7	20	78
353.5	0.2	300	24	5.8	2.2	8100	4.8	50	82
362.5	<0.1	70	22	4.8	1.3	9600	4.4	30	78
Core 1 (MUB-N1)									
498.5L	1.6	540	36	40	12	17700	59	110	90
498.5R	0.2	300	38	8.8	10	17800	11	40	81
500.5L	2.2	1900	100	92	14	51300	15	390	72
500.5R	0.4	270	30	20	7.4	26600	7.8	90	100
509.5	0.1	220	33	5.8	1.2	11400	3.9	60	150

Sample	Mo (µg/g)	Ni (µg/g)	K (µg/g)	Se (µg/g)	Ag (µg/g)	Na (µg/g)	Sr (µg/g)	TI (µg/g)	Sn (µg/g)
Core 2 (MUB-S1)									
355.5L	1.3	108	90	780	0.2	200	300	0.5	1.8
355.5R	<0.1	7.4	90	54	<0.1	60	30	<0.2	1.1
353.5	0.3	8.4	110	0.1	<0.1	70	22	<0.2	1.1
362.5	<0.1	10	80	0.2	<0.1	70	34	<0.2	1.1
Core 1 (MUB-N1)									
498.5L	4.1	60	130	1.6	<0.1	130	74	0.4	1.5
498.5R	0.8	19	150	0.4	<0.1	110	72	0.3	1.4
500.5L	12	151	80	4.0	0.2	280	140	2.8	4.0
500.5R	2.0	36	140	0.8	<0.1	80	32	0.7	1.2
509.5	0.1	11	70	0.1	<0.1	90	32	<0.2	1.1

Sample	Ti (µg/g)	U (µg/g)	V (µg/g)	Zn (µg/g)
Core 2 (MUB-S1)				
355.5L	1100	954	5840	14
355.5R	510	3.6	32	24
353.5	630	9.1	28	20
362.5	330	2.9	31	20
Core 1 (MUB-N1)				
498.5L	700	2.4	96	130
498.5R	520	1.5	53	47
500.5L	1800	22	576	35
500.5R	610	1.4	36	34
509.5	500	3.2	31	16

Appendix B

Table B-1: Sulfur reference compounds, quality of fit value (R-factor) and spoil values from PCA analyses.

Sulfur reference compounds	**Spoil[a]**	**R-factor**	**Quality (assessment based on spoil value)**
Gypsum	1.90	0.002	good
Marcasite	2.48	0.009	good
Pyrite	1.07	0.006	excellent
Sodium bisulfide	5.44	0.081	poor
Orpiment	2.62	0.013	good
Arsenopyrite	1.91	0.002	good
Pyrrotitie	2.31	0.070	good
Anhydrite	1.79	0.014	good
Thianthrene ($C_{12}H_8S_2$)	3.90	0.040	fair
Aluminum sulfate	1.91	0.056	good
Dibenzothiophene	4.04	0.025	fair
L-cysteine	2.65	0.033	good

[a]Values less than 1.5 are considered excellent fit, 1.5-3 are good, 3 - 4.5 are fair, 4.5 – 6 are poor and > 6 are unacceptable.

Table B-2: Iron reference compounds, quality of fit value (R-factor) and spoil value.

Iron reference compounds	Spoil[a]	R-factor	Quality
Pyrite	0.8023	0.00049	excellent
Goethite	1.3809	0.00032	Excellent
Vivianite	2.8276	0.00151	good
Ferrous sulfate (melanterite)	2.1922	0.00118	good
chlorite	1.6052	0.00071	good
Illite	1.2784	0.00019	excellent
Magnetite	1.7319	0.00041	good
Haematite	1.8534	0.00051	good
Siderite	5.2317	0.01029	poor
Smectite	1.6261	0.00033	good
Scorodite	1.6697	0.00076	good
Ilminite	2.6873	0.00054	good
Ferrihydrite	1.1818	0.00026	excellent

[a]Values less than 1.5 are considered excellent fit, 1.5-3 are good, 3 - 4.5 are fair, 4.5 – 6 are poor and > 6 are unacceptable.

Appendix C

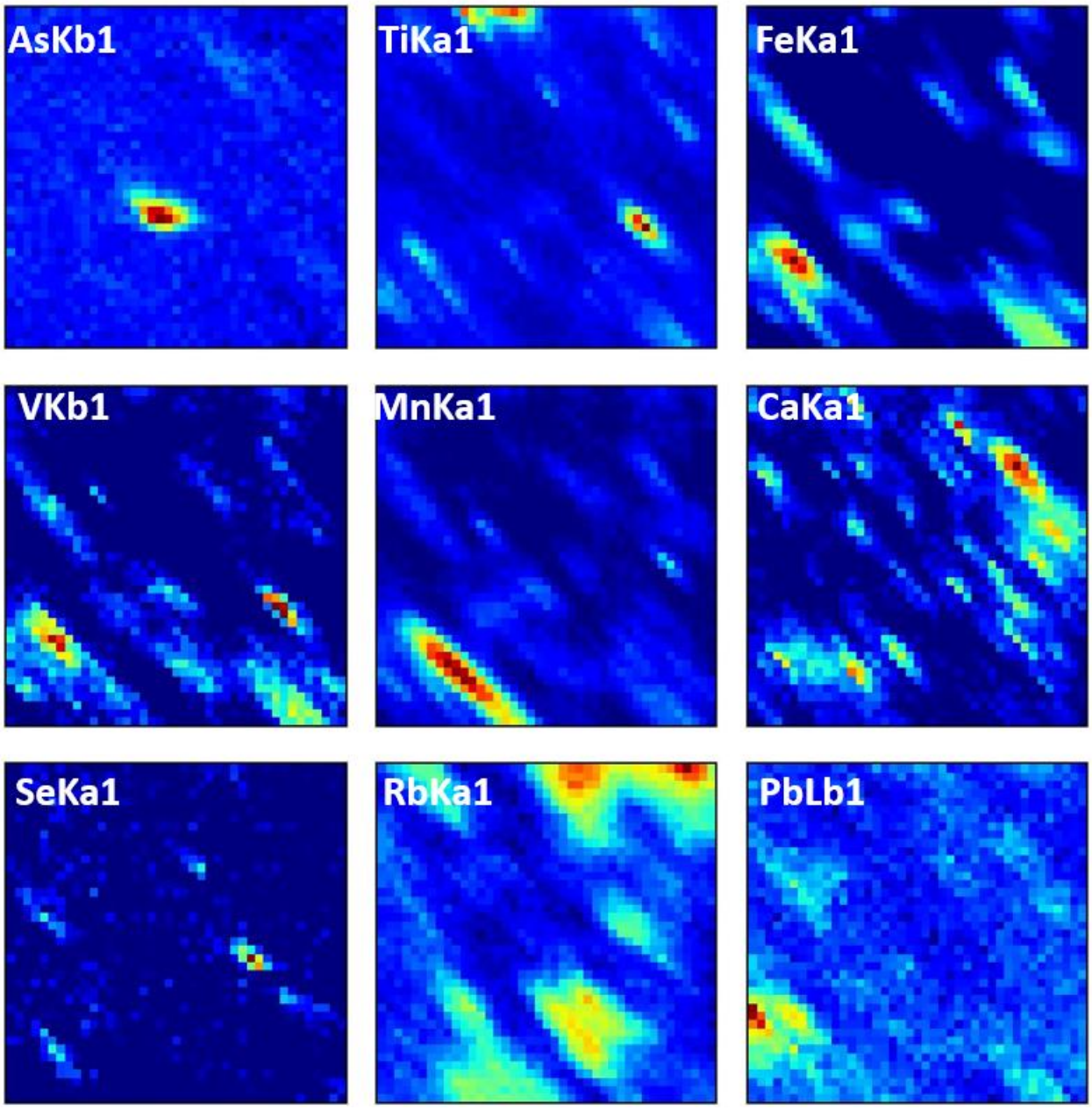

Figure C-1: X-ray flourescence elemental distribution map for sample 509.5. The size of each map is 200 µm x 200 µm. X-ray flourescence intensities of the element are scale between maximum (red) and minimum (blue).

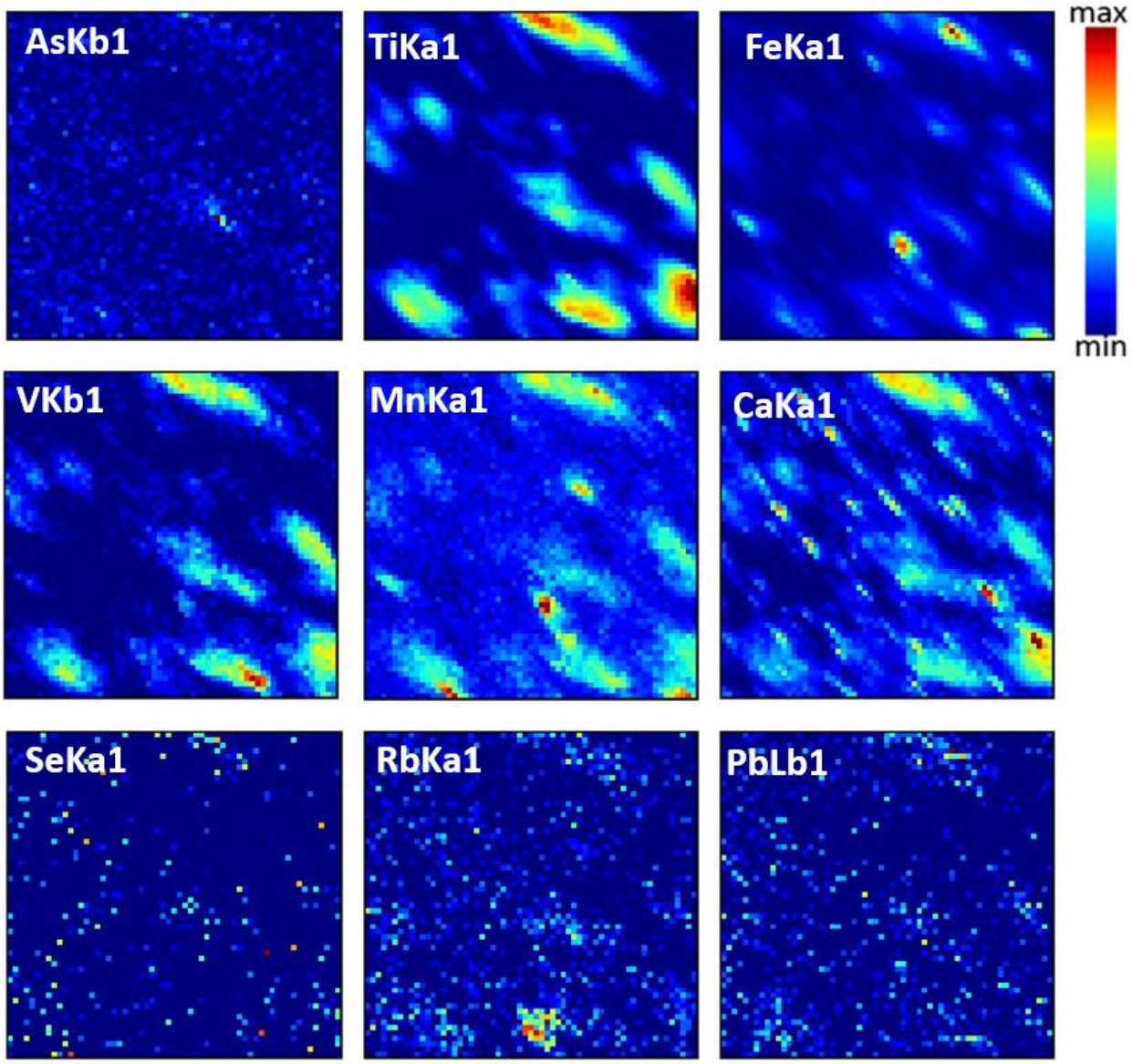

Figure C-2: X-ray flourescence elemental distribution map for sample 500.5L (coal lens). The size of each map is 300 µm x 300 µm. X-ray flourescence intensities of the element are scale between maximum (red) and minimum (blue).

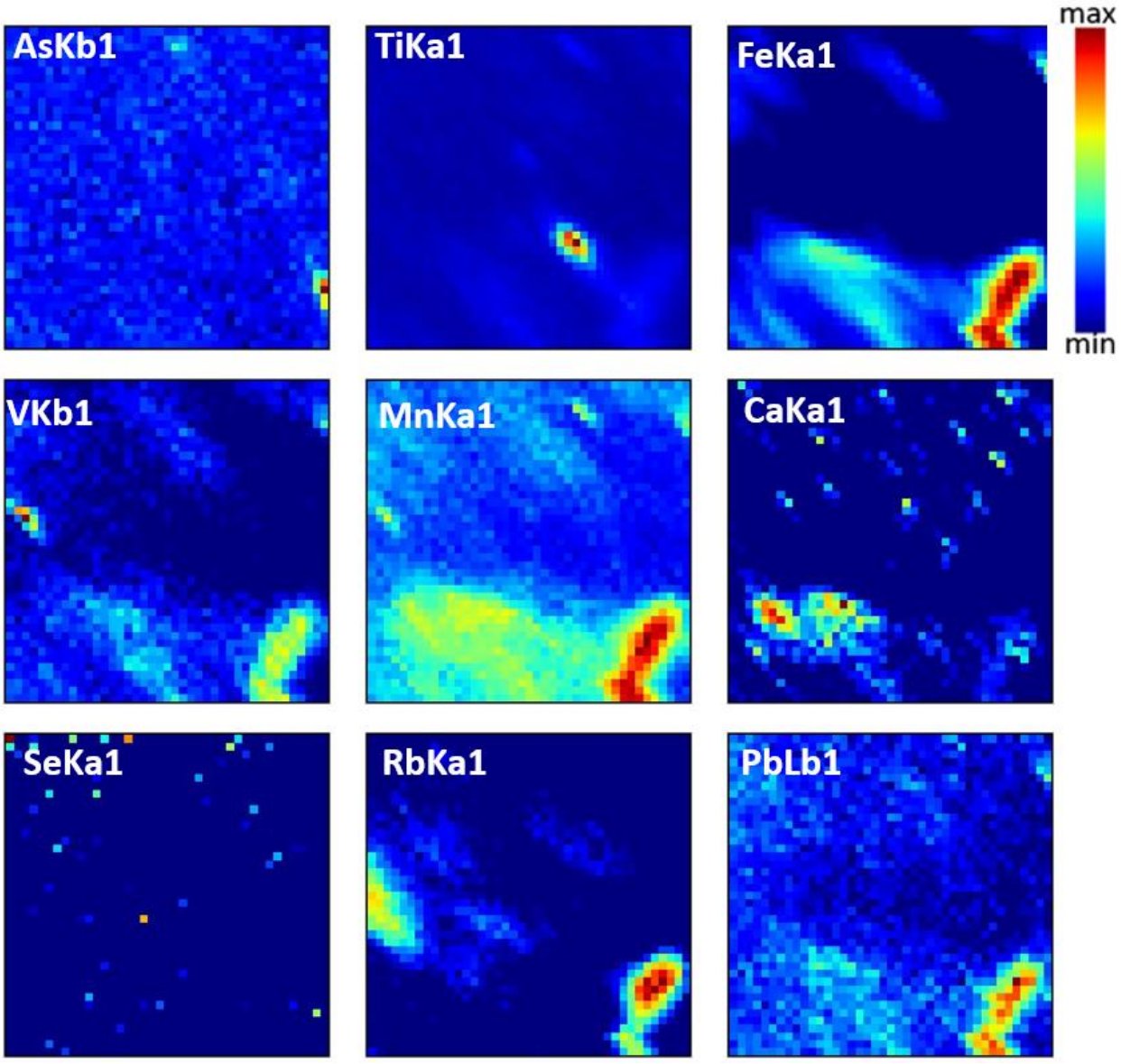

Figure C-3: X-ray flourescence elemental distribution map for sample 498.5L (coal lens). The size of each map is 200 µm x 200 µm. X-ray flourescence intensities of the element are scale between maximum (red) and minimum (blue).

Appendix D

Table D-1: Saturation state of mineral in groundwater from M39 and M20.

Minerals	Saturation Index		Chemical Formulae
	M39	M20	
a-U_3O_8(cr)	-17.05	-17.31	U_3O_8
Anhydrite	-1.81	-2.07	$CaSO_4$
Aragonite	0.46	0.45	$CaCO_3$
Artinite	-5.89	-5.71	$MgCO_3$:$Mg(OH)_2$:$3H_2O$
Birnessite	-14.65	-14.28	MnO_2
Bixbyite	-13.75	-13.23	Mn_2O_3
Boltwoodite	-4.64	-4.62	$KUO_2(SiO_3OH)$:H_2O
Brucite	-4.79	-4.65	$Mg(OH)_2$
Calcite	0.61	0.6	$CaCO_3$
Chalcedony	0.12	0.11	SiO_2
Chlorite	0.62	1.12	$Mg_5Al_2Si_3O_{10}(OH)_8$
Chrysotile	-2.26	-1.85	$Mg_3Si_2O_5(OH)_4$
Coffinite	-6.39	-6.61	$USiO_4$
Cristobalite	0.18	0.17	SiO_2
Diopside	-1.8	-1.58	$CaMgSi_2O_6$
Dolomite	0.7	0.73	$CaMg(CO_3)_2$
Dolomite(d)	0.1	0.13	$CaMg(CO_3)_2$
$Fe(OH)_3$(a)	1.98	2.28	$Fe(OH)_3$
Ferrihydrite-6L	3.67	3.97	$Fe(OH)_3$
Fluorite	-2.34	-2.44	CaF_2
Forsterite	-7.62	-7.34	Mg_2SiO_4
gamma-UO_3(cr)	-9.64	-9.66	UO_3
Goethite	6.6	6.9	FeOOH
Greenalite	3.8	4.4	$Fe_3Si_2O_5(OH)_4$
Gypsum	-1.56	-1.81	$CaSO_4$:$2H_2O$
H_2(g)	-19.2	-19.4	H_2
H_2O(g)	-1.83	-1.83	H_2O
Halite	-7.79	-7.91	NaCl
Hausmannite	-15.66	-14.97	Mn_3O_4
Hematite	16.81	17.41	Fe_2O_3
Huntite	-3.51	-3.39	$CaMg_3(CO_3)_4$
Illite	3.14	2.90	$K0.6Mg0.25Al_2.3Si_3.5O_{10}(OH)_2$
Jarosite(ss)	-5.02	-4.76	$(K0.77Na0.03H0.2)Fe_3(SO_4)_2(OH)_6$
Jarosite-K	-3.33	-3.07	$KFe_3(SO_4)_2(OH)_6$
Jarosite-Na	-8.68	-8.34	$NaFe_3(SO_4)_2(OH)_6$
JarositeH	-13.19	-12.97	$(H3O)Fe_3(SO_4)_2(OH)_6$
Kaolinite	4.31	4.11	$Al_2Si_2O_5(OH)_4$
K-mica	9.13	8.87	$KAl_3Si_3O_{10}(OH)_2$
Magadiite	-5.21	-5.09	$NaSi_7O_{13}(OH)_3$:$3H_2O$
Maghemite	7.36	7.96	Fe_2O_3

Magnesite	-0.45	-0.41	$MgCO_3$
Magnetite	19.05	19.85	Fe_3O_4
Metaschoepite(am)	-7.67	-7.69	$UO_3:2H_2O$
Metaschoepite(cr)	-6.78	-6.8	$UO_3:2H_2O$
Metaschoepite(syn)	-7.57	-7.59	$UO_3:2H_2O$
Mirabilite	-6.7	-6.79	$Na_2SO_4:10H_2O$
NaBoltwoodite	-5.22	-5.11	$NaUO_2(SiO_3OH):H_2O$
NaCompreignacite	-40.15	-40.02	$Na_2(UO_2)_6\,O_4(OH)_6:7H_2O$
Nahcolite	-4.5	-4.47	$NaHCO_3$
Natron	-8.26	-8.11	$Na_2CO_3:10H_2O$
NaWeeksite	-14.56	-14.36	$Na_2(UO_2)_2(Si_2O_5)3:4H_2O$
Nesquehonite	-2.85	-2.81	$MgCO_3:3H_2O$
Nsutite	-13.61	-13.25	MnO_2
O_2(g)	-49.03	-48.63	O_2
Portlandite	-10.39	-10.3	$Ca(OH)_2$
Pyrite	19.62	19.50	FeS_2
Pyrochroite	-5.44	-5.28	$Mn(OH)_2$
Pyrolusite	-14.43	-14.06	MnO_2
Quartz	0.58	0.58	SiO_2
Rhodochrosite	-0.33	-0.27	$MnCO_3$
Rhodochrosite(d)	-1.03	-0.96	$MnCO_3$
Rutherfordine	-7.78	-7.9	UO_2CO_3
Schwertmannite	5.76	7.62	$Fe_8O_8(OH)_4.8(SO_4)1.6$
Sepiolite	-1.07	-0.79	$Mg_2Si_3O_7.5OH:3H_2O$
Siderite(cr)	0.22	0.33	$FeCO_3$
Siderite(ppt)	-0.18	-0.08	$FeCO_3$
SiO_2(a)	-0.77	-0.77	SiO_2
Soddyite	-12.7	-12.74	$(UO_2)_2SiO_4:2H_2O$
Talc	1.5	1.91	$Mg_3Si_4O_{10}(OH)_2$
Thenardite	-8.24	-8.33	Na_2SO_4
Thermonatrite	-10.27	-10.11	$Na_2CO_3:H2O$
Tremolite	2.94	3.8	$Ca_2Mg_5Si_8O_{22}(OH)_2$
Trona	-14.98	-14.8	$NaHCO_3:Na_2CO_3:2H_2O$
$U(OH)_2SO_4$(cr)	-26.79	-27.35	$U(OH)_2SO_4$
U_4O_9(cr)	-21.74	-22.41	U_4O_9
UO_2(am,hyd)	-8.95	-9.17	UO_2
UO_2(cr)	-6.17	-6.39	UO_2
$UO_2SO_4:2.5H_2O$(cr)	-19.27	-19.63	$UO_2SO_4:2.5H_2O$
$UO_2SO_4:3.5H_2O$(cr)	-19.27	-19.63	$UO_2SO_4:3.5H_2O$
$UO_2SO_4:3H_2O$(cr)	-20.1	-20.46	$UO_2SO_4:3H_2O$
Uranophane	-7.49	-7.45	$Ca(UO_2)_2(SiO_3OH)_2:5H_2O$

Appendix E

Table E-1: Modelling results for saturation indices under different conditions of pH for M20 at Eh of +80 mV

MINERALS	pH					
	3	5	7	8.3	9	11
Calcite	-4.56	-2.67	-0.65	0.62	1.23	1.87
Dolomite	-10.19	-6.41	-2.42	0.14	1.99	2.70
Ferrihydrite	-11.77	-5.37	0.57	3.93	5.12	3.40
Goethite	-8.72	-2.46	3.49	6.85	8.05	6.32
Coffinite	2.67	1.87	-2.78	-6-62	-8.55	-11.70
Uraninite	2.61	2.17	-2.76	-6.40	-8.30	-10.43
Uranophane	-21.90	-10.11	-7.58	-7.48	-7.16	-1.60
Pyrite	2.52	10.52	17.83	19.50	19.94	12.79
Gypsum	-2.11	-1.81	-1.81	-1.82	-1.84	-1.87
Siderite	-4.28	-2.39	-0.49	0.28	0.02	-6.92
Quartz	0.86	0.59	0.59	0.58	0.55	-0.56
Albite	-13.72	-6.72	-0.42	-0.34	-0.44	-3.47
Kaolinite	-13.28	-2.10	6.56	4.11	2.65	-3.37
Illite	-22.44	-7.80	4.36	2.90	2.01	-3.37
Chlorite	-69.96	-38.07	-9.40	1.12	6.55	18.96
Mica	-22.33	-3.76	11.24	8.87	7.37	0.34

Table E-2: Modelling results for saturation indices under different conditions of pH for M39 at Eh of +80 mV

MINERALS	pH					
	3	5	7	8.3	9	11
Calcite	-4.45	-2.57	-0.57	0.61	1.32	1.94
Dolomite	-10.03	-6.26	-2.27	0.10	2.13	2.79
Ferrihydrite	-11.85	-5.46	0.48	3.69	5.06	3.33
Goethite	-8.80	-2.54	3.40	6.55	7.99	6.25
Coffinite	2.75	2.05	-2.83	-6.39	-8.59	-11.63
Uraninite	2.70	2.26	-2.62	-6.77	-8.33	-10.36
Uranophane	-21.58	-9.81	-7.58	-7.49	-7.12	-1.32
Pyrite	2.43	10.43	17.75	19.62	19.89	12.70
Gypsum	-1.85	-1.56	-1.56	-1.56	-1.58	-1.68
Siderite	-4.38	-2.50	-0.56	0.18	-0.06	-7.05
Quartz	0.85	0.59	0.59	0.58	0.55	-0.46
Albite	-13.77	-6.57	-0.24	-0.36	-0.47	-3.50
Kaolinite	-13.29	-2.10	6.56	4.31	2.64	-3.38
Illite	-22.41	-7.78	4.41	3.14	2.05	-3.91
Chlorite	-69.64	-37.78	-9.11	0.62	6.85	19.34
Mica	-22.28	-3.70	11.30	9.11	7.42	0.39

Appendix F

Table F-1: Modelling results for saturation indices under different redox conditions for M20.

MINERALS	pE							
	1.4	1.7	2.5	3.4	5.1	-1.7	-2.5	-3.4
Calcite	0.61	0.61	0.61	0.61	0.61	0.61	0.61	0.61
Dolomite	0.14	0.14	0.14	0.14	0.14	0.14	0.14	0.14
Ferrihydrite	3.93	4.22	4.97	5.57	5.82	0.83	0.03	-0.87
Goethite	6.85	7.15	7.89	8.50	8.75	3.76	2.96	2.06
Coffinite	-6.62	-7.22	-8.82	-10.62	-14.02	-0.42	1.80	2.98
Uraninite	-6.40	-7.00	-8.60	-10.00	-13.80	-0.20	1.40	3.20
Uranophane	-7.48	-7.48	-7.48	-7.48	-7.48	-7.48	-7.48	-7.48
Pyrite	10.70	20.30	21.90	23.64	25.92	13.50	11.90	10.10
Gypsum	-1.82	-1.82	-1.82	-1.82	-1.82	-1.82	-1.82	-1.82
Siderite	0.28	0.28	0.22	-0.07	-1.52	0.29	0.29	0.29
Quartz	0.58	0.58	0.58	0.58	0.58	0.58	0.58	0.58
Albite	-0.34	-0.34	-0.34	-0.34	-0.34	-0.34	-0.34	-0.34
Kaolinite	4.11	4.11	4.11	4.11	4.11	4.11	4.11	4.11
Illite	2.97	2.97	2.97	2.97	2.97	2.97	2.97	2.97
Chlorite	1.12	1.12	1.12	1.12	1.12	1.12	1.12	1.12
Mica	8.87	8.87	8.87	8.87	8.87	8.87	8.87	8.87

Table F-2: Modelling results for saturation indices under different redox conditions for M39.

MINERALS	pE							
	1.4	1.7	2.5	3.4	5.1	-1.7	-2.5	-3.4
Calcite	0.61	0.61	0.61	0.61	0.61	0.61	0.61	0.61
Dolomite	0.10	0.10	0.10	0.10	0.10	0.10	0.10	0.10
Ferrihydrite	3.63	3.93	4.69	5.39	5.76	0.53	-0.27	-1.17
Goethite	6.55	6.85	7.62	8.31	8.68	3.43	2.66	1.76
Coffinite	-6.39	-6.99	-8.59	-10.39	-13.74	-0.19	1.41	3.21
Uraninite	-6.17	-6.77	-8.37	-10.17	-13.57	0.03	1.63	3.43
Uranophane	-7.49	-7.49	-7.49	-7.49	-7.49	-7.49	-7.49	-7.49
Pyrite	19.62	20.22	21.81	23.57	25.89	13.42	11.82	10.02
Gypsum	-1.56	-1.56	-1.56	-1.56	-1.56	-1.56	-1.56	-1.56
Siderite	0.18	0.17	0.14	-0.06	-1.39	0.18	0.18	0.18
Quartz	0.58	0.58	0.58	0.58	0.58	0.58	0.58	0.58
Albite	-0.36	-0.36	-0.36	-0.36	-0.36	-0.36	-0.36	-0.36
Kaolinite	4.31	4.31	4.31	4.31	4.31	4.31	4.31	4.31
Illite	3.14	3.14	3.14	3.14	3.14	3.14	3.14	3.14
Chlorite	0.62	0.62	0.62	0.62	0.62	0.62	0.62	0.62
Mica	9.13	9.13	9.13	9.13	9.13	9.13	9.13	9.13